



**The Grid Technologies Collaborative
Next Generation Power Converter Development
2012 Research & Development Progress Report
UNIV-PUB-109**

February 28, 2013

**DOE/NETL
Innovative Process Technologies FWP: IPT_FY131415**

Task 7.5: Grid Technologies

Disclaimer

This report was prepared as an account of work sponsored by an agency of the United States Government. Neither the United States Government nor any agency thereof, nor any of their employees, makes any warranty, express or implied, or assumes any legal liability or responsibility for the accuracy, completeness, or usefulness of any information, apparatus, product, or process disclosed, or represents that its use would not infringe privately owned rights. Reference therein to any specific commercial product, process, or service by trade name, trademark, manufacturer, or otherwise does not necessarily constitute or imply its endorsement, recommendation, or favoring by the United States Government or any agency thereof. The views and opinions of authors expressed therein do not necessarily state or reflect those of the United States Government or any agency thereof.

The National Energy Technology Laboratory (NETL) conducts cutting-edge energy research and technology development and analyzes energy systems and international energy issues for the U.S. Department of Energy. The NETL-Regional University Alliance (NETL-RUA) is an applied research collaboration that combines NETL's energy research expertise with the broad capabilities of five nationally recognized, regional universities: Carnegie Mellon University (CMU), The Pennsylvania State University (PSU), the University of Pittsburgh (Pitt), Virginia Tech (VT), and West Virginia University (WVU), and the engineering and construction expertise of an industry partner (URS). The NETL-RUA leverages its expertise with current fossil energy sources to discover and develop sustainable energy systems of the future, introduce new technology, and boost economic development and national security.

**DOE NETL-RUA
GRID TECHNOLOGIES COLLABORATIVE**

DOE/NETL

Innovative Process Technologies FWP: IPT_FY131415

Task 7.5 Grid Technologies

**Next Generation Power Converter Development
2012 Research & Development Progress Report**

February 28, 2013

UNIV-PUB-109

NETL-RUA Contacts:

Gregory F. Reed, Ph.D.

GTC Director and Technical Lead

Swanson School of Engineering, University of Pittsburgh

Wayne Honath

**GTC Director of Program Development and Industry Relations
University Energy Partnership**

National Energy Technology Laboratory

www.netl.doe.gov

This page intentionally left blank

Table of Contents

TABLE OF CONTENTS	I
LIST OF EXHIBITS	III
PREPARED BY THE NETL-RUA INSTITUTIONS	VI
ACKNOWLEDGMENTS	VIII
EXECUTIVE SUMMARY	1
1. INTRODUCTION AND BACKGROUND	4
1.1 ADVANCED ELECTRICITY TRANSMISSION AND DISTRIBUTION NETWORK	4
1.2 APPLICATIONS AND BENEFITS OF ADVANCED GRID-SCALE POWER ELECTRONICS	5
1.2.1 <i>Mitigating the Need to Build New Transmission</i>	6
1.2.2 <i>Supporting Liberalized Electricity Markets</i>	7
1.2.3 <i>Integrating Renewable Generating Resources</i>	8
1.2.4 <i>Increasing Power System Stability, Security, and Reliability</i>	9
1.2.5 <i>How Industry and Consumers Realize the Benefits of Advanced Power Electronics</i>	10
1.2.6 <i>The Market for Grid-scale Power Electronics</i>	11
2. R&D PROGRAM OVERVIEW	13
3. TEST SYSTEMS AND SIMULATION TOOLS	16
3.1 SYSTEM MODELING OF TEST FEEDERS	16
3.2 MODEL OF THE SYNCHRONOUS GENERATOR	20
3.2.1 <i>Generator Model A</i>	20
3.2.2 <i>Generator Model B</i>	22
3.3 MODEL OF THE THREE-PHASE GRID-INTERFACE POWER CONVERTER	26
3.3.1 <i>Power Converter Model A – switching model</i>	28
3.3.2 <i>Power Converter Model B– average model</i>	30
3.3.3 <i>Power Converter Model C– simplified average model</i>	33
3.3.4 <i>Power Converter Model D – for P-f control</i>	34
3.4 INTERFACE AND COMMUNICATIONS PROTOCOLS.....	34
3.5 DEMONSTRATION SITE PLAN DEVELOPMENT	36
3.5.1 <i>Statement of the Problem</i>	36
3.5.2 <i>Approach</i>	36
3.5.3 <i>The Philadelphia Navy Yard: Background</i>	37
3.5.4 <i>PNY Microgrid Opportunity</i>	38
3.5.5 <i>Converter Characteristics</i>	38
4. METHODS, ANALYSIS, AND RESULTS	41
4.1 POWER SYSTEM NETWORK MODEL OF IEEE 13 NODE TEST FEEDER SYSTEM	41
4.2 CONVERTER PERFORMANCE, FUNCTIONALITY AND SPECIFICATIONS	62
4.2.1 <i>Scenario I</i>	63
4.2.2 <i>Scenario II</i>	67
4.3 COMMUNICATIONS AND INTERFACE PROTOCOLS.....	71
4.4 SMART CONTROL METHODOLOGY.....	79
4.5 THE POWER CONVERSION TEST STAND	101
4.5.1 <i>Initial Converter Test Configurations</i>	102
4.5.2 <i>Test Configurations Details</i>	106
4.5.3 <i>Evolution of UC test configuration</i>	106

4.5.4	<i>AC-to-AC Converter Testing</i>	107
4.5.5	<i>DC-to-DC UC Testing</i>	107
4.5.6	<i>Ancillary Testing Opportunities</i>	107
4.5.7	<i>Power System Simulation</i>	108
4.5.8	<i>Communications and Smart Grid Simulation</i>	108
4.6	MODELING PRODUCTION COST DECLINES FOR UNIVERSAL POWER CONVERSION TECHNOLOGIES	109
4.6.1	<i>Summary of Findings</i>	109
5.	CONCLUSIONS	111
5.1	SYSTEM MODELING CONCLUSIONS	112
5.2	CONVERTER PERFORMANCE, FUNCTIONALITY & DESIGN CONCLUSIONS	112
5.3	COMMUNICATIONS AND INTERFACE PROTOCOLS CONCLUSIONS	112
5.4	SMART CONTROL METHODOLOGY CONCLUSIONS	113
5.5	DEMONSTRATION SITE PLAN CONCLUSIONS	113
5.6	FUTURE WORK AND CONSIDERATIONS	113

List of Exhibits

Figure 1: An Advanced Electricity Transmission System Employing Advanced Power Electronics to Improve Performance.....	5
Figure 2: Collaborations between Universities in the NETL-RUA.....	15
Figure 3: IEEE 13 Node Test Feeder Expected and Simulated Results (Original Model).....	17
Figure 4: IEEE 13 Node Test Feeder Schematic.....	18
Figure 5: IEEE 13 Node Test Feeder PSCAD Simulation Schematic.....	19
Figure 6: WECC 9-bus system generator parameters.....	20
Figure 7: $d-q$ model of the synchronous generator.....	20
Figure 8: abc/dq transformation block.....	21
Figure 9: Simplified synchronous generator model.....	22
Figure 10: Synchronous generator (assumed) operating region map.....	23
Figure 11: WECC 9-bus system re-calculated generator parameters.....	23
Figure 12: Simplified synchronous generator model with voltage control and frequency droop implementation.....	24
Figure 13: Voltage control (simplified excitation control).....	25
Figure 14: Frequency droop for all the WECC generators.....	26
Figure 15: Grid-interface converter specifications.....	27
Figure 16: WECC 9-bus system with illustrated connection of the grid-interface converters at the bus. No1.....	27
Figure 17: The snapshot of the IEEE 1547 standard for allowable current distortion.....	28
Figure 18: The grid-interface switching model and its LCL filter.....	29
Figure 19: LCL filter parameter values.....	29
Figure 20: Converter output current.....	29
Figure 21: Harmonic spectrum of the output current.....	30
Figure 22: Average model of the grid-interface converter.....	31
Figure 23: Control block diagram.....	32
Figure 24: Control block diagram.....	32
Figure 25: Time domain simulation of the independent P (—) and Q (—) control of the grid-interface converter.....	33
Figure 26: Simplified model of the power converter for the system-level studies.....	33
Figure 27: CommSim module and SCMs within PSCAD IEEE 13node test feeder.....	36
Figure 28: GridSTAR Center Location at PNY.....	39
Figure 29: PNY Ring Bus Configuration.....	39
Figure 30: Building 664 Substation Single-Line Diagram.....	40
Figure 31: IEEE 13 Node Test Feeder Schematic.....	41
Figure 32: 3 Node IEEE 13 Node Test Feeder System.....	42
Figure 33: Bus 650 with Generation Source and Voltage Regulator.....	43
Figure 34: Bus 632 with Crossroads of Line Configurations 601, 602 and 603.....	44
Figure 35: Bus 633 with a Y-Y Transformer and Line Configuration 602.....	45
Figure 36: Bus 634 with Corresponding Three Phase Load.....	45
Figure 37: IEEE results compared with PSCAD results for Bus 634.....	46
Figure 38: Bus 645 with a Wye-Connected Single Phase Load on Phase C.....	46
Figure 39: IEEE results compared with PSCAD results for Bus 645.....	47
Figure 40: Bus 646 with a Delta-Connected Single Phase Load.....	47

Figure 41: Spot Load Data.....	48
Figure 42: IEEE results compared with PSCAD results for Bus 646.....	48
Figure 43: Bus 671 with Corresponding Delta-Connected Three Phase Load.....	49
Figure 44: IEEE results compared with PSCAD results for Bus 671.....	50
Figure 45: Bus 680 with No Immediate Load Connected.....	51
Figure 46: Bus 684 with Two Single Phase Lines Branching Off.....	52
Figure 47: Bus 611 with a Single-Phase Wye Connected Load and a Shunt Capacitance.....	53
Figure 48: Capacitor Data.....	53
Figure 49: IEEE results compared with PSCAD results for Bus 611.....	53
Figure 50: Bus 652 with a Single-Phase Wye Connected Impedance Load.....	54
Figure 51: IEEE results compared with PSCAD results for Bus 652.....	54
Figure 52: Bus 692 with a Single-Phase Delta Connected Load.....	55
Figure 53: IEEE results compared with PSCAD results for Bus 692.....	55
Figure 54: Bus 675 with a Three-Phase Load and a Shunt Capacitance.....	56
Figure 55: IEEE results compared with PSCAD results for Bus 675.....	57
Figure 56: Distributed Load Data.....	57
Figure 57: Distributed Load (on far right).....	57
Figure 58: Line Segment Data.....	58
Figure 59: Overhead Line Configuration Data.....	58
Figure 60: Underground Line Configuration Data.....	59
Figure 61: Tap Changing Configuration of Voltage Regulator.....	61
Figure 62: Regulator Data.....	61
Figure 63: Transformer Model in PSCAD.....	62
Figure 64: Transformer Data.....	62
Figure 65: WECC 9-bus system in the loss of generation scenario.....	63
Figure 66: Generator 1 active and reactive power waveforms before and after the transient (Generator 2 disconnected at 5s).....	64
Figure 67: Generator 1 power angle before and after the transient (Generator 2 disconnected at 5s).....	64
Figure 68: Generator 3 active and reactive power waveforms before and after the transient (Generator 2 disconnected at 5s).....	65
Figure 69: Generator 3 power angle before and after the transient (Generator 2 disconnected at 5s).....	65
Figure 70: Generator 3 active and reactive power waveforms before and after the transient (Generator 2 disconnected at 5s).....	66
Figure 71: Generator 3 power angle before and after the transient (Generator 2 disconnected at 5s).....	66
Figure 72: Grid-interface converter active and reactive power waveforms before and after the transient (Generator 2 disconnected at 5s).....	67
Figure 73: Reduced WECC 9-bus system with two grid-interface converters.....	67
Figure 74: One-line diagram of the grid-interface converter connection to the grid – given here for better understanding of condition (13).....	68
Figure 75: Reduced WECC system (—), and the equivalent source (—) output impedances in $d-q$	69
Figure 76: Active and reactive power of the two grid-interface converters before and after the transient (increasing grid output impedance at 1s).....	70

Figure 77: Angular frequencies of both converters' PLLs before and after the transient (increasing grid output impedance at 1s).....	70
Figure 78: Communication interface design within PSCAD, The whole system schematic	72
Figure 79: Communication network architecture coupled with PSCAD continuous time domain	72
Figure 80: An example of sampled signal along with its clock signal	74
Figure 81: Comm-Sim module components and how they can be used to have different network topologies.....	75
Figure 82: Wind Speed, Turbine Torque, Wind Power, Storage Power and Frequency for ideal communication	76
Figure 83: Wind and Storage Power, Frequency for 0.1 delay	77
Figure 84: Wind and Storage Power, Frequency for 0.5 delay	78
Figure 85: Wind Power Communicated to Storage component	78
Figure 86: Standard H Infinity Problem Configuration.....	83
Figure 87: WECC 9-bus Test System.....	84
Figure 88: Weighting Functions for Generator and Storage Power Output	85
Figure 89: Real Power Output in Frequency Domain	85
Figure 90: Frequency Deviations at Bus 3	86
Figure 91: Power Output Deviations of Gen 3 from the Operating Point	86
Figure 92: Bode Diagram of the Transfer Function from w to SOC.....	87
Figure 93: 3-bus Test System	93
Figure 94: Evolution of Coupling Variables and Multipliers using OCD_v1	94
Figure 95: Evolution of Coupling Variables and Multipliers using OCD_v2.....	94
Figure 96: Divergent Evolution of Coupling Variables and Multipliers using OCD_v1	95
Figure 97: Convergent Behavior for Evolution of Coupling Variables and Multipliers using OCD_v2.....	95
Figure 98: Evolution of Coupling Variables and Multipliers using OCD_v2 for the WECC 9-bus Test System.....	96
Figure 99: Two-Stage Stochastic Optimization.....	96
Figure 100: Economic Dispatch Model.....	97
Figure 101: Optimal Generation and Storage values for 24 hours	98
Figure 102: Modified WECC 9-bus Test System with Two Wind Generators.....	99
Figure 103: Optimal Storage Capacity and Variance in LMP Relationship	99
Figure 104: 9-Bus System with Line Limits Between Buses 4 and 6	100
Figure 105: 9-Bus System with Line Limits Between Buses 4 and 6; 7 and 8	100
Figure 106: Power-Conversion Test Stand.....	102
Figure 107: The Converter Interfacing between Storage and the Ring Bus.....	104
Figure 108: The Converter Controlling Power Factor on the Ring Bus.....	104
Figure 109: The Converter Operating as an ECC for a DC Household.	105
Figure 110: The Converter Operating Under a Dynamic AC Load	105

Prepared by the NETL-RUA Institutions:

University of Pittsburgh

PI: Gregory Reed, Ph.D.

Co-PI's: Thomas McDermott, Ph.D., Zhi-Hong Mao, Ph.D.

Graduate Student Researchers: Brandon Grainger, Patrick Lewis,
Adam Sparacino

Virginia Tech

PI: Dushan Boroyevich, Ph.D.

Co-PI's: Fred C. Lee, Ph.D., Rolando Burgos, Ph.D.

Graduate Student Researchers: Igor Cvetkovic, Zhiyu Shen

West Virginia University

PI: Parviz Famouri, Ph.D.

Co-PI: Yaser Fallah, Ph.D.

Graduate Student Researchers: Neda Nasiriani, Kaveh Rahimi,
Roopa Ramachandran

Carnegie Mellon University

PI: Gabriela Hug, Ph.D.

Co-PI: Michael McHenry, Ph.D.

Graduate Student Researchers: Dinghuan Zhu, Kyri Baker,
Vincent DeGeorge

The Pennsylvania State University

PI: Gregory M. Dobbs, Ph.D.

Co-PIs: Seth Blumsack, Ph.D, Dwight F. Macomber, Ph.D.

Graduate Student Researcher: Nicholas Johnson

National Energy Technology Laboratory

Steve Bossart, Keith Dodrill

University Energy Partnership

Wayne Honath

DOE/NETL

Innovative Process Technologies

FWP: IPT_FY131415

Task 7.5: Grid Technologies

UNIV-PUB-109

Acknowledgments

This report was prepared by the NETL-RUA Grid Technologies Collaborative (GTC) for the United States Department of Energy's National Energy Technology Laboratory. This work was completed under DOE NETL Contract Number DE-FE0004000. This work was performed under RES Activity 2.600.220.001 supporting the NETL-RUA Innovative Process Technologies Field Work Proposal.

The authors wish to acknowledge the excellent guidance, contributions, and cooperation of the NETL staff, particularly:

David Alman: Director, Materials Performance Division

Julianne Klara: Manager, Regional University Alliance

Robert Romanosky: Manager, Crosscutting Research Technology

NETL-RUA GTC also wishes to acknowledge the valuable input to this study provided by Terri Marts and Janet Nelson of URS Corporation but notes that this acknowledgement does not indicate their endorsement of the results of this study.

This page intentionally left blank

EXECUTIVE SUMMARY

This document reports on the progress of National Energy Technology Laboratory Regional University Alliance (NETL-RUA) research on the development of a next generation power converter for application in the transmission and distribution (T&D) of electrical power.

Improving the reliability and stability of T&D of electrical power and the development of the smart grid that includes large scale energy storage will: (i) enable the capacity to more efficiently manage electricity generation through “peak shaving or load shifting;” (ii) enable the integration of large scale renewable energy plants; (iii) and provide more stable and efficient delivery of electrical power. This will result in a more efficient delivery of electrical power, while reducing overall CO₂ emissions — including power generated from fossil fuel assets.

This report summarizes the first phase of NETL-RUA research aimed at providing solutions for an improved electrical grid. This report covers the period of August 2012 through December 2012. The initial phase of the project focused on modeling and simulation to develop validated steady state and dynamic models of system interactions at the converter-grid interface, including consideration of a next generation power converter, which will be established as a scalable bi-directional three-phase AC-DC interface for utility scale high power applications at T&D levels. Initial system applications for this advanced power electronics based converter topology were selected to address T&D grid performance including advanced control methodology development, interface and communications protocols, and integration of various renewable energy resources, energy storage, and evolving load entities, as well as emerging hybrid AC/DC systems.

Modeling platforms for the initial year efforts were chosen to include industry-standard tools and programs that are also common to each university’s capabilities and expertise, and are centered on models utilizing the PSCAD/EMTDC and MATLAB/Simulink program environments. The system models for initial project development consist of an accepted and widely used IEEE standard WECC transmission level test case system, as well as an IEEE standard distribution feeder test case system. This was established as a baseline to allow the ability to analyze interactions between T&D networks for both the converter and the control and interface methodologies to be developed. Various additional resources and loads will be integrated into these models, as well as the advanced converter model that is being developed separately.

This executive summary is ordered by the major areas of contribution made by each university on their respective lead scope, as follows: System Modeling (Pitt), Converter Design and Performance (VT); Communications and Interfaces (WVU); Smart Controls (CMU); and Site Planning and Costs (Penn State). While these lead roles and contributions have been initiated as somewhat individualized components of scope to-date, the work completed in 2012 will become the basis for higher levels of integration in the 2013 program plan. In all cases, each scope area is highly collaborative with one or more of the others in its definition and ultimate application, all of which will come together in an even more cohesive manner in the early stages of the 2013 efforts. The 2012 work herein, thus establishes a significant baseline of work in each of the core scope areas for the overall Next Generation Power Converter development.

System Modeling

As a starting platform for the project development, the system modeling aspect primarily consisted of the base case model development for the T&D power system network topology in the PSCAD/EMTDC program environment. Employment of standard PSCAD models have been utilized for all selected equipment and network facilities, including generation sources, power electronics converters, feeders, and loads. This has been done using IEEE standard test bus cases (IEEE 9 bus and IEEE 13 bus systems) for the transmission network and for the distribution feeder network. Also, Pitt has supported the following scopes of the partner universities: control methodology development, converter topology design, interface/communications development, and demonstration site plan selection.

Converter Performance, Functionality and Design

The power electronics converter technology development focused on a functional design which enables major improvements in performance, reliability, and maximal utilization of the renewable energy sources and energy storage systems that can be integrated into the electric power system. The main goal of this work was to explore functionality and performance of the bidirectional three-phase ac/dc (micro)grid interface converter for the medium-voltage high-power applications (through functional average models). In order to conduct performance analysis and obtain reasonable results, some preliminary specifications for design of the power converter have been developed (power rating, switching frequency, LCL filter, control loops, etc.), and several simulation models have been built in MATLAB/Simulink for that purpose. An on-demand active and reactive power delivery, as well as P - f control of the grid, has been explored as functional modes of the 100 MVA grid-interface converter interfacing (ideal) energy storage. It has been shown that if operated as a current source, active and reactive power delivered from the grid-interface converter with the energy storage can be independent and fast. However, the converter's phase-locked loop would cause frequency instability in the case when grid output impedance becomes very high (an islanded mode for instance). It has also been shown that if operated as a voltage source, the grid-interface converter could have significant stabilizing effects on the system dynamics due to the non-delayed power delivery.

Communication and Interface Protocols

The emergence of distributed communication based control schemes and associated infrastructure in power systems emphasizes the need for a realistic power systems simulation tool that allows inclusion of communication components. Communication performance parameters, such as delay and loss in transfer of measurements and commands, affect the result of control and are taken into account while studying a control mechanism over power system dynamics. The method and tools have been developed to allow simulation of communication networks inside off-the-shelf product for power system transient simulation in PSCAD. In particular this research presents the structural designs and interfaces of modules that are needed for implementing an embedded communication network simulator in PSCAD, and provide a brief guide on how power system engineers could use these modules in their designs. This research also provides a foundation for future development of standard power system communication protocols such as DNP-3.

Smart Control Methodology

The objectives of the smart control methodology development were to integrate energy storage devices into the future electric power system via next generation power converters with respect to energy management. The challenges are not only the power limits, but also the energy limits on energy storage devices, all of which have to be taken into account. Two types of power balancing problems in energy management were considered, i.e. the frequency control problem and the economic dispatch problem. More specifically, the aim is to safely and optimally control and schedule conventional generation and energy storage in multiple timescales (i.e. from primary frequency control to economic dispatch) to reduce the frequency deviations and the ramp rates of conventional generators, and in the meantime to minimize total operation costs of providing energy for the system under the uncertainties introduced by variable energy sources such as wind and solar energy. The relevant energy storage applications include primary and secondary frequency control, load shifting, load leveling, transmission deferral, congestion management, integration of renewable generation, and power output smoothing of conventional generation. In addition, the problem of optimal sizing and placement of storage devices is investigated as a complementary research topic to the development of the energy storage enabled smart control methodology. Therefore, this smart control method was organized to include three major technical parts: 1) Real-time frequency control: a novel H_∞ -based approach with a storage enabled frequency differentiated power balancing scheme is proposed and verified; 2) Advanced economic dispatch: a decomposed stochastic model predictive control approach is proposed to optimally dispatch generators and storage devices under uncertainties. The resulting singularity issue is analyzed and solved; and 3) Optimal sizing of storage devices: stochastic optimization is used to quantify the optimal storage capacity. It is found that without congestion, the optimal storage capacity is correlated with the variance in the locational marginal price.

Site Plan Development and Estimated Production Cost Declines

One of the two main objectives of the site plan and costing evaluations was to determine whether the unregulated microgrid at the Philadelphia Navy Yard (PNY) and the Penn State GridSTAR plug-and-play test microgrid would be a suitable venue for the testing and demonstration of future power electronics devices to be developed. Preliminary evaluations show that several avenues of in-line testing for the converter are possible, the simplest being as an interface between the DC output of the energy storage system and the ring bus via a 480-V-to-13.2-kV step-up transformer, which would require modification and up-grades of existing facilities. The second objective was to determine an appropriate method for estimating production-cost declines for advanced power converters as they move from bench scale to commercial/utility scale and eventually to high volume production. It was found that modeling declines in production costs involve challenges related to data availability. While data-driven approaches exist for estimating learning curves or decline curves for energy technologies, scarcity of data in the public domain on power converter or component costs makes such an approach infeasible at present (or at best, highly speculative). Thus, it was determined that methods would need to be established to achieve this objective, with a focus on costs and capabilities of advanced power conversion technologies, which can be used to develop probabilistic projections of uncertain variables.

1. INTRODUCTION AND BACKGROUND

Improving the reliability and stability of T&D of electrical power and the development of the smart grid that includes large scale energy storage will: (i) enable the capacity to more efficiently manage electricity generation through “peak shaving or load shifting;” (ii) enable the integration of large scale renewable energy plants; (iii) and provide more stable and efficient delivery of electrical power. This will result in a more efficient delivery of electrical power, while reducing overall CO₂ emissions — including power generated from fossil fuel assets.

This report summarizes the first phase of NETL-RUA research aimed at providing solutions for an improved electrical grid. This report covers the period of August 2012 through December 2012. The initial phase of the project focused on modeling and simulation to develop validated steady state and dynamic models of system interactions at the converter-grid interface, including consideration of a next generation power converter, which will be established as a scalable bi-directional three-phase AC-DC interface for utility scale high power applications at T&D levels. Initial system applications for this advanced power electronics based converter topology were selected to address T&D grid performance including advanced control methodology development, interface and communications protocols, and integration of various renewable energy resources, energy storage, and evolving load entities, as well as emerging hybrid AC/DC systems.

The research was planned and executed through the NETL-RUA Grid Technologies Collaborative (GTC). A GTC Steering Committee was established with members from all the NETL-RUA Institutions. This ensured leveraging the complementary capabilities of the partner organizations related to power grid technologies could effectively and efficiently be utilized for this research. The GTC Steering Committee has the responsibility for identifying research objectives, planning and completing the research plan. In order to execute this research, a team consisting of 23 faculty members, graduate students and post-doctoral researchers across the NETL-RUA was established. Each NETL-RUA university assumed a defined lead role responsibility in the project, along with strong ties to input and support from the other organizations, while also providing similar input and support to others’ lead scopes. This synergistic approach provided strong team interactions and interdisciplinary collaboration among the NETL-RUA partners.

1.1 ADVANCED ELECTRICITY TRANSMISSION AND DISTRIBUTION NETWORK

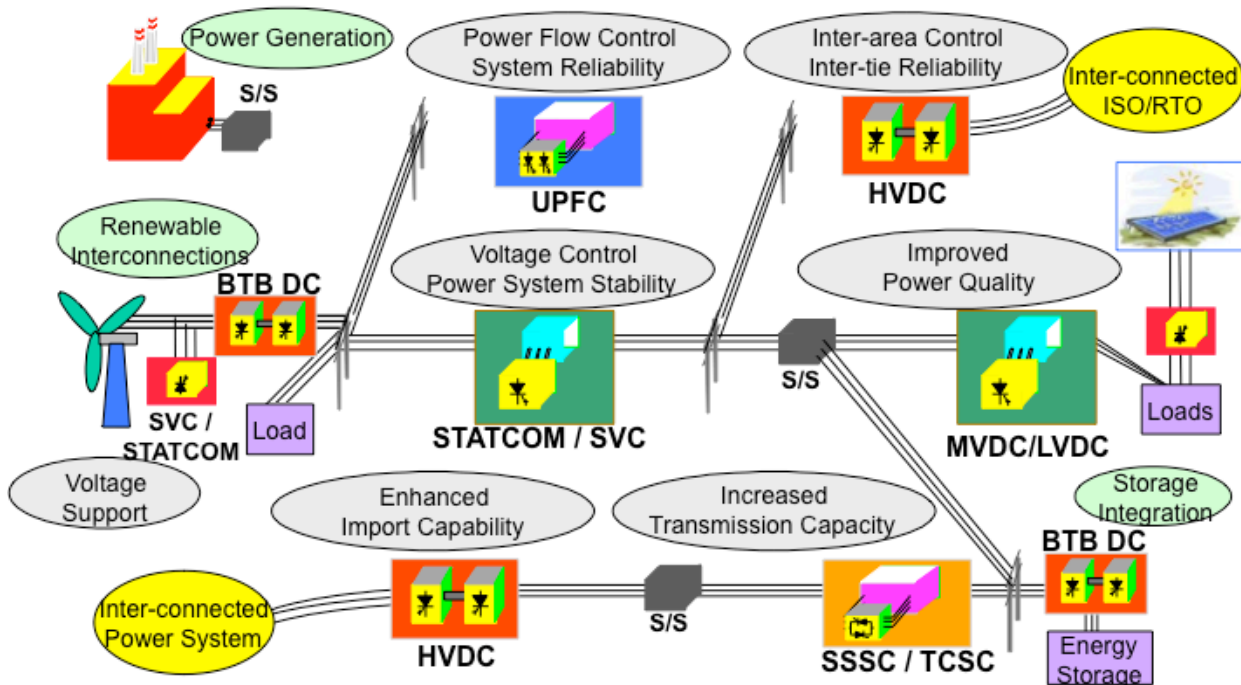
Ultimately, the vision for the grid is the realization of an advanced electricity transmission and distribution network that:

- is efficient, reliable, and resilient to disruptions and other contingency events on the power grid
- integrates clean energy generation resources, energy storage capacity, emerging hybrid AC/DC networks, and alternate operational concepts

- delivers the most suitable forms of electricity in the most economic manner to end-users and enables greater levels of consumer participation

Advanced power electronics technologies are at the core of improved grid performance and enhanced reliability, and include Flexible Alternating Current Transmission Systems (FACTS), High Voltage and Medium Voltage Direct Current Systems (HVDC and MVDC), and hybrid AC/DC systems and topologies. These highly integrated, engineered systems incorporate advanced devices, components and equipment; control architecture, and engineering design to facilitate the optimal delivery of electrical energy from generation resources to end-users, advancing the vision. A depiction of this vision appears in Figure 1, below.

Figure 1: An Advanced Electricity Transmission System Employing Advanced Power Electronics to Improve Performance



Notes: HVDC–High-voltage direct current; SSSC/TCSC–Static synchronous series compensator/thyristor-controlled series compensator; STATCOM/SVC–Static synchronous controller/static reactive power compensator; UPFC–Unified power flow controller; ISO/RTO–Independent system operator/Regional transmission operator.

1.2 APPLICATIONS AND BENEFITS OF ADVANCED GRID-SCALE POWER ELECTRONICS

Improvements to the current electric power grid infrastructure, whose design dates back over a century, have been identified as a key component of a U.S. strategy to improve energy efficiency, grid reliability, and power security. Improving the efficiency and performance of electrical energy transmission, distribution and utilization in the United States may be the largest single opportunity for carbon footprint reduction that currently exists. Considerable efforts are

devoted to developing and deploying technologies for “smart grids” — a collection of technologies and methodologies that enable better point of use control of power usage and improved flexibility of delivery at several levels of grid infrastructure. Surprisingly, less effort to date has been devoted to the design of advanced grid infrastructures — components, systems, and operating approaches — that incorporate the technologies underlying the “smart grid”, address key challenges facing electricity transmission, and help to integrate distributed and renewable power generation and storage systems.

At the core of these systems are advanced power electronics. Grid-scale advanced power electronics refer to devices and systems used to facilitate the delivery of electricity from generators to end users. The electricity transmission system in the United States was designed to be a passive system — delivering electricity from central generating stations to load centers— and still largely is. Control devices are mechanical switches and circuit breakers, which largely are incapable of dynamically controlling power flows through the system. For several decades, advanced power electronics systems have demonstrated their value in the ability to maximize real power flows through the system, support deregulated electricity markets, and provide additional security to the system. These systems are now considered an essential component of any project to expand transmission capacity and support the operations of the existing system: “To achieve both operational reliability and financial profitability, it has become clear that more efficient utilization and control of the *existing* transmission system infrastructure is required.”¹

Below we describe some of the key benefits of advanced power electronics.

1.2.1 Mitigating the Need to Build New Transmission

The amount of electricity that can flow through an alternating current (AC) transmission line depends principally on the thermal capacity of the line.² Because the line has resistance, current flowing through the line generates heat, which requires that thermal capacity limits be placed on the lines. These limits depend on a number of time-varying environmental factors—such as the ambient temperature and the relative humidity — and the time history of loading on the line. When the U.S. transmission system was constructed, load limits were set conservatively, so in practice there is significantly more safe capacity available on lines than is rated. Recent advances in sensors and communication technologies allow real time monitoring of the status of the line.

Increasing the flow of power is more complex than allowing additional loads on the line based on the measurements of sensors. Generators and transmission operators receive payments for deliveries of power that service end-use loads, also referred to as *real power*. But the thermal capacity is related to the *apparent power*, which includes real power and the power that is required to “charge” the system, also known as *reactive power*. The amount of real power that flows through the system depends on the parameters of the transmission system and can be

¹ Paserba, John J. (2004), “How FACTS Controllers Benefit AC Transmission Systems,” in Proceedings of the IEEE Power Engineering Society General Meeting, Denver, CO, June 10.

² Hingorani, Narain G. and Laszlo Gyugyi (2000), *Understanding FACTS: Concepts and Technology of Flexible AC Transmission Systems*, New York, NY: IEEE Press, John Wiley and Sons, Inc.

controlled actively through the application of flexible AC transmission systems (FACTS). In combination with line sensors and appropriate control protocols, FACTS systems increase the amount of power flowing through the transmission system, and also ensure that more of it is real power. When applied as part of a new transmission system, FACTS can reduce system costs by as much as 30 percent.³

That advanced power electronics can increase capacity and mitigate expansions of the transmission system is good news. Acquiring rights-of-way for new transmission lines has become especially challenging and far more controversial than previously.⁴ The Energy Policy Act of 2005 attempted to address this issue by allowing the U.S. Department of Energy (DOE) to designate “National Interest Energy Transmission Corridors” for areas in which electricity transmission systems are overloaded. The DOE designated “national interest” corridors in 2007, but the U.S. Court of Appeals invalidated them. On October 10, 2011, the DOE announced a plan to allow the Federal Energy Regulatory Commission, an organization with a large staff and deep experience in electricity transmission, to designate the corridors on behalf of the DOE. The DOE retracted the plan on October 11, 2011, in part because of the concerns of utilities and states that the corridors would bypass their historic role in power plant siting and transmission planning. Unsurprisingly, the uncertainty surrounding these “national interest” corridors has not resulted in any planning or development activity to relieve transmission constraints throughout the system.⁵

1.2.2 Supporting Liberalized Electricity Markets

In many areas of the United States, the U.S. transmission system delivers electricity today in a fundamentally different way than it did when it was designed. The dispatch of electricity is based on the bids of generators into a power pool, which is managed by an independent system operator (ISO). The ISO is supposed to dispatch power according to the bids of generators into long-term (next day) and near-term (next hour) markets. The ISO must satisfy these bids to the best of its ability within the constraints of the transmission system.

Prior to the arrival of liberalized electricity markets, system operators would control flows of power by turning on and off generating assets as needed. Today, to carry out these duties, system operators must be able to control dynamically the flow of electricity through the system. FACTS systems can control the impedance of the transmission system, giving system operators more control over how electricity flows from generators to users. Moreover, renewable energy generator installations, such as photovoltaic systems, are typically small and increase the number of generator-owners. This will require appropriate commercial contracts and technical requirements for connecting these generators, which the ISO must enforce.

³ Reed, Gregory, John Paserba, and Peter Salavantis (2003), “The FACTS on Resolving Transmission Gridlock,” *IEEE Power and Energy Magazine*, September/October.

⁴ Reed (2003).

⁵ Behr, Peter (2011), “DOE shelves controversial plan to hand off ‘national corridor’ power line role to FERC,” *Energy and Environmental News*, October 12.

High-voltage direct current (HVDC) transmission systems can also play a significant role in flow control. HVDC systems convert power from AC to DC, transmit it as HVDC, and then reconvert it to DC to AC. Flows through HVDC lines can be controlled precisely.⁶

1.2.3 Integrating Renewable Generating Resources⁷

Renewable resources are typically non-dispatchable, meaning that their energy source is inherently variable. Non-dispatchable resources include wind, solar, wave, and tidal power. Fluctuations in the availability of the energy sources can result in variations in the voltage and power that they produce. When turbines are involved in producing the electricity—as is the case with wind, wave, and tidal power—these fluctuations can also result in undesirable changes in operating frequencies as rotational speeds vary. All of these variations have the potential to damage the quality and safety of power being transmitted to end users. The highly intermittent nature of many renewable resources, introduces challenges related to dispatching and integrating them into the transmission system, including:

- *Voltage instability.* To interconnect renewable resources to the grid, the output voltage of the generating utility and the grid operating voltage must be equal at the point of common coupling (PCC). A large difference between the two voltages can lead to instability on the transmission grid. Voltage fluctuations for renewable energy systems can be caused by many factors, including changes in wind speeds, sunlight intensity, or tidal heights.
- *Voltage flicker.* Fluctuations in output voltage can cause an inconvenient and noticeable voltage flicker; this is similar to the flicker seen from older fluorescent lights. In the case of wind power systems, this is most noticeable when wind turbines are switched on and off due to wind changes at the cut-in speed.

Similarly, issues arise when renewable generation sources utilize rotating machines for electrical generation:

- Reactive power consumption: Induction generators, especially wind turbine generators, require substantial amounts of reactive power to operate. This power is pulled from the grid, and can cause depressed voltages and voltage stability problems. In addition, this issue may conflict with the low voltage ride-through requirement for wind turbines, which states that a generator must be connected during grid faults and disturbances, and supply the grid with reactive power at low voltage.
- Voltage regulation: For wind turbines, reactive power consumption increases in proportion to wind speed. This can result in an unacceptable low voltage level at the receiving end. Due to changes in the load, renewable power systems need to adjust the consumption and supply of reactive power, to maintain a constant receiving-end voltage. This allows utilities to maintain power quality and interconnection standards for renewable integration.

⁶ Wang, Shu, Jinxiang Zhu, Lan Trinh, and Jiuping Pan (2008), “Economic Assessment of HVDC Project in Deregulated Energy Markets,” Proceedings of the DRPT 2008, Nanjing, China, April 6-9.

⁷ Reed, Gregory F., Brandon M. Grainger, Hussain Bassi, Emmanuel Taylor, Zhi-Hong Mao, Alex K. Jones (2010), “Analysis of High Capacity Power Electronic Technologies for Integration of Green Energy Management,” Panel Session on FACTS Applications to Improve Power System Dynamic Performance, IEEE Power and Energy Society Transmission and Distribution Conference and Exposition, New Orleans, LA, April.

- **Voltage sag:** When the turbines start up, the machines act as large motors, operating in motoring mode until reaching grid voltage and synchronizing with the grid, and then changing to the generating mode of operation. During the motoring mode, a large reactive current (i.e. inrush current) resulting from the difference in the voltage between two systems, flows from the grid to the machines. This current can be two to three times the machine rated current, and can cause voltage sags in the area around the turbines. Eventually, the voltage difference and inrush current tapers to zero after the two systems are synchronized.
- **Turbine tripping:** A transmission system fault may result in the loss of a power line. As a result, control systems on the wind turbines can cause them to disconnect from the grid—“trip”—to protect the machinery. The sudden loss in generation can be the start of a major cascading outage event. This problem has a direct impact on system stability.
- **Subsynchronous resonance:** The shafts of wind turbines bend and flex, vibrating as a torsional spring. Sometimes this flexing occurs as a frequency below that of the power system to which the wind turbines are connected. Moreover, the flexing can be amplified by series capacitors, which are installed to cancel the line inductive reactance, but also reduce the damping that would decrease the vibration. Subsynchronous resonance is especially problematic where renewable generation requires long distance transmission to the point of system interconnection.

As renewable generation resources reach higher levels of system penetration, these challenges will become more acute, requiring improvements and expansions to the transmission system. The key to integrating green and renewable resources requires appropriate grid planning supported by detailed simulation tools. Operators of the equipment also require new methods and tools for detecting and responding to these problems. These tools include accurate forecasting of resource availability and intelligent decision-making of renewable energy dispatch for both operation and investment. For example, wind farm electricity production, at times, may need to be reduced for system security reasons. Variable generation influences system operation scheduling on all time frames and will necessitate investigation into new scheduling techniques such as stochastic unit commitment.

Power electronics technology is an efficient, powerful, and a reliable solution to these issues and challenges. FACTS systems can be used to correct voltage and frequency deviations and supply reactive power when it is needed. They can also be used to provide additional system damping, resolving issues of subsynchronous resonance. Finally, HVDC systems are required to integrate distant offshore wind installations. While the technical systems and solutions exist, systematic and robust integration of these systems still does not occur. As penetration levels increase advanced power electronics will be an essential component of the solution.

1.2.4 Increasing Power System Stability, Security, and Reliability

To properly support economic activity the electricity generating, transmission, and distribution system must deliver high quality electricity—electricity that conforms tightly to voltage and frequency specifications—that is also highly reliable. However, a system operating near its capacity limits and supporting an increased number of smaller and unpredictable generating sources would seem to run counter this need.

Security issues, which are an extension to power system dynamic performance, exist at both the transmission and distribution levels. With regards to the transmission level, renewable energy generators must:

- Ride-through disturbances in the power system to avoid contributing to cascading outages
- Reduce output to avoid overloaded or insecure power system operation
- Contribute to voltage and frequency control and help stabilize system operation following a disturbance

If transmission expansion and upgrade needs are not addressed, steady-state stability limits can be reached. Specifically, as the power flows to or from the grid, it must be kept below the maximum allowed power value, referred to as the steady-state stability limit. Otherwise, the line will lose its ability to transfer power and can become unstable while transients emanate through the system. Therefore, a new maximum power level below the steady-state stability value, the dynamic stability limit, must be established to avoid line instability.

1.2.5 How Industry and Consumers Realize the Benefits of Advanced Power Electronics

The preceding discussion illustrates that grid-scale power electronics systems are essential for continued operation of the existing transmission network and distribution systems, and also are a critical component of the future grid. The benefits afforded by these systems benefit directly power producers, transmission system operations, distribution companies, and customers.

- From the perspective of renewable electricity generators, advanced power electronics systems facilitate their integration into the transmission grid, protect systems from damage, and improve the availability of these resources (especially when combined with grid-scale storage). As a result, renewable energy producers can more confidently bid into higher-value electricity markets, increasing their revenues.
- From the perspective of the transmission system owner, systems are able to operate closer to their thermal capacity limits while also delivering more real power to customers. Thus current systems are better utilized, forestalling investments in new capacity. And new capacity, when it is constructed, operates more effectively than it had in the past. Moreover, the reduced losses of the transmission system have an aggregate benefit for all generators.
- HVDC transmission systems can carry 2 to 5 times more power over the same physical right-of-way corridor than do AC systems of equivalent voltage and are capable of controlling the power flow flowing through the line. This minimizes the footprint of transmission expansions, reducing environmental impacts.
- The system operator is able to control flows through the transmission grid more effectively, minimizing the amount of out-of-merit generation that is dispatched. Moreover, control systems are able to control actively these flows, enabling quick responses to disturbances and avoiding dips in power quality and system wide failures.
- Citizens and customers benefit from increased reliability and quality of electricity and reduced requirements for additional transmission capacity.
- The recent merchant transmission provider activity in large scale HVDC and FACTS installations is driving an era of unprecedented investment in the transmission and distribution sector, from both the private and the public sectors.

1.2.6 The Market for Grid-scale Power Electronics

The benefits and advantages of grid-scale advanced power electronics are established and are proven by the existing and growing applications of the technology. FACTS are a de facto component of new transmission installations, where they help to ensure that lines are fully utilized. HVDC interconnections and transmission lines provide essential services and are becoming more cost competitive as compared to traditional high-voltage AC transmission. Given the range of growing challenges that advanced power electronics address, the market for these systems is growing too.

Despite the economic downturn, investments in transmission infrastructure continue to grow. Compiling information from its members, the Edison Electric Institute estimates that \$55.3 billion was invested in transmission infrastructure improvements from 2001 through 2009.⁸ As described above, many of these improvements include the installation of advanced power electronics to maximize system performance.

The annual value of global FACTS installations is expected to grow from \$330 million in 2010 to \$780 million in 2017.⁹ This represents up to 16 GVAR of reactive power compensation installed per year with the potential to offset up to 800 MW of real power generation and new transmission requirements. The reason for such a significant increase in FACTS installation is twofold: FACTS are needed to bolster existing transmission systems, and because they help to maximize real power flows, they are a critical component of new transmission installations. For example, Southern California Edison plans to invest over \$17 billion in transmission systems during this decade. All of those investments will include FACTS devices to maximize the return on investment for the utility. Also, the Electricity Reliability Council of Texas (ERCOT) is in the process of installing over 6 GW of reactive power compensation in the form of FACTS compensators for the Competitive Renewable Energy Zone project. These devices will facilitate the integration of 10 GW of new wind generation capacity into the ERCOT grid by means of over 2,300 miles of new 345 kV transmission lines.

For HVDC, Pike Research estimates growth in annual HVDC installations from \$8.4 billion in 2010 to \$12 billion in 2015.¹⁰ This estimate for the size of the HVDC market includes the complete costs of such a project, including: the enabling power electronics and transmission lines; procuring rights-of-way; engineering; and construction. In a typical HVDC project approximately 25 percent of the cost is for the key HVDC valves.¹¹ Therefore a more comparable estimate of the market for HVDC equipment is \$2.1 billion in 2010 to \$3 billion in 2015. There are currently 38 HVDC systems in operation today in North America dating back to early 1970's, including links between the U.S. and Mexico, and long distance transmission between the U.S. and Canada – this represents about one major HVDC project per year historically. But, there are currently 27 newly planned HVDC projects between now and 2020,

⁸ Edison Electric Institute (2011) "Transmission Projects: At a Glance," Washington, DC, March.

⁹ Fairley, Peter (2011) "Flexible AC Transmission: The FACTS Machine," *IEEE Spectrum*, January.

¹⁰ Pike Research (2010), "High Voltage DC Transmission Market to Grow 44% by 2015," Press release, Boulder, CO, November 15.

¹¹ Rudervall, Roberto, Charpentier, J.P., and Raghuvver Sharma (2000), "High Voltage Direct Current (HVDC) Transmission Systems Technology Review Paper," in *Energy Week*, Washington, DC, March.

representing nearly a doubling of total project installations in the coming decade, and a tripling the number of projects per year. This also provides major infrastructure expansion and investment for the U.S. transmission sector.

The relative size of the HVDC market as compared to the FACTS market is a result of the characteristics of the devices: HVDC systems must handle the full load of the transmission line and are installed at both ends of the line, whereas the capacity of FACTS solutions can be a fraction of the line's load. Also, HVDC system costs include the DC transmission line itself, while FACTS installations typically are implemented at existing substations without major infrastructure changes. Reducing these power electronics costs would have the benefit of making HVDC a viable alternative to AC transmission at shorter distances. Major equipment manufacturers are also expecting large-scale growth in the market.

Beyond the United States, developing countries are rapidly expanding their electricity transmission and distribution systems, making investments in infrastructure that is to provide essential services for many decades. For example, in India, between 2007 and 2012 the national power transmission utility will add 25,000 miles of transmission lines throughout the country, representing a 40 percent increase in existing transmission lines.¹² The rate of China's growth in transmission, including large-scale HVDC systems, is unprecedented with new facilities to support load growth and new generation developing at a rapid pace. China's current plans involve 5 GW of newly installed HVDC capacity per year for at least the next decade, totaling 50 GW or more in China alone by 2020. India plans on five new HVDC systems of 6 GW each, totaling at least 30 GW of newly installed capacity, also by 2020. Brazil, northern Africa, and other developing parts of the world are all planning new power transmission systems with HVDC as a core technology solution.

¹² International Bank for Reconstruction and Development, the World Bank Group (2010), "Meeting India's Demand for Electricity."

2. R&D PROGRAM OVERVIEW

The Next Generation Power Converter will serve as a key interface to power grid modernization and advancement, providing an efficient, bidirectional connection and control point. Initial application of the converter will be at the utility-scale distribution level, with extension of control concepts and interfaces to the transmission system. The 2012 modeling efforts focused on establishing base cases developed by utilizing standard IEEE test bus scenarios, that were used to incorporate the advanced converter model and to eventually analyze various interactions of renewable energy integration, energy storage interconnection, and integration of traditional and emerging AC and DC loads.

The initial test cases were based on single line diagrams of the WECC 9-bus transmission test case and the IEEE 13-bus distribution feeder test case. The transmission and distribution systems were modeled and used for the project development applications. These models were developed in PSCAD/EMTDC. Applications for control method development and other aspects that will build upon the base models of the project will be done in both PSCAD/EMTDC and in MATLAB/Simulink.

The five GTC research universities collaborated on the modeling and simulation phase of the converter's development, with additional support from NETL and UEP.

Each participating institution assumed a lead role in a particular area, with support roles tied to multiple areas of the research. The lead roles are as follows:

University of Pittsburgh

- Development of the transmission and distribution power system network topology base case models in the PSCAD/EMTDC program environment.
- Employment of standard PSCAD models for all selected equipment and network facilities, including generation sources, power electronics converters, feeders, and loads.

Virginia Polytechnic Institute and State University

- Exploration of functionality and performance of the grid-interface power electronics converter for medium-voltage high-power applications, through functional average models.

West Virginia University

- Development of communication protocols and interface models for selected equipment and network facilities, including generation sources, and power electronics converters at connection points.

Carnegie Mellon University

- Development of smart control methodology, focusing on system level aspects and the integration of storage devices via the next generation power electronics converter.

The Pennsylvania State University

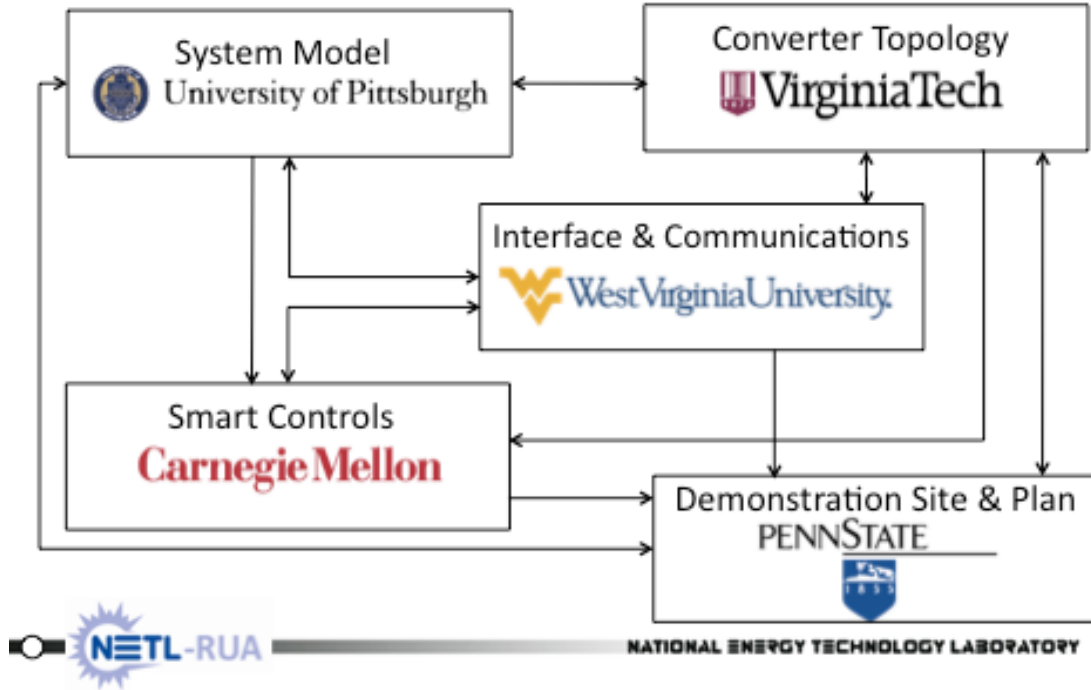
- Analysis of converter specifications as developed by the GTC team with respect to microgrid test facilities at the Philadelphia Navy Yard (PNY) to determine how the device should be tested in its various stages of development, and the appropriateness of the PNY for such testing at various voltage levels. This will require modeling of the relevant part of the PNY test loop.
- Investigation of exporting developed models MATLAB/Simulink, using a new export function that is in beta test.

The National Energy Technology Laboratory

The NETL Advanced Virtual Energy Simulation Training And Research (AVESTAR™) Center will integrate high-fidelity, real-time dynamic power plant simulators with base case models of the transmission and distribution power network. In the modern grid era, multiple power generation facilities and multiple consumer networks will be optimally integrated to maximize throughput of the system while reducing energy consumption. Smart power plants will consist of conventional fossil energy systems (e.g., natural gas, coal) integrated with variable renewable power generators (e.g., wind, solar) and fast-ramping energy storage (e.g., batteries) to supply a stable source of power to active consumers who can vary their consumption based on the real-time electricity price or can sell back surplus power to their utilities. Conceptually, such an integrated system can improve the profitability, efficiency, and reliability of grid operations while still delivering a significant and environmentally meaningful fraction of that power from renewable sources. Using the AVESTAR™ infrastructure for integration would enable NETL to evaluate the effectiveness of different control strategies when coupling generation assets with a smart transmission and distribution system. The AVESTAR™ simulators can be used to study the dynamic response of modern power systems to changes in generation and load; to power disturbances including outages; and to the interactions between the power and communication networks. Although a modern power system has many benefits, there are many challenges to its operation and control. These challenges include moving to an electric power trading market with dynamic real-time pricing; controlling an increased number of generation and energy storage assets including variable renewables; and availability of large amounts of real-time data. The AVESTAR™ simulators can be used to create various designs of a modern power system and evaluate the effectiveness of different control schemes under normal and edge conditions. In the future, the AVESTAR™ simulators could be also be used for training operators of a modern power system.

Every project deliverable is a collaborative effort between the following universities as portrayed in Figure 2 below.

Figure 2: Collaborations between Universities in the NETL-RUA



3. TEST SYSTEMS AND SIMULATION TOOLS

In this section, an overview is provided of the test systems and their simulations in PSCAD.

3.1 SYSTEM MODELING OF TEST FEEDERS

Simulation models have been developed and analyzed for this work under different conditions in PSCAD and have been made available to all the team members for further evaluation and research. The following paragraphs list and briefly explain developed models of the system components. Models have been created for two different benchmark platforms for this research work: namely the WECC 9-bus system and the IEEE 13 node test feeder system.

The purpose of the system modeling portion of this report is to validate and give an explanation of a PSCAD model created to simulate the results obtained in the IEEE 13 Node Test Feeder report¹³. This model was validated through examination and the collection of the power flow results. The PSCAD model of the 13 bus system was originally created by the University of Pittsburgh and refined with the aid of West Virginia University using the basis of the IEEE 13 Node Test Feeder report created by the Power and Energy Society (PES) Distribution System Analysis Subcommittee.

Figure 3 provides the first set of validation power flow results with a comparison between the original IEEE Node Test Feeder report and the 13 node test feeder model created in PSCAD.

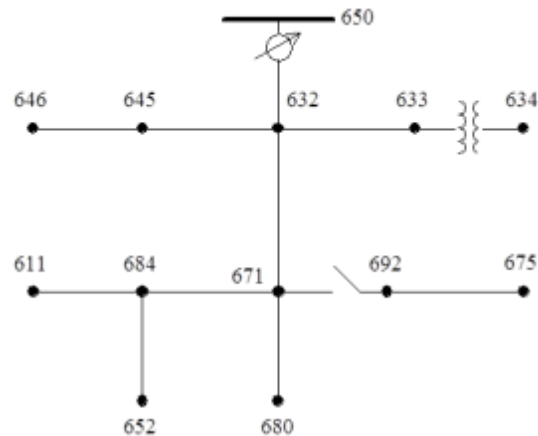
¹³ Distribution Test Feeders. *IEEE PES Distribution System Analysis Subcommittee's Distribution Test Feeder Working Group.*

Figure 3: IEEE 13 Node Test Feeder Expected and Simulated Results (Original Model)

BUS	Real Power (p=MW) and Reactive Power (q=Mvar)								
	Phase A (MW)			Phase B (MW)			Phase C (MW)		
	IEEE	PSCAD	% Diff	IEEE	PSCAD	% Diff	IEEE	PSCAD	% Diff
634_p	0.16	0.1579	1.312	0.12	0.1205	0.417	0.12	0.1229	2.417
634_q	0.11	0.1077	2.091	0.09	0.08929	0.789	0.09	0.09115	1.278
645_p	-	-	-	0.17	0.18	5.882	-	-	-
645_q	-	-	-	0.125	0.132	5.600	-	-	-
646_p	-	-	-	0.2466	0.2412	2.190	-	-	-
646_q	-	-	-	0.13812	0.13796	0.116	-	-	-
671_p	0.385	0.3847	0.078	0.385	0.396	2.857	0.385	0.3755	2.468
671_q	0.22	0.2026	7.909	0.22	0.2485	12.955	0.22	0.2095	4.773
611_p	-	-	-	-	-	-	0.16554	0.1563	5.582
611_q	-	-	-	-	-	-	0.0779	0.07299	6.303
652_p	0.12356	0.1181	4.419	-	-	-	-	-	-
652_q	0.08302	0.07877	5.119	-	-	-	-	-	-
692_p	-	-	-	-	-	-	0.16837	0.16845	0.048
692_q	-	-	-	-	-	-	0.14955	0.15935	6.553
675_p	0.485	0.46425	4.278	0.068	0.0754	10.882	0.29	0.2764	4.690
675_q	0.19	0.1809	4.789	0.06	0.06598	9.967	0.212	0.2	5.660

Note: No load is directly related to the following busses: 650, 632, 633, 680, 684

These PSCAD results were obtained using the 13 bus network model by plotting each power flow with respect to time and then measuring the steady-state RMS value. As needed, there were edits made to the model created by WVU in order to obtain better results. These modifications are also recorded within this report. In order to demonstrate the system on a high level, the IEEE 13 Node Test Feeder is depicted in Figure 4 shown below.

Figure 4: IEEE 13 Node Test Feeder Schematic

The ultimate result desired is a 3 node IEEE 13 node test feeder system where three of the systems specified in Figure 4 will be connected in parallel.

A simulation schematic of the 13 node test feeder system created in PSCAD is shown in Figure 5 on the following page.

Deliverables:

IEEE_13_Pitt_Rev0_110112.psc

- Basis of the written documentation found in this report and from which the results displayed had been obtained. This is the IEEE 13 Bus model.

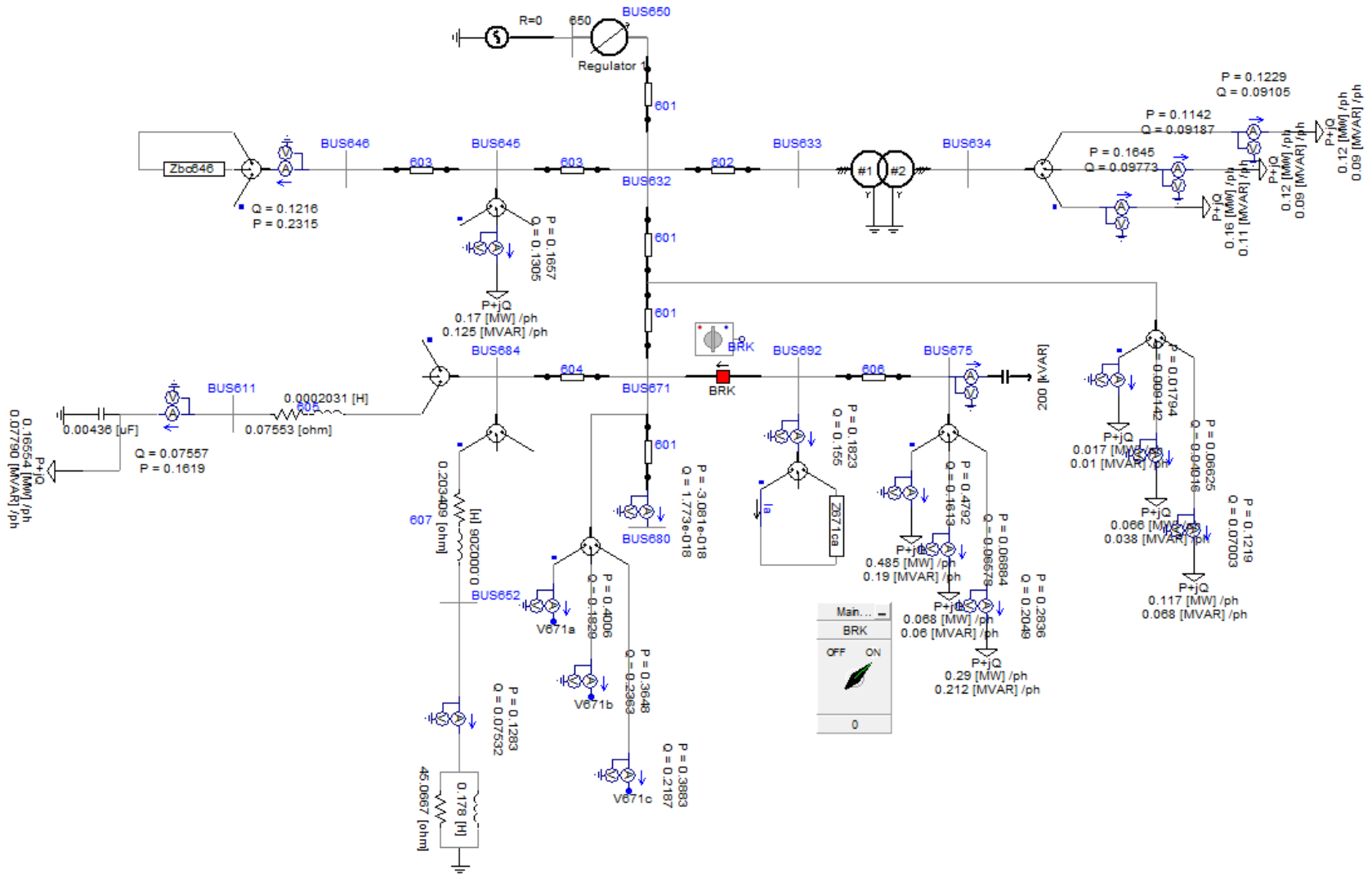
IEEE_13x3_Pitt_Rev0_110112.psc

- This model is simply the IEEE 13 bus model (IEEE_13_Pitt_Rev0_110112) connected in parallel three times (see EX-2).

IEEE_nodeWVU_Model_Roopa.psc

- This is the refined model of the IEEE 13 bus model provided by West Virginia University. This file might not be accessible by all university parties because of the PSCAD version used to create the model. This file was created in PSCAD X4, which Pitt has not upgraded too due to other ongoing research activities in an older version of PSCAD. If a university has PSCAD X4, they should consult this file because stronger agreement with published IEEE 13 bus test reports would be found.

Figure 5: IEEE 13 Node Test Feeder PSCAD Simulation Schematic



3.2 MODEL OF THE SYNCHRONOUS GENERATOR

Two different models of the synchronous generator have been developed for the purpose of system dynamics analysis.

3.2.1 Generator Model A

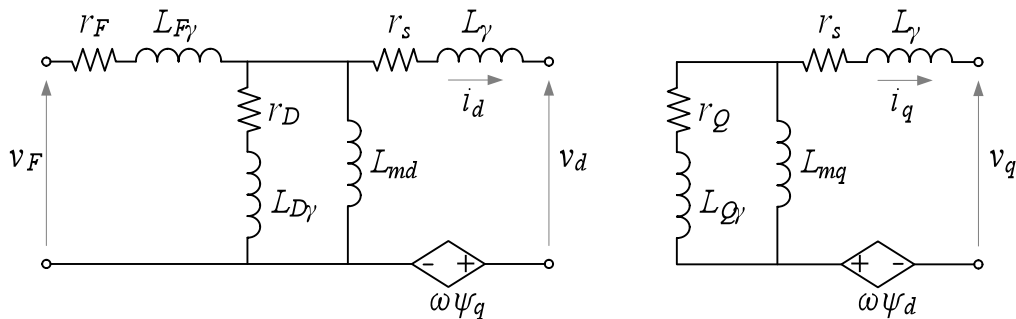
The WECC 9-bus model¹⁴ gives the common generator parameters: standard synchronous and transient reactances (in p.u. on a 100 MVA base), and characteristic time constants as shown in the Figure 6.

Figure 6: WECC 9-bus system generator parameters

Generator	1	2	3	Generator	1	2	3
Rated MVA	247.5	192	128	x'_q	0.0969	0.1969	0.25
kV	16.5	18	13.8	x'_d	0.0336	0.0521	0.0742
x_d	0.146	0.8958	1.3125	τ'_{d0}	8.96	6	5.89
x'_d	0.0608	0.1198	0.1813	τ'_{q0}	0	0.535	0.6
x'_q	0.0969	0.8645	1.2578	H	23.64	6.4	3.01

The d - q model of the generator is shown in the Figure 7.

Figure 7: d - q model of the synchronous generator



This model is built according to the following set of equations:

¹⁴ P. W. Sauer and M. A. Pai. *Power System Dynamics and Stability*. Prentice-Hall, Upper Saddle River, NJ, 1998.

$$\begin{aligned}
 v_d &= -r_s i_d - \frac{d\psi_d}{dt} - \omega\psi_q & 0 &= r_D i_D + \frac{d\psi_D}{dt} \\
 v_q &= -r_s i_q - \frac{d\psi_q}{dt} + \omega\psi_d & 0 &= r_D i_D + \frac{d\psi_D}{dt} \\
 v_F &= R_F i_F + \frac{d\psi_F}{dt} & J \frac{d\omega}{dt} &= T_m - T_e; \quad \omega = \frac{d\theta}{dt}
 \end{aligned}$$

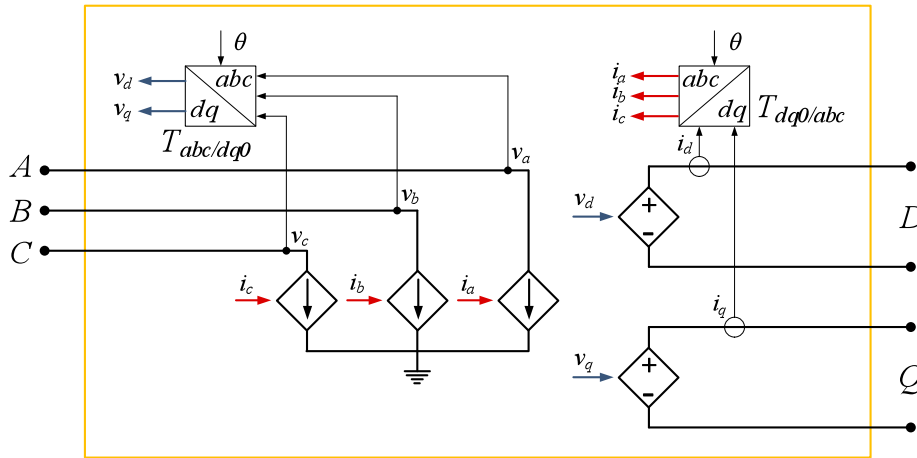
$$\begin{bmatrix} \psi_d \\ \psi_F \\ \psi_D \end{bmatrix} = \begin{bmatrix} L_d & L_{md} & L_{md} \\ L_{md} & L_F & L_{md} \\ L_{md} & L_{md} & L_D \end{bmatrix} \cdot \begin{bmatrix} i_d \\ i_F \\ i_D \end{bmatrix}$$

$$\begin{bmatrix} \psi_q \\ \psi_Q \end{bmatrix} = \begin{bmatrix} L_q & L_{mq} \\ L_{mq} & L_Q \end{bmatrix} \cdot \begin{bmatrix} i_q \\ i_Q \end{bmatrix}$$

(1)

In order to connect this model to the WECC system, one would need to put *abc/dq* transformation block between the generators and proper buses due to the fact that the WECC system model is modeled in *abc* frame, while the generator is in *d-q*. The following *abc/dq* transformation block has been modeled for that purpose:

Figure 8: *abc/dq* transformation block



where:

$$\mathbf{T}_{dq0/abc} = \sqrt{\frac{2}{3}} \begin{bmatrix} \cos(\omega t) & \cos(\omega t - 2\pi/3) & \cos(\omega t + 2\pi/3) \\ -\sin(\omega t) & -\sin(\omega t - 2\pi/3) & -\sin(\omega t + 2\pi/3) \\ 1/\sqrt{2} & 1/\sqrt{2} & 1/\sqrt{2} \end{bmatrix}, \quad \mathbf{T}_{abc/dq0} = \mathbf{T}_{dq0/abc}^{-1} \quad (2)$$

Deliverables:

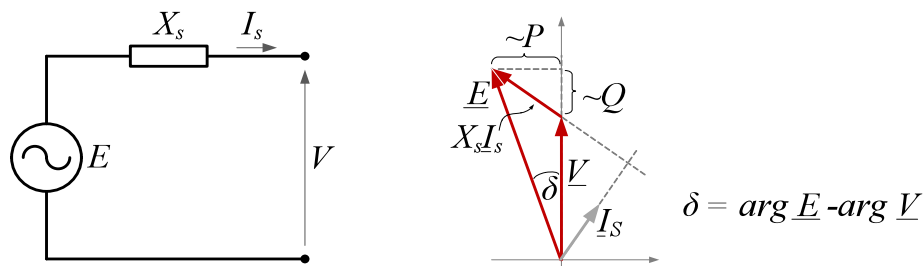
MATLAB (Simulink/SimPowerSystems) $d-q$ model of the synchronous generator. The model called “**gen_d_q.mdl**” has been uploaded to the NETL members SharePoint website. When using with the WECC 9-bus system for the system-level simulation, our recommendation is to use Model B instead (significantly reduces the simulation time). Please note that the model initialization m -file “**init_file.m**” has to be run before starting the model.

3.2.2 Generator Model B

Although more detailed and accurate, the Model A above is computationally very demanding (slow) when run together with the WECC 9-bus system mainly due to the algebraic loops for the dq/abc transformation in SimPowerSystems. In order to provide faster simulation platform, simplified generator model explained in this section was used.

Figure 9 shows the simplified model of the generator used for the further system-level study in this work.

Figure 9: Simplified synchronous generator model



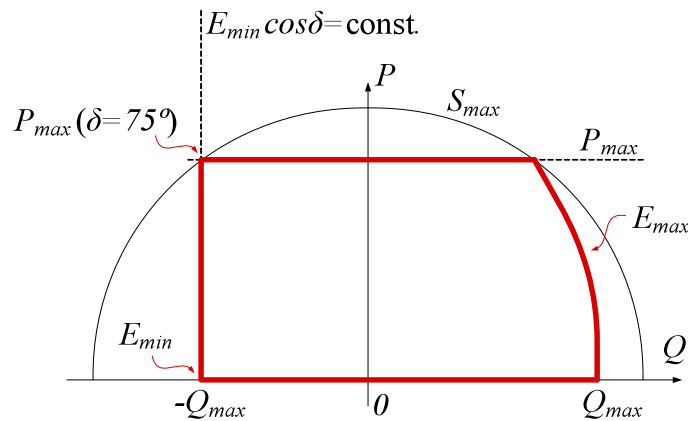
As it can be seen, the simplified model comprises voltage source E (electromotive force (EMF)) in series with the synchronous reactance X_s that is not given by the model (Figure 6) due to the fact that those generators are anisotropic (salient pole) machines, while parameter X_s characterizes the isotropic machines. For the purpose of the low-frequency dynamic analysis (performed under this work), the “equivalent or virtual” synchronous reactance X_s can be calculated out from the existing machine parameters with no loss of generality.

According to the phasor diagram of the isotropic machine above, it can be written for active, reactive and apparent power:

$$\begin{aligned}
 P &= 3 \frac{EV}{X_s} \sin \delta \\
 Q &= 3 \frac{(EV \cos \delta - V^2)}{X_s} \\
 S &= \sqrt{P^2 + Q^2}
 \end{aligned} \tag{3}$$

Since the apparent power has been given for all three WECC generators (Figure 6), a few assumptions on the operating regions of those generators will be made and are shown below on the synchronous generator operating region map.

Figure 10: Synchronous generator (assumed) operating region map



Assumptions: The maximum apparent power does not exceed the value given in the Figure 6; the maximal power angle (δ) allowed in any mode of operation is 75° ; maximal active power for the negative Q (capacitive) happens for this angle (75°);

According to the assumptions above, Figure 10 and power ratings from Figure 6, the system of equations (3) can be solved giving the following parameters:

Figure 11: WECC 9-bus system re-calculated generator parameters

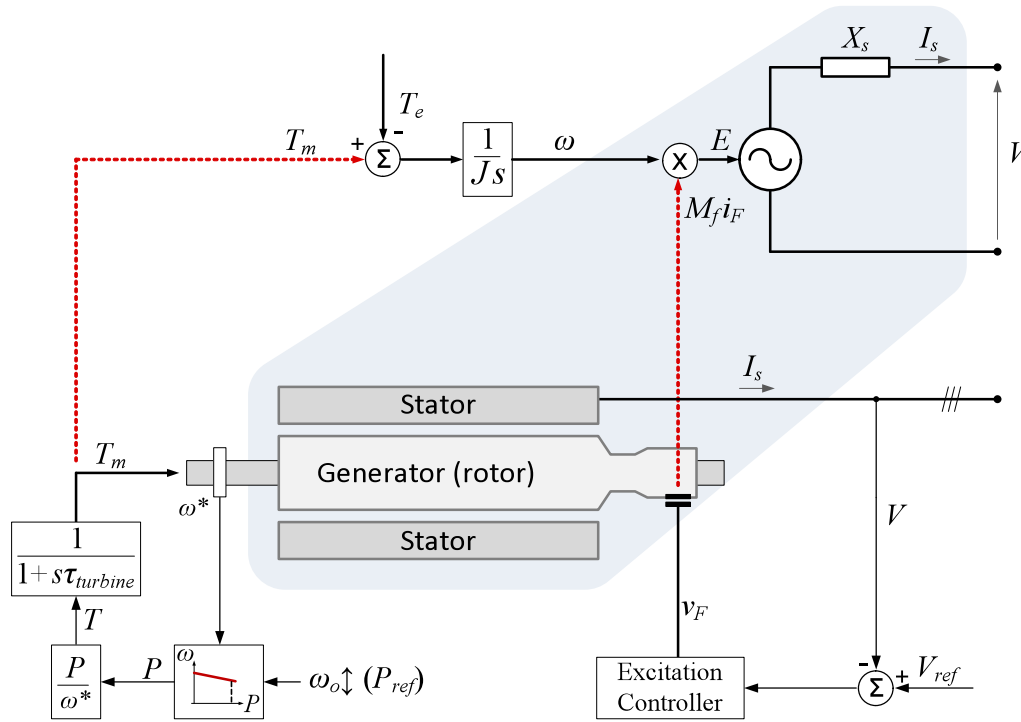
Generator	1	2	3
S_{max} [MVA]	247.5	192	128
P_{max} [MW]	220	165	100
Q_{max} [Mvar]	120	95	80
Q_{min} [Mvar]	-120	-95	-80

Generator	1	2	3
E_{max} [V]	15446	15510	15960
E_{min} [V]	6806	6678	5862
X_s [Ω]	0.93	1.22	1.77
L_s [mH] for ω_n	2.4	3.2	4.7

A small winding resistance of $1\text{m}\Omega$ has been added to all three generators (per phase - in addition to L_s) to provide damping and improve model's numerical convergence.

Figure 12 shows the voltage control and the frequency droop added to the simplified generator models in order to describe the WECC system with the more realistic representation. An explanation about parameters shown in this figure is given below.

Figure 12: Simplified synchronous generator model with voltage control and frequency droop implementation



The flux linkages of the synchronous machine stator windings can be written as:

(4)

i_a, i_b, i_c are stator phase currents, i_f is an excitation current, and M_f is amplitude of the mutual inductance of rotor and stator windings.¹⁵ The phase terminal voltages are then:

¹⁵ Z. Qing-Chang and G. Weiss, "Synchronverters: Inverters That Mimic Synchronous Generators," *Industrial Electronics, IEEE Transactions on*, vol. 58, pp. 1259-1267, 2011.

(5)

where the machine's EMF can be represented as

(6)

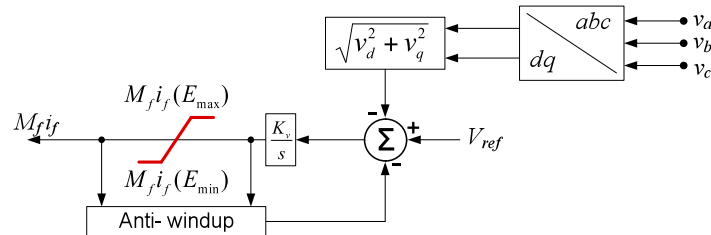
The second part of (6) can be neglected due to the fact that the main focus of the work will be frequency, not voltage stability, thus the EMF vector of the WECC generators becomes:

(7)

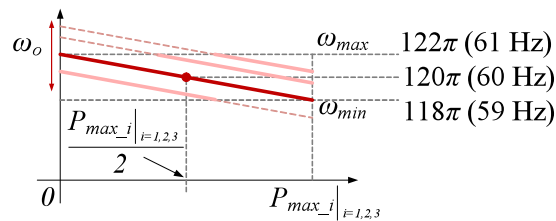
Now looking at Figure 12, it can be noticed that EMF regulation comprises two loops, voltage control loop provides the product $M_f i_f$, while torque control gives ω and, consequently (after the integrator), θ .

Voltage loop features the simple integrator as shown in Figure 13 and is the same for all WECC generators (the $M_f i_f$ limits are different according to Figure 11 and (7)).

Figure 13: Voltage control (simplified excitation control)



For all the WECC generators, “default” frequency droop has been designed in such a way to feature the nominal speed (60 Hz) when the delivered active power of a particular generator is exactly half of the maximal value shown in the Figure 11. Maximal frequency of 61 Hz happens for 0 MW active power delivery, while the minimal frequency of 59 Hz occurs for P_{max} of the specific generator. By changing ω_o from Figure 14, different amounts of active power can be achieved. All these assumptions correspond to the 3.33% speed droop algorithm often seen in practice.

Figure 14: Frequency droop for all the WECC generators

Thus, it can be written for the droop law:

(8)

As shown in Figure 12, the angular frequency ω is measured, fed back to the droop (Figure 13), and the demanded active power is obtained as an output. This output is then divided by the same measured speed to get the demanded torque which is then brought to the machine model through the low pass filter as shown in Figure 12. The low pass filter is used to model the reaction of the steam turbine in a simplified way using only single time constant τ_{turbine} .

Deliverables:

MATLAB (Simulink/SimPowerSystems) models of the WECC synchronous generators. The model called “wecc_gens.mdl” has been uploaded to the NETL members SharePoint website. Please note that the model initialization *m*-file “init_file.m” has to be run before starting the model.

3.3 MODEL OF THE THREE-PHASE GRID-INTERFACE POWER CONVERTER

The grid-interface converter considered for analysis under this work is a bidirectional three-phase ac/dc power electronics converter for the medium-voltage high-power applications. The main goal has been exploring functionality and performance together with some preliminary specification and design requirements that allow: a bi-directional interface between two grids (*dc*- and *ac*-microgrid) and/or interface to different types of *dc* energy storage systems (batteries, fuel cells). If two such converters were used in the back-to-back configuration, the application can be easily extended to interfacing two *ac*-microgrids (grids), wind turbines, or variety of *ac* energy storage systems (flywheels, compressed air).

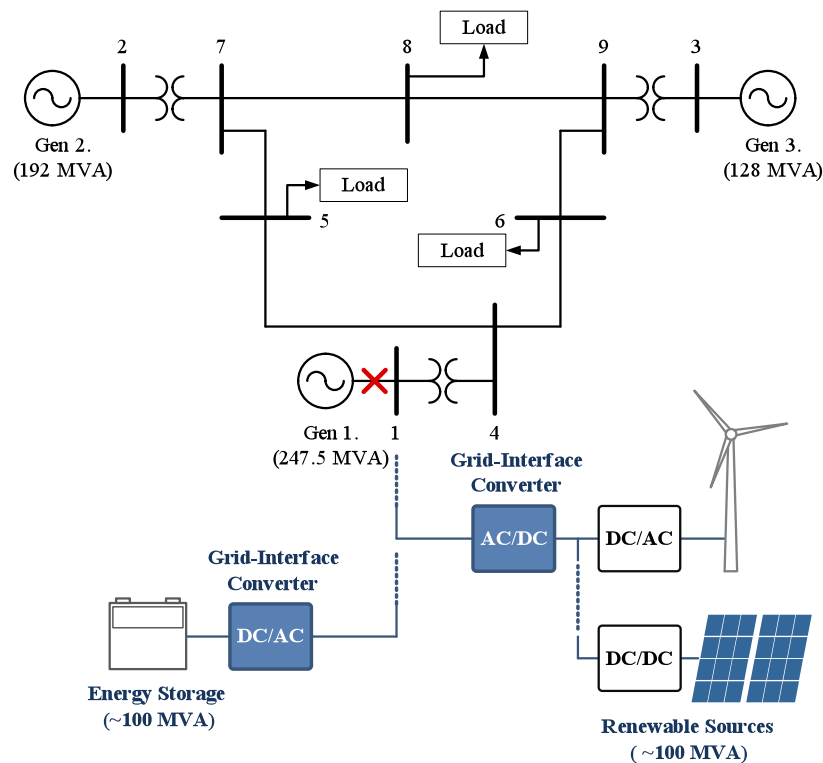
This converter’s behavior and performance has been explored through simulations with the WECC 9-bus system by connecting it to the WECC bus No.1 (arbitrary chosen point) as depicted in the Figure 16.

To develop some basic specifications that will be used later for the filter and control design, it has been planned to consider the grid-interface converter rated about 30% of the nominal WECC system power level. Assuming that connection is made at the bus No.1, losing Generator 1, the converters nominal power is then accordingly assumed to be 100 MVA. The other specification parameters shown in the table Figure 15 have been chosen to correspond to some practical, grid-related power converter applications (HVDC, STATCOM, etc...).

Figure 15: Grid-interface converter specifications

Voltage rating (V_n):	18 kV
Power rating ($S_n (P_n, Q_n)$):	100 MVA (80 MW, 60 Mvar)
Current rating (I_n):	3.2 kA
Switching frequency (f_{sw}):	2000 Hz
DC side voltage (V_{dc}):	36 kV
Topology:	Two-level

Figure 16: WECC 9-bus system with illustrated connection of the grid-interface converters at the bus. No1



The two-level topology has been chosen due to the fact that this decision has pretty insignificant impact on the system dynamics that has been researched in this work, but offers reduced complexity of the models, control loop, filter design, etc., putting the main focus of the research to the low-frequency dynamic behavior rather than the electromagnetic interference (EMI), switching and conduction losses, modulation techniques, etc. Additional research effort needs to be put on the suitable topology selection of the grid-interface converter in this and similar application, thus has not been performed in this particular work.

There are three models of the grid-interface converter developed for the purpose of analysis under this work. All three of them will be briefly explained in this report as they feature quite different usability levels.

3.3.1 Power Converter Model A – switching model

The first model of the power converter developed was the switching model used only for the purpose of designing (and inspection) of the suitable LCL filter for the grid-interface converter. IEEE standards^{16,17} strictly suggest the amount of allowed harmonic content into the current injected into the grid from the power generating device, and grid-interface converter that is an objective of this work belongs to this category, hence must comply with those standards.

Figure 17: The snapshot of the IEEE 1547 standard for allowable current distortion

Current Distortion Limits for General Dist. Systems (120 V – 69 000 V)						
Maximum Harmonic Current Distortion in Percent of I_L						
Individual Harmonic Order (Odd Harmonics)						
I_{sc}/I_L	<11	11<h<17	17<h<23	23<h<25	35<h	TDD
<20*	4.0	2.0	1.5	0.6	0.3	5.0
20<50	7.0	3.5	2.5	1.0	0.5	8.0
50<100	10.0	4.5	4.0	1.5	0.7	12.0
100<1000	12.0	5.5	5.0	2.0	1.0	15.0
>1000	15.0	7.0	6.0	2.5	1.4	20

Even harmonics are limited to 25% of the odd harmonic limits above.

Current distortions that result in a dc offset, e.g., half-wave converters, are not allowed

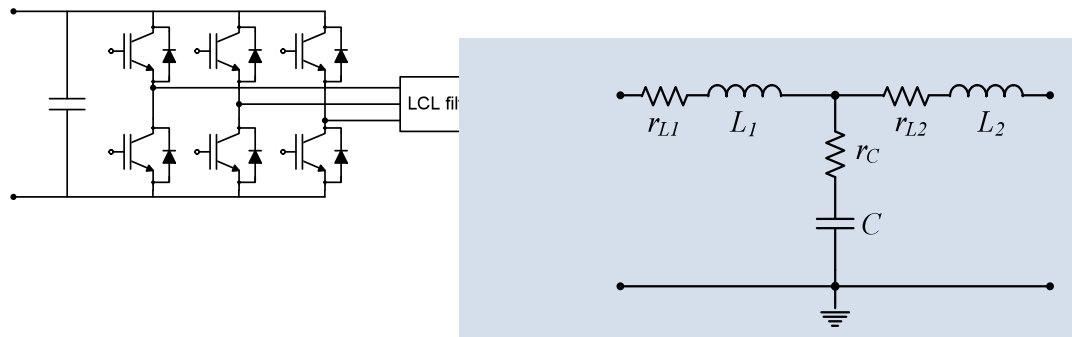
* All power generation equipment is limited to these values current distortion, regardless of actual I_{sc}/I_L

The red rectangle in Figure 17 highlights requirements related to the power generation equipment, and the Figure 18 shows the structure of the LCL filter.

¹⁶ "IEEE Recommended Practices and Requirements for Harmonic Control in Electrical Power Systems," *IEEE Std 519-1992*, p. 0_1, 1993.

¹⁷ "IEEE Application Guide for IEEE Std 1547, IEEE Standard for Interconnecting Distributed Resources with Electric Power Systems," *IEEE Std 1547.2-2008*, pp. 1-207, 2009.

Figure 18: The grid-interface switching model and its LCL filter



The following LCL filter parameters meet current distortion requirements, and were obtained after several iterations using the switching model:

Figure 19: LCL filter parameter values

r_{L1}	1 m Ω	C	500 μ F
L_1	450 μ H	r_{L2}	1 m Ω
r_C	3 m Ω	L_2	494 μ H

It should be mentioned that the parameter L_2 is actually the series inductance of the 18kV/230kV block transformer between buses 1 and 4 in the WECC system (Figure 16), and there was no need to design the separate inductor due to the fact that only grid-interface converter will be connected to the primary side of transformer. A small series resistance r_{L2} was added to provide damping and improve model’s numerical convergence.

The following figures show converter’s output currents before and after the filter, and the harmonic spectrum of the output current at the Point of Common Coupling (PCC – bus 4).

Figure 20: Converter output current

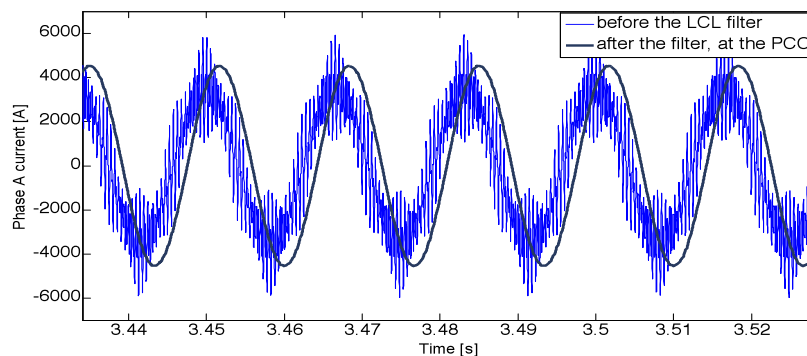
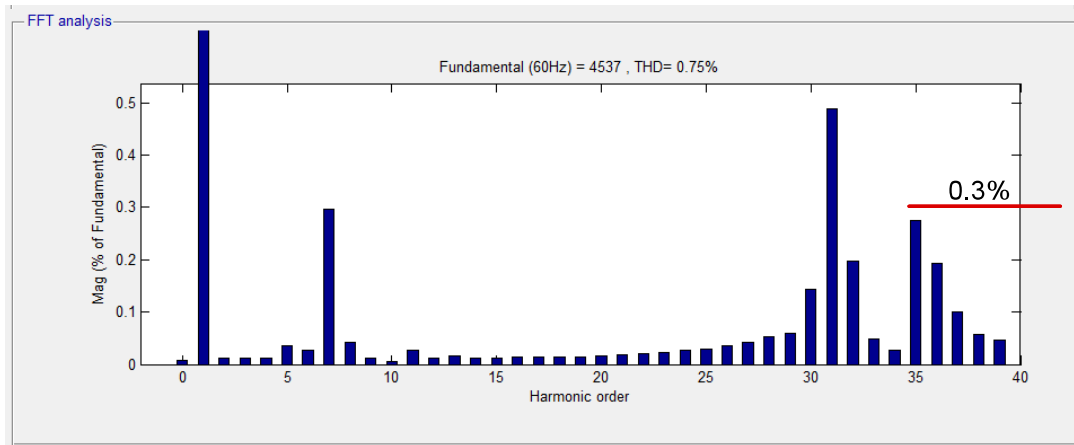


Figure 21: Harmonic spectrum of the output current**Deliverables:**

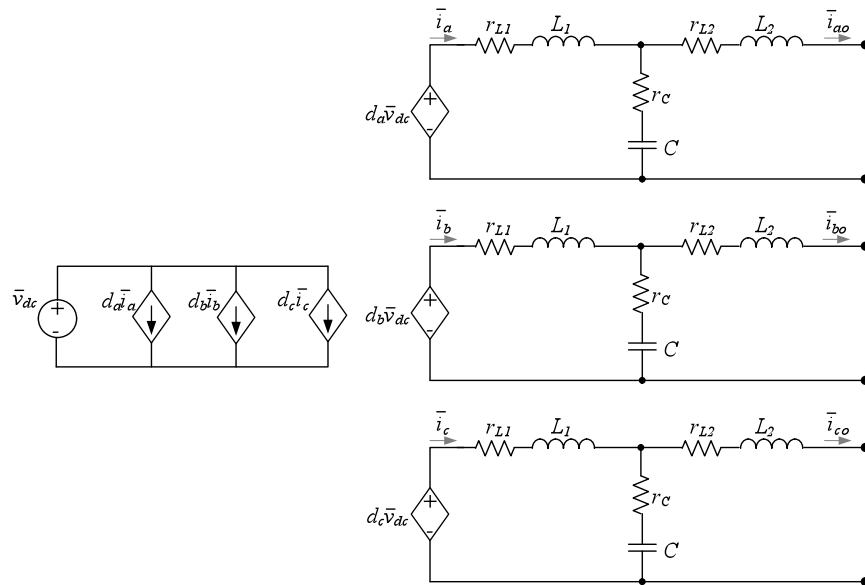
MATLAB (Simulink /SimPowerSystems) switching models of the grid-interface converter. The model called “**switchingM.mdl**” has been uploaded to the NETL members SharePoint website. Please note that the model initialization *m*-file “**init_file.m**” has to be run before starting the model.

3.3.2 Power Converter Model B– average model

Figure 22 shows the large-signal average model (open loop) of the grid-interface converter. The overlined variables have been obtained after applying an average operator (9) to the switching model variables:

$$\bar{x}(t) = \frac{1}{T} \int_{t-T}^t x(\tau) d\tau \quad (9)$$

Figure 22: Average model of the grid-interface converter



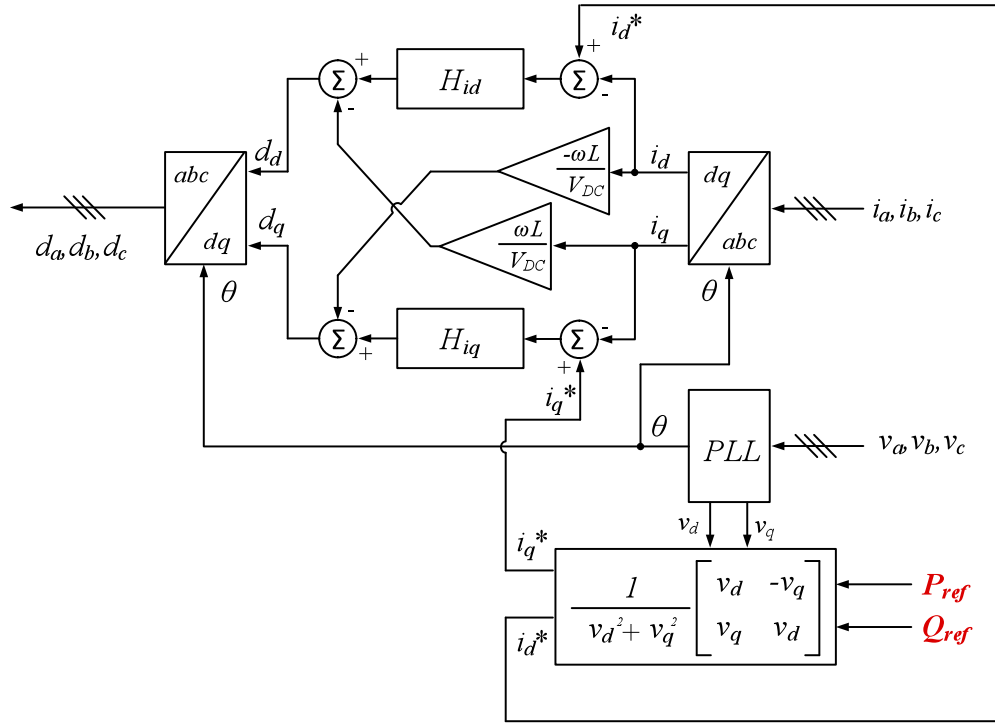
d_a , d_b and d_c represent converter's duty cycles.

Although the power stage (Figure 22) is in the abc , which makes it convenient to be connected to the WECC system, the control design has been done in $d-q$ frame as this allows voltages, currents and duty cycles from the Figure 22 to be seen as a dc values in steady state.

The following Figure 23 depicts the control block diagram implemented on this converter. The current controller is the same in both d - and q - axis, features the PI structure and bandwidth of around 200 Hz ($f_{sw}/10$). It is shown below in (10).

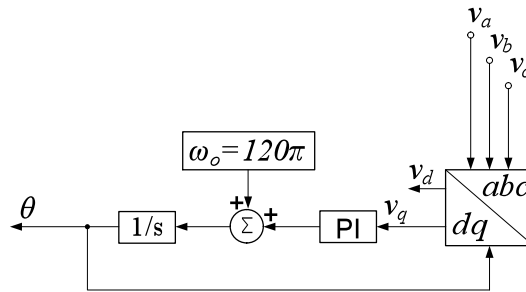
(10)

Figure 23: Control block diagram



The Phase-locked Loop (PLL) is a synchronous reference frame PLL as shown below in Figure 24. The PI controller used with it has parameters shown in (11).

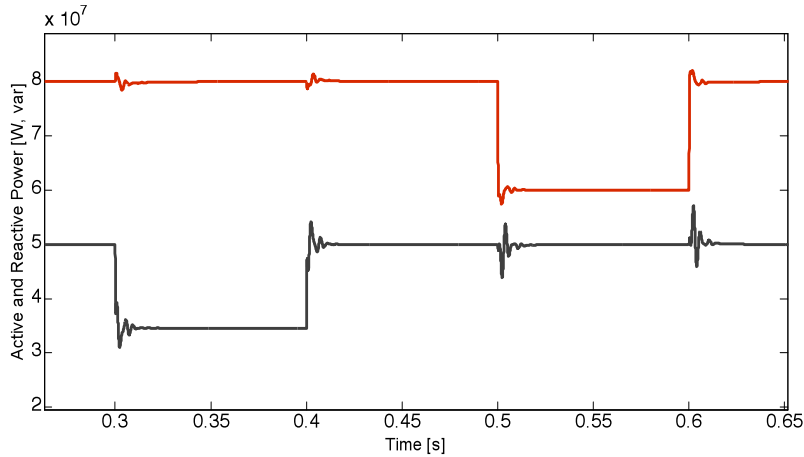
Figure 24: Control block diagram



$$PI = \frac{0.5(1 + s)}{s} \quad (11)$$

The following Figure 25 shows the time domain simulation results for the P-Q control. It should be noted that the power demands P_{ref} and Q_{ref} in the model refer the active and reactive power delivered at the WECC bus No.1 (before the block transformer), or looking at the LCL filter - before the r_{L2} and L_2 branch (Figure 22).

Figure 25: Time domain simulation of the independent P (—) and Q (—) control of the grid-interface converter



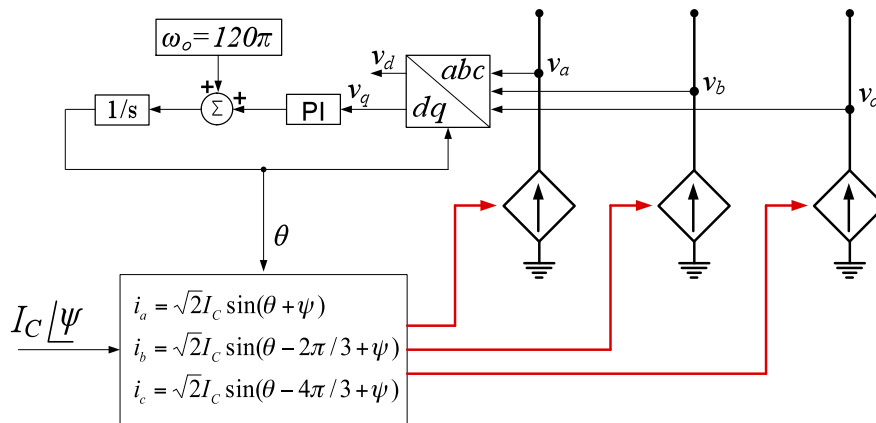
Deliverables:

MATLAB (Simulink /SimPowerSystems) average model of the grid-interface converter. The model called “**averageM.mdl**” has been uploaded to the NETL members SharePoint website. Please note that the model initialization *m*-file “**init_file.m**” has to be run before starting the model.

3.3.3 Power Converter Model C– simplified average model

For the very slow dynamics in the power system, the previous average model can be simplified without making a big impact on the low-frequency dynamic behavior; this means that the current control loops can be regarded as the infinite bandwidth ones, thus the power stage of the grid-interface converter can be modeled as three ideal current sources as shown in the Figure 26. The only dynamics of the converter modeled this way would be the one influenced by the PLL, which, even in the real systems, is dominant in the low-frequency range.

Figure 26: Simplified model of the power converter for the system-level studies



Deliverables:

MATLAB (Simulink /SimPowerSystems) simplified average model of the grid-interface converter. The model called “**simple_averageM.mdl**” has been uploaded to the NETL members SharePoint website. Please note that the model initialization *m*-file “**init_file.m**” has to be run before starting the model.

3.3.4 Power Converter Model D – for *P-f* control

This forth model was developed for the purpose of enabling the *P-f* control of the grid via the grid-interface converter. In other words, the idea is to use this power electronics converter in place of the synchronous generator and explore the benefits of its significantly faster response and when possible, bidirectional operation (for instance when dc-side of this converter interfaces batteries or dc-microgrid). There are two ways of developing such model of the power converter; the first one is to extend the average model B (section 1.3.2) by closing the voltage loop around existing current one, and second is to actually use the model B of the synchronous generator (with both voltage control and frequency droop implemented – section 1.2.2) by bringing the inertia coefficient *J* down to a very small value (small enough to correspond to the slow bandwidth of the PLL shown in Figure 24), and neglecting the turbine time constant $\tau_{turbine}$.

The second approach was chosen here with *J* being 100 times smaller than the one given for the generator No.1, and the $\tau_{turbine} = 0$.

Deliverables:

MATLAB (Simulink /SimPowerSystems) simplified model of the grid-interface converter. The model called “**P_f_controlGIC.mdl**” has been uploaded to the NETL members SharePoint website. Please note that the model initialization *m*-file “**init_file.m**” has to be run before starting the model.

3.4 INTERFACE AND COMMUNICATIONS PROTOCOLS

Power system simulators cannot perform network simulations, so whenever communication between components is required an external network simulator should be utilized. By using the developed communication interface module defined as the Application Layer Communication Interface (ALCI), power simulations and network simulations can be provided simultaneously in PSCAD without the need of an external network simulator. The developed communication module in PSCAD can be used in power system simulations especially where communication plays the first role such as smart grid simulations, energy management systems (EMS) and multi-agents systems (MAS). In this work an easy to use method for putting the power system and communication network dynamics together using power system simulator EMTDC/PSCAD is introduced. PSCAD simulates the power system as a continuous system for transient analysis, while it is operating on time step basis. We have used this configurable time step in PSCAD and embed the communication network simulation inside the PSCAD. And hence, for studying communication vulnerabilities on power systems there is no need to go outside the PSCAD. The effects of communication will be applied on the system by using components and modules

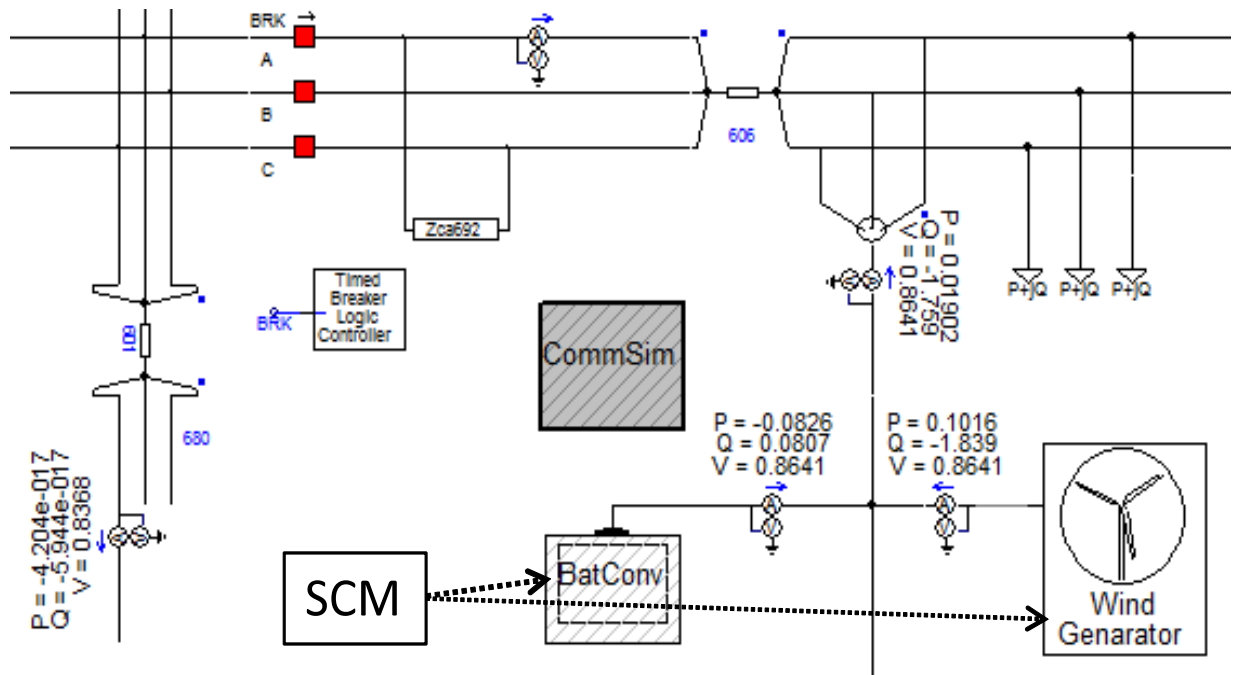
introduced to set up a network topology inside PSCAD and make communication between different modules possible. A set of easy to use components and modules have been developed which are easy to configure and have desirable network properties within the power system and more importantly inside PSCAD with no considerable overhead for federation or going outside PSCAD. The modules and components were developed during the initial stages of the project and implemented during the final stage.

Initially the idea for a Communication Simulator for use within PSCAD was developed. The interface points within PSCAD were defined and their connection with other modules of the power system was identified. A study was conducted on existing communication protocols for power systems; the results were shared with the group during the August meeting. Then the first version of the designed Communication simulator for use within PSCAD was developed during the month of September. This development included the first version of the Application Layer Communication Interface (ALCI) designed as a Communication Module inside the Sensor and Control Modules (SCM) and the Communication Simulator Module (Comm-Sim Module). An IEEE 13-nodes test feeder with a wind generation module was also developed in parallel as a test bench for implementing the Comm-Sim module.

During October we did some refinements and added generic characteristics on the first developed version of the designed Communication simulator for use within PSCAD. Features to provide different medium for communication by applying specific medium characteristics (like delay and loss profile) in the Comm-Sim module were added. ALCI design was also improved as a Communication Module inside the SCM. The Communication Simulator Module (Comm-Sim Module) simulates the lower level communication allowing the joint simulation of the network and power system. This uses the PSCAD time step to integrate the discrete simulation of network into continuous simulation of the power system. We did the implementation of the Comm-Sim module according to the design developed in November. The other implemented component is Comm-Router; this component acts as a router and will allow more dynamic links by routing each packet to its destination. The Comm-Router will allow broadcasting to all SCMs connected to it too. By having these two components the most typical network topologies for power systems are supported however any other network conditions can be easily added to the existing modules. The components as Comm-Link and Comm-Router were implemented and tested in the test case. The Comm-Sim module was designed and implemented in a generic and easy to use way so any PSCAD user can easily integrate it with their power system design. The Application layer communication simulated by Comm-Module was implemented as well; the signals were monitored for stability purposes, which were inputted to the module.

The other activity that was accomplished during the month of November was improving IEEE 13-nodes test feeder by adding storage beside wind generator. These two modules are considered as SCMs according to their dynamical behavior and will stabilize the whole system by help of communication simulation within PSCAD. This will allow the study of communication vulnerabilities and their effects on control applied on the system without going outside PSCAD. The final result was an embedded simulation environment inside PSCAD.

Figure 27: CommSim module and SCMs within PSCAD IEEE 13node test feeder



3.5 DEMONSTRATION SITE PLAN DEVELOPMENT

3.5.1 Statement of the Problem

This work had two objectives. The first was to assess whether the Philadelphia Navy Yard (PNY) is a good test venue for the power electronic systems, simulation tools, and grid control strategies being developed and evaluated. The second objective was to determine the incremental resources required to carry out such testing. The GridSTAR Center, a Smart-Grid Training Application and Resource Center, has constructed a plug-and-play feeder within the larger PNY micro-grid that is to be used both as an educational and research resource. Other areas of the PNY may also be suitable to carry out testing, particularly for electronic devices operating at higher power levels than what GridSTAR can accommodate. The Pennsylvania PUC has declared that the PNY grid is unregulated. Hence, the operating entity at the PNY, The Philadelphia Industrial Development Corporation (PIDC) has the authority to decide on grid connections without PUC approval. While it is assumed that the flexibility that should arise from this situation should be helpful in testing of prototype devices and control and communications strategies, a deeper analysis was needed to better understand the configurations to be evaluated and how such testing could be economically and efficiently implemented.

3.5.2 Approach

The coordinated work being done by the universities in the GTC is to develop a conceptual power electronic device—the *next generation power converter*—that would operate at the

substation level or above, assess the grid impact and value proposition for such a device, and produce a cost-benefit analysis for the device when produced in the quantities needed. The assessment herein represents an initial evaluation based on what was known at the date of the report. As the next generation power converter concept matures, this assessment will require refinement and updating. Information gathering was limited to journal research, interviews, and the use of existing drawings and other materials that were readily at hand.

The PNY is a legacy underground distribution system that is being converted to 13.2 kV feeders. Individual customers can decide whether to use the 13.2 kV supply or have it stepped down to 480V. An Energy Master Plan (EMP) has recently been developed to be consistent with the real-estate master plan and growth rates at the PNY. This EMP will convert the distribution system from a legacy Phase 1 micro-grid to a more evolved Phase 2 micro-grid that may incorporate new substations and feeders, distributed generation, partial islanding, supervisory controls, and other features. At somewhat lower probability, and depending on future events, there are options for future ring buses that may operate at about 68kV. Hence, more information was needed about how power electronic devices, communications, and controls are developed and tested at various stages of development, and what useful testing could be done at substation voltages and below of devices that would operate at substation voltages and above after commercialization.

A literature search was conducted on power electronic devices for grid applications at substation levels and below. This was done to gain familiarity with the current state of the art, the product development process, and test requirements and configurations. It was anticipated that in the early stages of product development of the higher-voltage device that there would be considerable overlap in capabilities with some lower-voltage systems already available. While the isolated testing of individual components is of course required (e.g., inputs, outputs, transfer functions) to assure basic functionality and robustness, it is also necessary to document the value-proposition to the grid. This may require testing a component as part of a complete system, where sizing is appropriate and the local and supervisory controls are coordinated to optimize the system as a whole. Under these conditions, the component interactions and overall system behavior can be documented to characterize the full benefit to the grid.

3.5.3 The Philadelphia Navy Yard: Background

The public and non-profit Philadelphia Industrial Development Corporation (PIDC) manages the electric distribution system of the 1200-acre Philadelphia Navy Yard, providing electric power for the Navy and the other commercial and institutional tenants and owners situated there. Under Pennsylvania statute, the Navy Yard has been declared an unregulated grid by the Pennsylvania Public Utility Commission (PUC). Hence, the PIDC functions like a small quasi-municipal utility. Actual maintenance and operation of the PNY grid is performed by DTE Energy, under contract to the PIDC. This unregulated status creates flexibility in that non-standard or novel configurations may be used without obtaining prior approval from regulators. Power is served to the PNY by the local utility, PECO, by seven feeder lines into two substations. While regulatory approval is not needed, sometimes an interconnection study must be done for equipment large enough to possibly impact the PECO distribution system. Clearly PIDC is greatly concerned with the reliability of the system and they are developing as part of an Energy Master Plan (EMP) their own requirements for safe insertion of prototype components.

The PNY grid is presently fed by multiple PECO 13.2-kV feeders, presently with a peak power capacity of about 28 MW. The EMP was undertaken to address the expanding needs for power and the financing mechanisms necessary to execute that expansion. It is clear that as the PNY grows from its current employment of 8500 worker per day, to 25-30,000 with full development, the peak power requirement might almost triple. To mitigate this need in a partially congested distribution area, the EMP not only considers the introduction of distributed generation devices within the PNY to reduce the future peak demand, but also carries out aggressive education programs to incentivize energy conservation by tenants and owners. It is clear that at least one new substation will be needed and one of the options considered was a ~68kV loop circuit that would feed the substations where it would get stepped down to 13.2kV. In addition, Philadelphia's commitment to fostering *green* development within the City extends to renewal and development projects of the PIDC at the PNY. This attitude is also manifest in its fostering of alliances with institutional tenants who are early adopters of new technology or carry out research and development in advanced energy technologies.

3.5.4 PNY Microgrid Opportunity

The GridSTAR facility at the PNY is currently under construction in the historical section of the development, identified in Figure 28. It contains a research structure, which looks like a two-story house that is to be used to demonstrate smart-grid and solar technologies, a solar training facility. These structures, along with a PV solar array (with a capacity of a few kilowatts), a 100-kWhr energy-storage system, and electric vehicle (EV) charging stations are currently on dedicated circuits. In later phases they could be linked by a circumscribed electrical loop, or *ring bus*. This physical collection is shown in Figure 29. This area is fed from PNY radial feeder line number 908, a 13.2-kV feeder which also supplies PNY Buildings 100, 101, and 796. See

Figure 30, Building 664 Substation Single-Line Diagram. (The #908 feeder appears at the extreme lower-left of the diagram.) The storage capabilities planned for the larger PNY micro-grid combine with the GridSTAR micro-grid to create a more complex distributed energy resource (DER) system worthy of supporting the technical study of dynamic stability, control, and possibly dispatch issues. Among the opportunities outlined below, is power-factor control and reactive power compensation on the PNY #908 feeder line.

3.5.5 Converter Characteristics

The characteristics for the initial development concepts of the next generation power converter provide a good match and opportunity for eventual demonstration at the PNY facilities, allowing for both operational flexibility and various control implementations. The bi-directional aspects of the converter design will allow for various interconnection scenarios for load supply, renewable and storage integration, and other options. Specifically, the converter topology will ideally allow an interface between grid-connected resources of various types, and transmit energy both *from* the AC grid to DC storage devices or loads of various types, and *to* the AC grid from DC storage devices or various DC generators. With circuit enhancements, the converter will be capable of transmitting energy in either of two directions, in either AC or DC form, controlling power factor, and providing dynamic system control and stability.

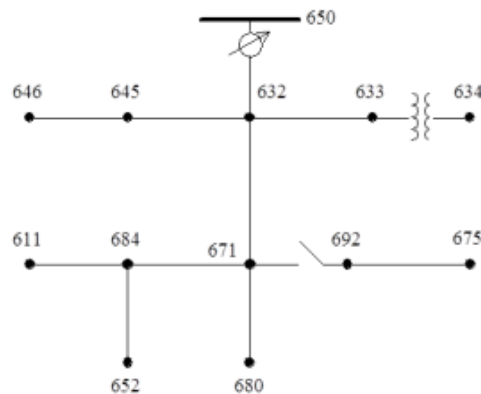
4. METHODS, ANALYSIS, AND RESULTS

4.1 POWER SYSTEM NETWORK MODEL OF IEEE 13 NODE TEST FEEDER SYSTEM

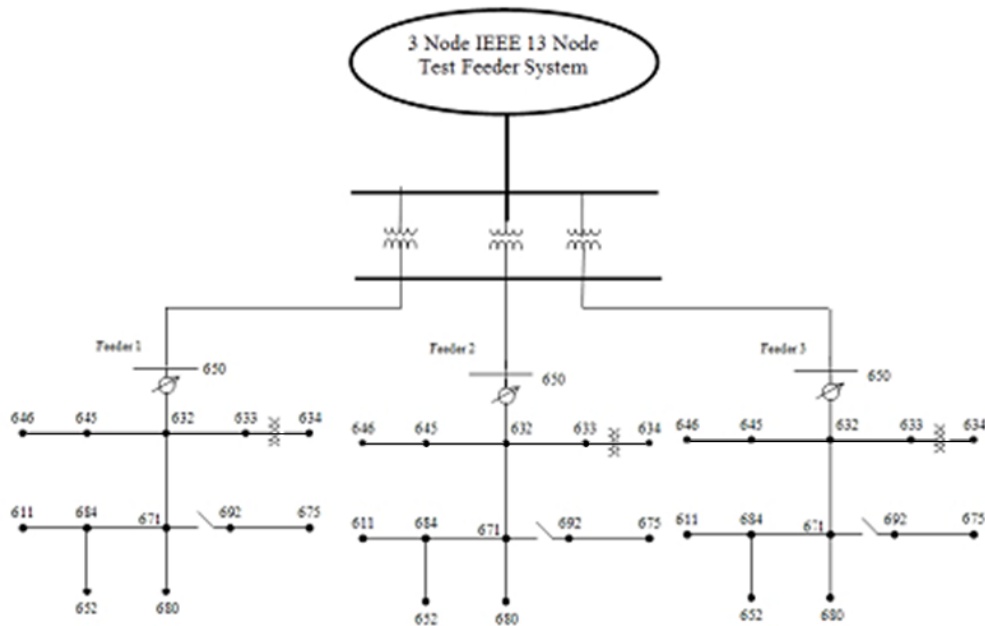
As a starting platform for the project development, the system modeling aspect primarily consisted of the base case model development for the T&D power system network topology in the PSCAD/EMTDC program environment. Employment of standard PSCAD models have been utilized for all selected equipment and network facilities, including generation sources, power electronics converters, feeders, and loads. This has been done using IEEE standard test bus cases (IEEE 9 bus and IEEE 13 bus systems) for the transmission network and for the distribution feeder network.

The IEEE 13 Node Test Feeder is depicted below.

Figure 31: IEEE 13 Node Test Feeder Schematic



The ultimate result desired is a 3 node IEEE 13 node test feeder system where three of the systems specified in Figure 31 will be connected in parallel. This 3 node system is depicted in Figure 32 shown below.

Figure 32: 3 Node IEEE 13 Node Test Feeder System

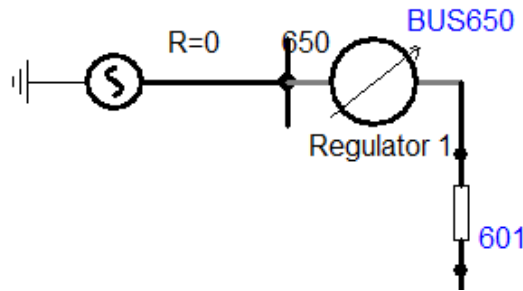
Each bus or node in the system is described below in detail. These descriptions provide clarity on the properties of each node as well as the function of the corresponding equipment connected to each node. Explanations are given as to why each item is modeled in PSCAD the way it is. Modeling of each bus is reasoned from the IEEE 13 Node Test Feeder report (referenced previously).

Bus Descriptions of IEEE 13 Node Test Feeder

Bus 650

Bus 650 is the node on the system designating the location of the generation in this 13 bus network. Connected to this bus is both the simulated power source as well as the regulator (described further in its own section). Shown in Figure 33 is a schematic showing how this bus was constructed in the PSCAD simulation.

Figure 33: Bus 650 with Generation Source and Voltage Regulator



Shown below is the power flow data from the IEEE 13 Node Test Feeder report. The IEEE 13 Node Test Feeder report recorded the power flow data for each bus. The data corresponding to bus 650 is shown below. For bus 650, the PSCAD simulation required a 4.16kV_{LL} RMS voltage for its generation source.

NODE	VALUE	PHASE A (LINE A)	PHASE B (LINE B)	PHASE C (LINE C)	UNT O/L< 60.%
-----*-----*-----*-----*-----*					
NODE: 650	VOLTS:	1.000	.00	1.000 -120.00	1.000 120.00 MAG/ANG
kv11	4.160	NO LOAD OR CAPACITOR REPRESENTED AT SOURCE NODE			
TO NODE RG60 <VRG>..:	593.30	-28.58	435.61 -140.91	626.92	93.59 AMP/DG <
<RG60 > LOSS=	.000:	(.000)	(.000)	(.000)	kw

Bus RG60

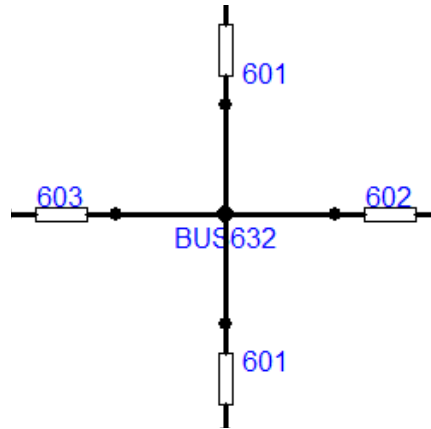
Node RG60 is located immediately after the voltage regulator and before a 601 line configuration. This node is not specifically shown in the model due to having no necessary simulation purposes. It is not counted as one of the 13 nodes (IEEE 13 Node Test Feeder System). The data for node RG60 is shown below, gathered from the IEEE report.

NODE	VALUE	PHASE A (LINE A)	PHASE B (LINE B)	PHASE C (LINE C)	UNT O/L< 60.%
-----*-----*-----*-----*-----*					
NODE: RG60	VOLTS:	1.062	.00	1.050 -120.00	1.069 120.00 MAG/ANG
kv11	4.160	-LD:	.00	.00	.00 kw/kVR
		CAP:	.00	.00	.00 kVR
FROM NODE 650 <VRG>:	558.40	-28.58	414.87 -140.91	586.60	93.59 AMP/DG <
<RG60 > LOSS=	.000:	(.000)	(.000)	(.000)	kw
TO NODE 632	558.40	-28.58	414.87 -140.91	586.60	93.59 AMP/DG <
<632 > LOSS=	59.716:	(21.517)	(-3.252)	(41.451)	kw

Bus 632

Bus 632, shown in Figure 34, on the system does not have load directly connected to it but functions as a crossroad of the system. Connected to bus 632 are two 601 line configurations, a 602 line configuration and also a 603 line configuration. This bus simply functions to interconnect multiple branches of the system.

Figure 34: Bus 632 with Crossroads of Line Configurations 601, 602 and 603



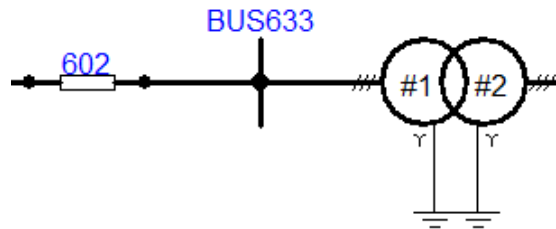
The data provided in the IEEE report made it clear as to how bus 632 intertied busses RG60, 633, 645 and 671 – each to be discussed in their separate subsection. The data also clarified that there was no load associated with bus 632.

NODE	VALUE	PHASE A (LINE A)		PHASE B (LINE B)		PHASE C (LINE C)		UNT	O/L< 60. %
-----*		-A-		-B-		-C-		-----*	
NODE: 632	VOLTS:	1.021	-2.49	1.042	-121.72	1.017	117.83	MAG/ANG	
	-LD:	.00	.00	.00	.00	.00	.00	kW/kVR	
kv11	4.160	CAP:	.00	.00	.00	.00	.00	kVR	
FROM NODE RG60	558.41	-28.58	414.87	-140.91	586.60	93.59	AMP/DG <	
<632 >	LOSS= 59.716:	(21.517)		(-3.252)		(41.451)		kW	
TO NODE 633	81.33	-37.74	61.12	-159.09	62.70	80.48	AMP/DG	
<633 >	LOSS= .808:	(.354)		(.148)		(.306)		kW	
TO NODE 645			143.02	-142.66	65.21	57.83	AMP/DG <	
<645 >	LOSS= 2.760:			(2.540)		(.220)		kW	
TO NODE 671	478.29	-27.03	215.12	-134.66	475.50	99.90	AMP/DG <	
<671 >	LOSS= 35.897:	(10.484)		(-6.169)		(31.582)		kW	

Bus 633

Bus 633 has a wye-wye connected transformer and a 602 line configuration connected to either of its sides as shown in Figure 35. The transformer has its own section within this report. Reference the power system equipment section for further description. Bus 632 is to the left-hand side of line 602.

Figure 35: Bus 633 with a Y-Y Transformer and Line Configuration 602



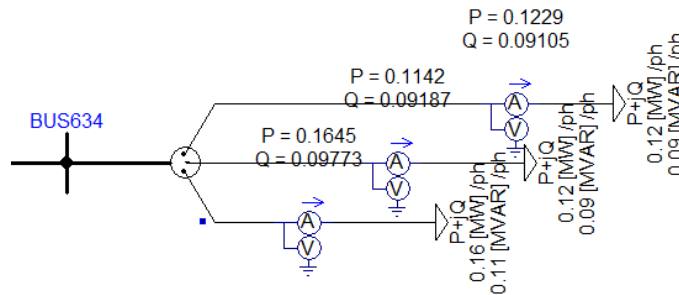
The data provided in the IEEE report gives reason to the way that the model is constructed the way it is. It is apparent in the last four lines of this data that bus 633 is located between bus 632 and the transformer. Also apparent is that there is no load on this bus.

NODE	VALUE	PHASE A (LINE A)	PHASE B (LINE B)	PHASE C (LINE C)	UNT O/L< 60.%			
-----*								
		A	B	C				
-----*								
NODE: 633	VOLTS:	1.018	-2.56	1.040	-121.77	1.015	117.82	MAG/ANG
	-LD:	.00	.00	.00	.00	.00	.00	kW/kVR
kv11	4.160	CAP:	.00	.00	.00	.00	.00	kVR
FROM NODE 632:	81.33	-37.74	61.12	-159.09	62.71	80.47	AMP/DG
<633 >	LOSS=	(.354)	(.148)	(.306)				kW
TO NODE XFXFM1:	81.33	-37.74	61.12	-159.09	62.71	80.47	AMP/DG <
<XFXFM1>	LOSS=	(2.513)	(1.420)	(1.494)				kW

Bus 634

Connected to bus 634 is one of the first appearances of load on the system. As seen in Figure 36 there is a three phase load directly connected to bus 634. Located to the left of bus 634 is the transformer previously mentioned. This can be seen clearly in Figure 35 – the general figure of the entire 13 bus test feeder system.

Figure 36: Bus 634 with Corresponding Three Phase Load



The amount of load simulated was defined by the data from the IEEE report. This data for bus 634 is shown below. Also specified in the data is the fact that this is a wye-connected load (Y-LD). The PSCAD simulation was created according to this information.

NODE	VALUE	PHASE A (LINE A)		PHASE B (LINE B)		PHASE C (LINE C)		UNT	O/L< 60.%
		A		B		C			
NODE: 634	VOLTS:	.994	-3.23	1.022	-122.22	.996	117.34	MAG/ANG	
	Y-LD:	160.00	110.00	120.00	90.00	120.00	90.00	kW/kVR	
kV11	.480	Y CAP:	.00	.00	.00	.00	.00	kVR	
FROM NODE XFXFM1.....:		704.83	-37.74	529.73	-159.09	543.45	80.47	AMP/DG <	
<634 > LOSS=	.000:	(.000)	(.000)	(.000)	(.000)	(.000)	(.000)	kW	

In comparison to the results from the IEEE report, our PSCAD simulation results are comparable as shown in Figure 37.

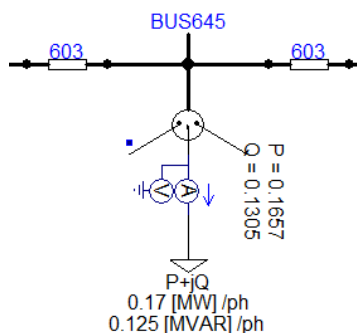
Figure 37: IEEE results compared with PSCAD results for Bus 634

BUS	Real Power (p=MW) and Reactive Power (q=Mvar)								
	Phase A (MW)			Phase B (MW)			Phase C (MW)		
	IEEE	PSCAD	% Diff	IEEE	PSCAD	% Diff	IEEE	PSCAD	% Diff
634_p	0.16	0.1579	1.312	0.12	0.1205	0.417	0.12	0.1229	2.417
634_q	0.11	0.1077	2.091	0.09	0.08929	0.789	0.09	0.09115	1.278

Bus 645

Connected to bus 645 is a single phase wye-connected load, specifically on phase B. On either side of bus 645 are 603 line configurations. As seen in Figure 38 the simulation was created accordingly.

Figure 38: Bus 645 with a Wye-Connected Single Phase Load on Phase C



All information used to create this portion of the PSCAD model was taken from the IEEE data shown below. The data specifying line 603 configurations on either side of the load is described further in the Line Configuration Descriptions section.

NODE	VALUE	PHASE A (LINE A)	PHASE B (LINE B)	PHASE C (LINE C)	UNT	O/L< 60.8
		A	B	C		
NODE: 645	VOLTS:		1.033 -121.90	1.015 117.86	MAG/ANG	
	Y-LD:		170.00 125.00	.00 .00	kW/kVR	
kV11 4.160	Y CAP:		.00	.00	kVR	
FROM NODE 632:		143.02 -142.66	65.21 57.83	AMP/DG <	
<645 > LOSS=	2.760:		(2.540)	(.220)	kW	
TO NODE 646:		65.21 -122.17	65.21 57.83	AMP/DG	
<646 > LOSS=	.541:		(.271)	(.270)	kW	

In comparison to the results from the IEEE report, our PSCAD simulation results are comparable as shown in Figure 39.

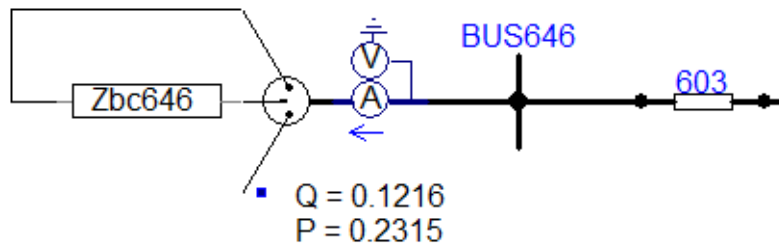
Figure 39: IEEE results compared with PSCAD results for Bus 645

Real Power (p=MW) and Reactive Power (q=Mvar)									
	Phase A (MW)			Phase B (MW)			Phase C (MW)		
BUS	IEEE	PSCAD	% Diff	IEEE	PSCAD	% Diff	IEEE	PSCAD	% Diff
645_p	-	-	-	0.17	0.18	5.882	-	-	-
645_q	-	-	-	0.125	0.132	5.600	-	-	-

Bus 646

Connected to bus 646 is a delta-connected single phase impedance load. Figure 40 gives a schematic of how this bus was constructed in the PSCAD simulation.

Figure 40: Bus 646 with a Delta-Connected Single Phase Load



As for previous busses, the information needed to create the PSCAD simulation appropriately was found in the IEEE 13 Node Test Feeder report. Only for this load specifically it was necessary to look at the Spot Load Data table in order to find that this load on bus 646 was an impedance (Z) load. The Spot Load Data shown in Figure 41 is also from the IEEE report. This table is referenced multiple times throughout this report.

Figure 41: Spot Load Data

Node	Load	Ph-1	Ph-1	Ph-2	Ph-2	Ph-3	Ph-3
	Model	kW	kVAr	kW	kVAr	kW	kVAr
634	Y-PQ	160	110	120	90	120	90
645	Y-PQ	0	0	170	125	0	0
646	D-Z	0	0	230	132	0	0
652	Y-Z	128	86	0	0	0	0
671	D-PQ	385	220	385	220	385	220
675	Y-PQ	485	190	68	60	290	212
692	D-I	0	0	0	0	170	151
611	Y-I	0	0	0	0	170	80
	TOTAL	1158	606	973	627	1135	753

The load flow expected was gathered from the data provided by the IEEE report, shown below.

NODE	VALUE	PHASE A (LINE A)	PHASE B (LINE B)	PHASE C (LINE C)	UNT	O/L< 60.8
		A	B	C		
NODE: 646	VOLTS:		1.031 -121.98	1.013 117.90	MAG/ANG	
	D-LD:		240.66 138.12	.00 .00	kW/kVR	
kVll 4.160	Y CAP:		.00	.00	kVR	
FROM NODE 645:		65.21 -122.18	65.21 57.82	AMP/DG	
<646 > LOSS=	.541:		(.271)	(.270)	kW	

In comparison to the results from the IEEE report, our PSCAD simulation results are comparable as shown in Figure 42.

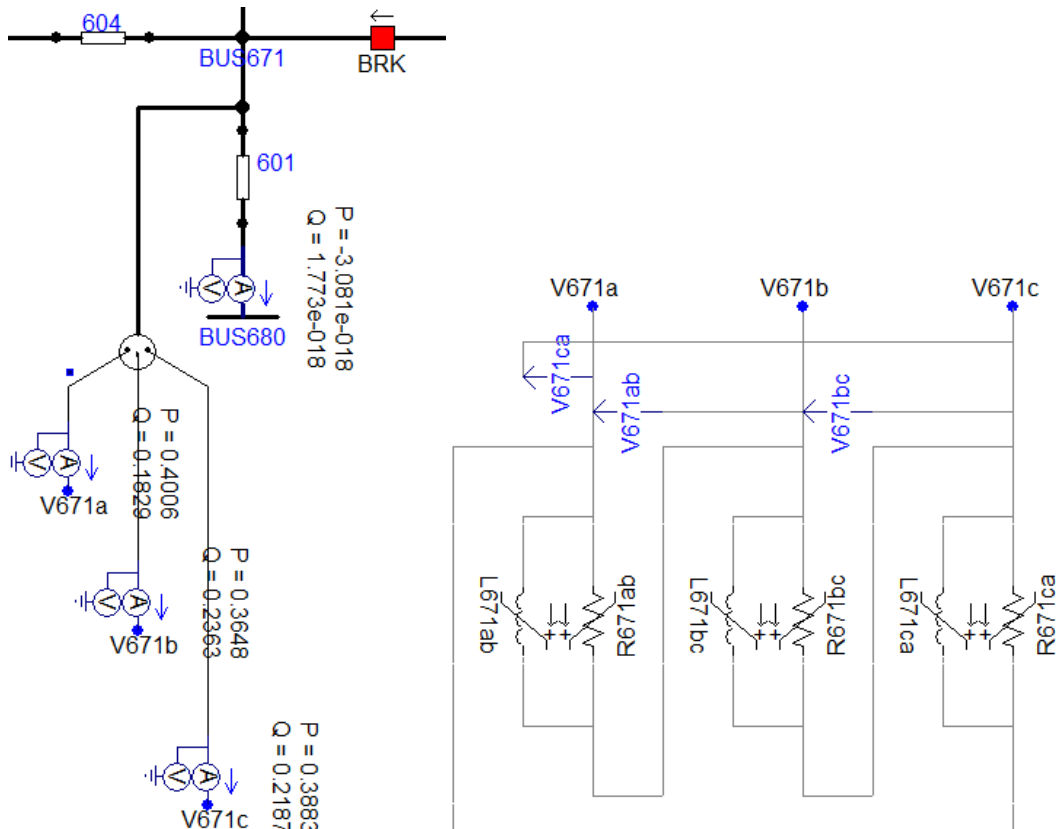
Figure 42: IEEE results compared with PSCAD results for Bus 646

Real Power (p=MW) and Reactive Power (q=Mvar)									
BUS	Phase A (MW)			Phase B (MW)			Phase C (MW)		
	IEEE	PSCAD	% Diff	IEEE	PSCAD	% Diff	IEEE	PSCAD	% Diff
646_p	-	-	-	0.2466	0.2412	2.190	-	-	-
646_q	-	-	-	0.13812	0.13796	0.116	-	-	-

Bus 671

Directly connected to bus 671 is a delta-connected three phase load as seen in Figure 43. The breaker located to the right of bus 671 was specified in the line configuration data table (Figure 58 located in the line configuration section of this report).

Figure 43: Bus 671 with Corresponding Delta-Connected Three Phase Load



The amount of load simulated was defined by the data from the IEEE report. This data for bus 671 is shown below, corresponding to what is simulated in Figure 43. Also specified in the data is the fact that this is a delta-connected load (D-LD). The PSCAD simulation was created according to this information.

NODE	VALUE	PHASE A (LINE A)		PHASE B (LINE B)		PHASE C (LINE C)		UNT	O/L< 60.8
-----*		-A-		-B-		-C-		-----*	
NODE: 671	VOLTS:	.990	-5.30	1.053	-122.34	.978	116.02	MAG/ANG	
	D-LD:	385.00	220.00	385.00	220.00	385.00	220.00	kW/kVR	
kv11	4.160	Y CAP:	.00		.00		.00	kVR	
FROM NODE 632	470.20	-26.90	186.41	-131.89	420.64	101.66	AMP/DG <	
<671 >	LOSS=	35.897:	(10.484)	(-6.169)	(31.582)			kW	
TO NODE 68000	.00	.00	.00	.00	.00	AMP/DG	
<680 >	LOSS=	.000:	(-.001)	(.001)	(.000)			kW	
TO NODE 684	63.07	-39.12			71.15	121.62	AMP/DG	
<684 >	LOSS=	.580:	(.210)			(.370)		kW	
TO NODE 692	229.11	-18.18	69.61	-55.19	178.38	109.39	AMP/DG	
<692 >	LOSS=	.008:	(.003)	(-.001)	(.006)			kW	

In comparison to the results from the IEEE report, our PSCAD simulation results are comparable as shown in Figure 44.

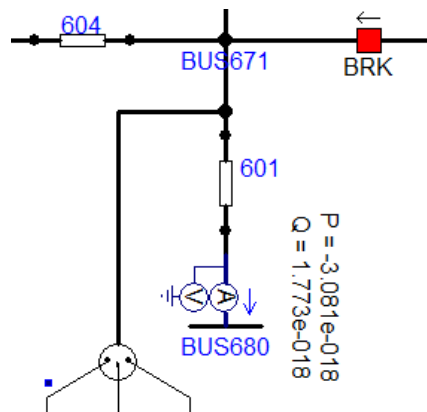
Figure 44: IEEE results compared with PSCAD results for Bus 671

BUS	Real Power (p=MW) and Reactive Power (q=Mvar)								
	Phase A (MW)			Phase B (MW)			Phase C (MW)		
	IEEE	PSCAD	% Diff	IEEE	PSCAD	% Diff	IEEE	PSCAD	% Diff
671_p	0.385	0.3847	0.078	0.385	0.396	2.857	0.385	0.3755	2.468
671_q	0.22	0.2026	7.909	0.22	0.2485	12.955	0.22	0.2095	4.773

Bus 680

Bus 680, Figure 45, does not have any load directly connected to it. A 601 line configuration is between bus 680 and the three phase delta-connected load (directly connected to bus 671 as discussed in previous section). Therefore bus 680 has essentially no load flow related to it. This bus does not have an apparent purpose with respect to the model in its entirety other than providing a node on the end of a line 601 configuration.

Figure 45: Bus 680 with No Immediate Load Connected



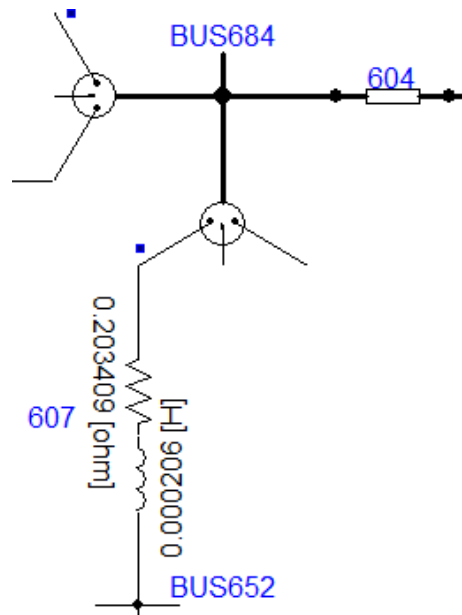
The information needed to create the PSCAD simulation of bus 680 accordingly is found in the IEEE 13 Node Test Feeder report. The corresponding data is shown below.

NODE	VALUE	PHASE A (LINE A)		PHASE B (LINE B)		PHASE C (LINE C)		UNT O/L< 60.%
		A	B	A	B	A	B	
NODE: 680	VOLTS:	.990	-5.30	1.053	-122.34	.978	116.02	MAG/ANG
	-LD:	.00	.00	.00	.00	.00	.00	kW/kVR
kv11	4.160	CAP:	.00		.00		.00	kVR
FROM NODE 671:	.00	.00	.00	.00	.00	.00	AMP/DG
<680 > LOSS=	.000:	(-.001)		(.001)		(.000)		kW

Bus 684

Bus 684, Figure 46, does not have any load directly connected to it. A 604 line configuration is between bus 684 and bus 671. Below bus 684, there is a single-phase line to bus 652 (to which load is connected). To the left of bus 684 is another single-phase line to bus 611 (also to which load is directly connected). Consequently bus 684 has no load flow related to it. This bus simply functions as a node at which single-phase lines branch off from.

Figure 46: Bus 684 with Two Single Phase Lines Branching Off



The data needed to model this bus appropriately was gathered from the IEEE report. This data is shown below.

NODE	VALUE	PHASE A (LINE A)	PHASE B (LINE B)	PHASE C (LINE C)	UNT O/L< 60.8
-----*					
		A	B	C	
NODE: 684	VOLTS:	.988	-5.32	.976	115.92 MAG/ANG
	-LD:	.00	.00	.00	.00 kW/kVR
kV11 4.160	CAP:		.00		.00 kVR
FROM NODE 671:	63.07	-39.12	71.15	121.61 AMP/DG
<684 > LOSS=	.580:	(.210)	(.370) kW
TO NODE 611:			71.15	121.61 AMP/DG
<611 > LOSS=	.382:			(.382) kW
TO NODE 652:	63.07	-39.12		AMP/DG
<652 > LOSS=	.808:	(.808)		kW

Bus 611

Connected to bus 611 is a single-phase wye connected load as well as a shunt capacitance. Bus 611 was simulated in PSCAD according to Figure 47 where the capacitance is modeled simply as a shunt capacitor on 611. This capacitance is modeled here according to Figure 48, capacitor data provided by the IEEE report. One can see in this table that there is also shunt capacitance on bus 675. What is connected to bus 675 is discussed further in its appropriate section.

Figure 47: Bus 611 with a Single-Phase Wye Connected Load and a Shunt Capacitance

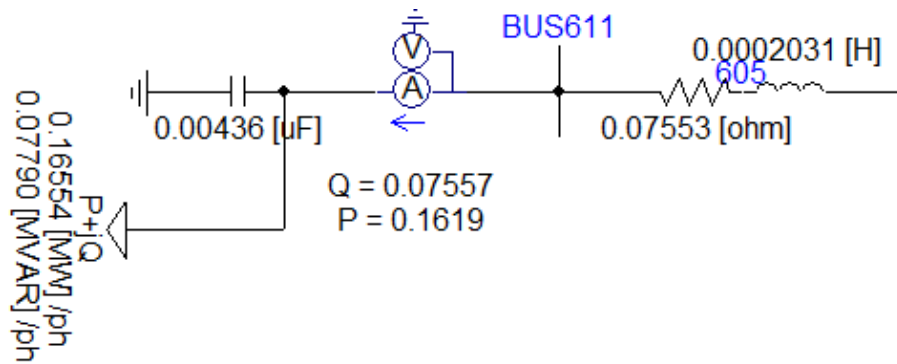


Figure 48: Capacitor Data

Node	Ph-A	Ph-B	Ph-C
	kVAr	kVAr	kVAr
675	200	200	200
611			100
Total	200	200	300

The single-phase load was modeled to obtain the specific load flow according to the data provided by the IEEE report as shown below.

NODE	VALUE	PHASE A (LINE A)	PHASE B (LINE B)	PHASE C (LINE C)	UNT	O/L< 60.%
NODE: 611	VOLTS:			.974	115.78	MAG/ANG
	Y-LD:			165.54	77.90	kW/kVR
kVLL 4.160	Y CAP:				94.82	kVR
FROM NODE 684:			71.15	121.61	AMP/DG
<611 > LOSS=	.382:			(.382)		kW

In comparison to the results from the IEEE report, our PSCAD simulation results for bus 611 are comparable as shown in Figure 49.

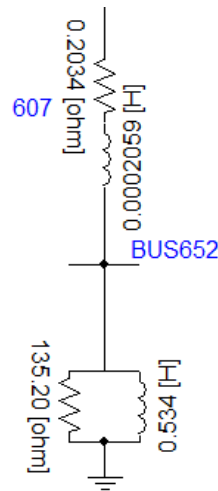
Figure 49: IEEE results compared with PSCAD results for Bus 611

BUS	Real Power (p=MW) and Reactive Power (q=Mvar)								
	Phase A (MW)			Phase B (MW)			Phase C (MW)		
	IEEE	PSCAD	% Diff	IEEE	PSCAD	% Diff	IEEE	PSCAD	% Diff
611_p	-	-	-	-	-	-	0.16554	0.1563	5.582
611_q	-	-	-	-	-	-	0.0779	0.07299	6.303

Bus 652

Connected to bus 652 is a single-phase wye connected load as well as a line connecting to bus 684. This line originates from bus 684 (previously discussed) and terminates at bus 652. This single-phase load was specified in the Spot Load Data (Figure 41) to be a wye connected impedance load. This is the reason for modeling this load as we did in Figure 50.

Figure 50: Bus 652 with a Single-Phase Wye Connected Impedance Load



The IEEE report also provided data for this bus as shown below.

NODE	VALUE	PHASE			UNT	O/L< 60.8
		A (LINE A)	B (LINE B)	C (LINE C)		
-----*-----*-----*-----*						
NODE: 652	VOLTS:	.983	-5.25			MAG/ANG
	Y-LD:	123.56	83.02			kW/ kVR
kv11 4.160	Y CAP:		.00			kVR
FROM NODE 684:	63.08	-39.15			AMP/DG
<652 > LOSS=	.808:	(.808)			kW

In comparison to the results from the IEEE report, our PSCAD simulation results are comparable as shown in Figure 51.

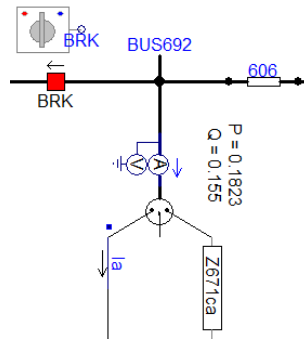
Figure 51: IEEE results compared with PSCAD results for Bus 652

BUS	Real Power (p=MW) and Reactive Power (q=Mvar)								
	Phase A (MW)			Phase B (MW)			Phase C (MW)		
	IEEE	PSCAD	% Diff	IEEE	PSCAD	% Diff	IEEE	PSCAD	% Diff
652_p	0.12356	0.1181	4.419	-	-	-	-	-	-
652_q	0.08302	0.07877	5.119	-	-	-	-	-	-

Bus 692

Bus 692 has a single-phase delta connected load as shown in Figure 52. The Spot Load Data table (Figure 41) is what provided the information for the impedance nature of the load. There is also a switch on the system isolating bus 692 and beyond from bus 671 and above. This was specified by Figure 58 (Line Segment Data) located in the next section.

Figure 52: Bus 692 with a Single-Phase Delta Connected Load



The single-phase load was modeled to obtain specific load flow according to the data provided by the IEEE report as shown below. This data is also what specified that the load was single-phase and delta connected (D-LD).

NODE	VALUE	PHASE A (LINE A)		PHASE B (LINE B)		PHASE C (LINE C)		UNT	O/L<
		A		B		C		60. %	
NODE: 692	VOLTS:	.990	-5.31	1.053	-122.34	.978	116.02	MAG/ANG	
	D-LD:	.00	.00	.00	.00	168.37	149.55	kW/kVR	
kv11	4.160	Y CAP:	.00		.00		.00	kVR	
FROM NODE 671:	229.11	-18.18	69.61	-55.19	178.38	109.39	AMP/DG	
<692 > LOSS=	.008:	(.003)		(-.001)		(.006)		kW	
TO NODE 675:	205.33	-5.15	69.61	-55.19	124.07	111.79	AMP/DG <	
<675 > LOSS=	4.136:	(3.218)		(.345)		(.573)		kW	

In comparison to the results from the IEEE report, our PSCAD simulation results are comparable as shown in Figure 53.

Figure 53: IEEE results compared with PSCAD results for Bus 692

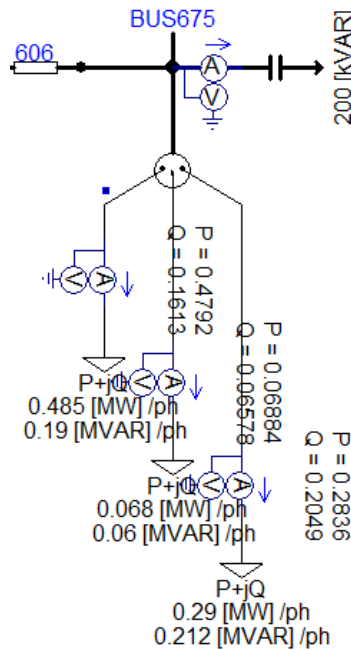
BUS	Real Power (p=MW) and Reactive Power (q=Mvar)								
	Phase A (MW)			Phase B (MW)			Phase C (MW)		
	IEEE	PSCAD	% Diff	IEEE	PSCAD	% Diff	IEEE	PSCAD	% Diff
692_p	-	-	-	-	-	-	0.16837	0.16845	0.048
692_q	-	-	-	-	-	-	0.14955	0.15935	6.553

Bus 675

Connected to bus 675 is a three phase load on the system as seen in

Figure 54. Bus 675 is connected to the system as a whole by a 606 line configuration. Also connected to bus 675 is a voltage compensating capacitance. This capacitor was modeled according to Figure 48 referenced once before in this report. This table of capacitor data was provided in the IEEE 13 node test feeder report.

Figure 54: Bus 675 with a Three-Phase Load and a Shunt Capacitance



The amount of load simulated was defined by the data from the IEEE report. This data for bus 675 is shown below. This data corresponds to what is shown in

Figure 54. Also specified in the data is the fact that this is a wye-connected load (Y-LD). The PSCAD simulation was created according to this information.

NODE	VALUE	PHASE A (LINE A)	PHASE B (LINE B)	PHASE C (LINE C)	UNT	O/L<
-----*-----A-----*-----B-----*-----C-----*						
NODE: 675	VOLTS:	.983	-5.56	1.055	-122.52	.976 116.03 MAG/ANG
	Y-LD:	485.00	190.00	68.00	60.00	290.00 212.00 kW/kVR
kv11	4.160	Y CAP:	193.44		222.75	190.45 kVR
FROM NODE 692:	205.33	-5.15	69.59	-55.20	124.07 111.78 AMP/DG <
<675	> LOSS=	4.136:	(3.218)	(.345)	(.573)	kW

In comparison to the results from the IEEE report, our PSCAD simulation results for bus 675 are comparable as shown in Figure 55.

Figure 55: IEEE results compared with PSCAD results for Bus 675

BUS	Real Power (p=MW) and Reactive Power (q=Mvar)								
	Phase A (MW)			Phase B (MW)			Phase C (MW)		
	IEEE	PSCAD	% Diff	IEEE	PSCAD	% Diff	IEEE	PSCAD	% Diff
675_p	0.485	0.46425	4.278	0.068	0.0754	10.882	0.29	0.2764	4.690
675_q	0.19	0.1809	4.789	0.06	0.06598	9.967	0.212	0.2	5.660

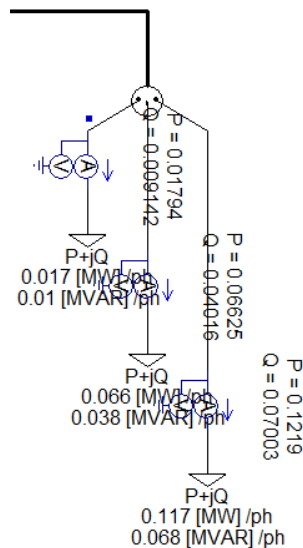
Distributed Load Bus

This bus or node on the system is not counted as one of the IEEE 13 node test system. It is located between bus 632 and bus 671 as seen in Figure 5. Nonetheless it functions as a bus on the network. The data that specifies this distributed load and where it is located is provided in Figure 56. This table was given in the IEEE report, hence the necessity to include it in the PSCAD model. As specified in the table, this is a wye connected three-phase load.

Figure 56: Distributed Load Data

Node A	Node B	Load	Ph-1	Ph-1	Ph-2	Ph-2	Ph-3	Ph-3
		Model	kW	kVAr	kW	kVAr	kW	kVAr
632	671	Y-PQ	17	10	66	38	117	68

Figure 57: Distributed Load (on far right)



Line Impedance Configurations of IEEE 13 Node Test Feeder

There are various line impedance configurations on the IEEE 13 Node Test Feeder system. This section shows the data used for each configuration modeled in PSCAD. There are seven different line configurations in the system. Each configuration has differing line impedance values in ohms per mile, and more specifically, within one configuration each phase can have a differing impedance value. This data is provided in this section in order to clarify what went into modeling each line in PSCAD. Figure 58 through 60 provide line segment data, overhead line configuration data, and underground line configuration data. Figure 58 provides the location of each line in the system, its length and its configuration type. Figure 59 and Figure 60 specify details per configuration type such as overhead or underground.

Figure 58: Line Segment Data

Node A	Node B	Length(ft.)	Config.
632	645	500	603
632	633	500	602
633	634	0	XFM-1
645	646	300	603
650	632	2000	601
684	652	800	607
632	671	2000	601
671	684	300	604
671	680	1000	601
671	692	0	Switch
684	611	300	605
692	675	500	606

Figure 59: Overhead Line Configuration Data

Config.	Phasing	Phase	Neutral	Spacing
		ACSR	ACSR	ID
601	B A C N	556,500 26/7	4/0 6/1	500
602	C A B N	4/0 6/1	4/0 6/1	500
603	C B N	1/0	1/0	505
604	A C N	1/0	1/0	505
605	C N	1/0	1/0	510

Figure 60: Underground Line Configuration Data

Config.	Phasing	Cable	Neutral	Space
606	A B C N	250,000 AA, CN	None	515
607	A N	1/0 AA, TS	1/0 Cu	520

The following data for each line configuration was provided by the IEEE report. These impedance values were used in order to model the exact impedances per phase per configuration in the PSCAD simulation model. The impedance data (Z) is separated into three columns for phases A, B, and C, and each phase has real and reactive values ($R+jX$). The susceptance (B) is separated likewise into phases A, B, and C.

Configuration 601:

```

      Z (R +jX) in ohms per mile
0.3465  1.0179  0.1560  0.5017  0.1580  0.4236
          0.3375  1.0478  0.1535  0.3849
                                0.3414  1.0348
      B in micro Siemens per mile
        6.2998  -1.9958  -1.2595
          5.9597  -0.7417
                                5.6386
    
```

Configuration 602:

```

      Z (R +jX) in ohms per mile
0.7526  1.1814  0.1580  0.4236  0.1560  0.5017
          0.7475  1.1983  0.1535  0.3849
                                0.7436  1.2112
      B in micro Siemens per mile
        5.6990  -1.0817  -1.6905
          5.1795  -0.6588
                                5.4246
    
```

Configuration 603:

```

      Z (R +jX) in ohms per mile
0.0000  0.0000  0.0000  0.0000  0.0000  0.0000
          1.3294  1.3471  0.2066  0.4591
                                1.3238  1.3569
      B in micro Siemens per mile
        0.0000  0.0000  0.0000
          4.7097  -0.8999
                                4.6658
    
```

Configuration 604:

```

      Z (R +jX) in ohms per mile
1.3238  1.3569   0.0000  0.0000   0.2066  0.4591
              0.0000  0.0000   0.0000  0.0000
                              1.3294  1.3471

      B in micro Siemens per mile
      4.6658   0.0000  -0.8999
              0.0000   0.0000
                              4.7097
    
```

Configuration 605:

```

      Z (R +jX) in ohms per mile
0.0000  0.0000   0.0000  0.0000   0.0000  0.0000
              0.0000  0.0000   0.0000  0.0000
                              1.3292  1.3475

      B in micro Siemens per mile
      0.0000   0.0000   0.0000
              0.0000   0.0000
                              4.5193
    
```

Configuration 606:

```

      Z (R +jX) in ohms per mile
0.7982  0.4463   0.3192  0.0328   0.2849 -0.0143
              0.7891  0.4041   0.3192  0.0328
                              0.7982  0.4463

      B in micro Siemens per mile
      96.8897   0.0000   0.0000
              96.8897   0.0000
                              96.8897
    
```

Configuration 607:

```

      Z (R +jX) in ohms per mile
1.3425  0.5124   0.0000  0.0000   0.0000  0.0000
              0.0000  0.0000   0.0000  0.0000
                              0.0000  0.0000

      B in micro Siemens per mile
      88.9912   0.0000   0.0000
              0.0000   0.0000
                              0.0000
    
```

Major Power System Equipment in the System

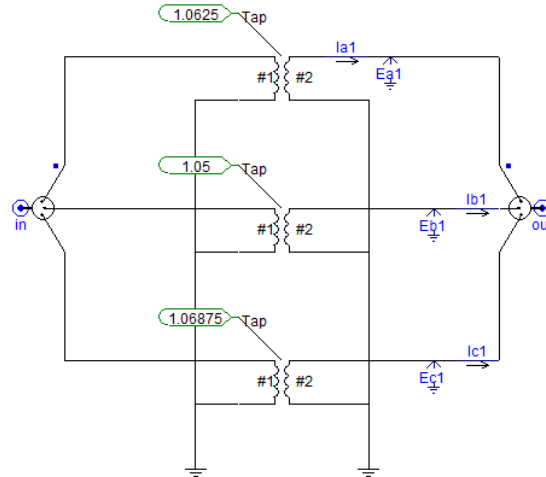
This section accounts for the pieces of power system equipment that do not fall under the categories of bus description or line configuration. The two items discussed in this section are the power system voltage regulator and the power transformer present in the system.

Regulator

The regulator of this system is located immediately after the primary source of the system. The regulator in this system does not seem to be doing much for the 13 node system. The function of the regulator will be appreciated and useful once the 3 node IEEE 13 bus network is created.

Shown here is a picture of the internals of the regulator. This picture shows the transformer taps that are necessary in order to regulate the voltage appropriately.

Figure 61: Tap Changing Configuration of Voltage Regulator



All data that was used to model this regulator was provided in the IEEE report in the form of Figure 62 shown below. This table specifies all of the necessary data such as the location, connection, ratings, settings and voltage level, etc.

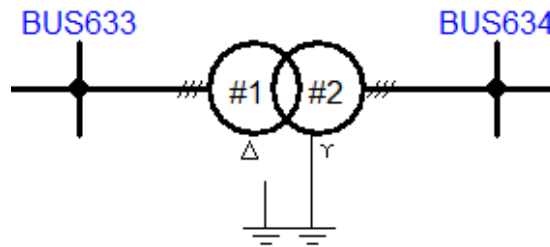
Figure 62: Regulator Data

Regulator ID:	1		
Line Segment:	650 - 632		
Location:	50		
Phases:	A - B -C		
Connection:	3-Ph,LG		
Monitoring Phase:	A-B-C		
Bandwidth:	2.0 volts		
PT Ratio:	20		
Primary CT Rating:	700		
Compensator Settings:	Ph-A	Ph-B	Ph-C
R - Setting:	3	3	3
X - Setting:	9	9	9
Voltage Level:	122	122	122

Transformer

There is one transformer in the IEEE 13 node test feeder system.. The data necessary to model this transformer was found in the IEEE report in table form (Figure 64). Figure 63 is a snapshot of the transformer model used in PSCAD.

Figure 63: Transformer Model in PSCAD



Transformer data from the IEEE report is given in Figure 64:

Figure 64: Transformer Data

	kVA	kV-high	kV-low	R - %	X - %
Substation:	5,000	115 - D	4.16 Gr. Y	1	8
XFM -1	500	4.16 - Gr.W	0.48 - Gr.W	1.1	2

All additional information needed to model the transformer was found also in the IEEE report as shown below. This data primarily provided the location of the device, between busses 633 and 634.

NODE	VALUE	PHASE A (LINE A)		PHASE B (LINE B)		PHASE C (LINE C)		UNT	O/L< 60.%
		A	B	A	B	A	B		
NODE: XFXFM1	VOLTS:	.994	-3.23	1.022	-122.22	.996	117.35	MAG/ANG	
	-LD:	.00	.00	.00	.00	.00	.00	kW/kVR	
kv11	.480	CAP:	.00	.00	.00	.00	.00	kVR	
FROM NODE 633:	704.83	-37.74	529.73	-159.09	543.45	80.47	AMP/DG <	
<XFXFM1> LOSS=	5.427:	(2.513)		(1.420)		(1.494)		kW	
TO NODE 634:	704.83	-37.74	529.73	-159.09	543.45	80.47	AMP/DG <	
<634 > LOSS=	.000:	(.000)		(.000)		(.000)		kW	

4.2 CONVERTER PERFORMANCE, FUNCTIONALITY AND SPECIFICATIONS

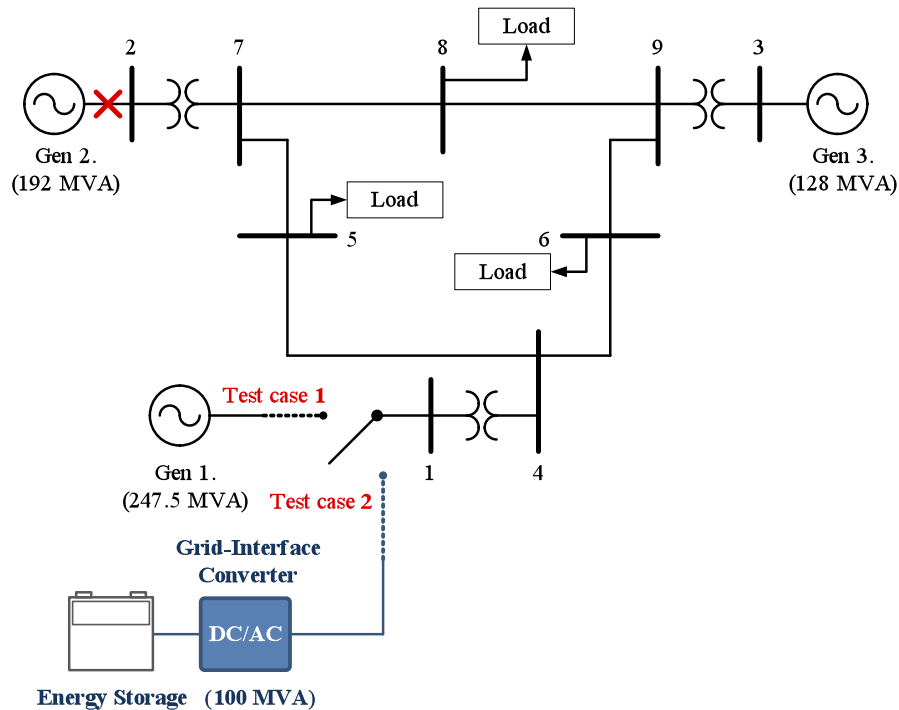
The models described in the section above have been built for the purpose of performing system-level simulations and exploring the dynamic behavior of the grid-interface converter and the system it connects to (here WECC 9-bus system). Two scenarios have been explored either using

elements of the above described models, or combining them into the different groups. Both scenarios are described in this section.

4.2.1 Scenario I

This scenario explores how grid-interface converter can support the grid stability during the loss of generation. Figure 65 shows the one line diagram of the simulation model used for this purpose.

Figure 65: WECC 9-bus system in the loss of generation scenario



The first simulation performed (Test case 1) was the loss of generation (generator 2 off) in the original WECC 9-bus system when both, generator 1 and generator 3 were connected to the system (no grid-interface converter added at this point). Generator 2 was disconnected from the system at 5s. The following figures show the time domain waveforms of active and reactive powers as well as the power angles of the remaining two generators (Gen 1 and Gen 2) as a result of the imposed transient.

Figure 66: Generator 1 active and reactive power waveforms before and after the transient (Generator 2 disconnected at 5s)

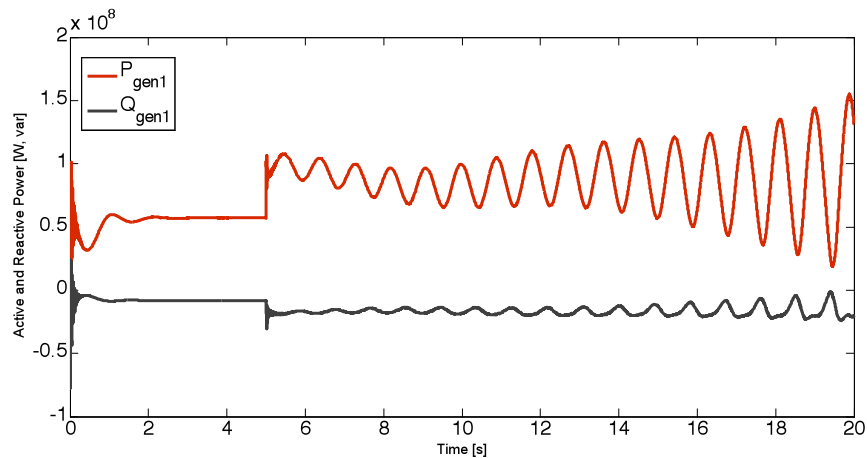
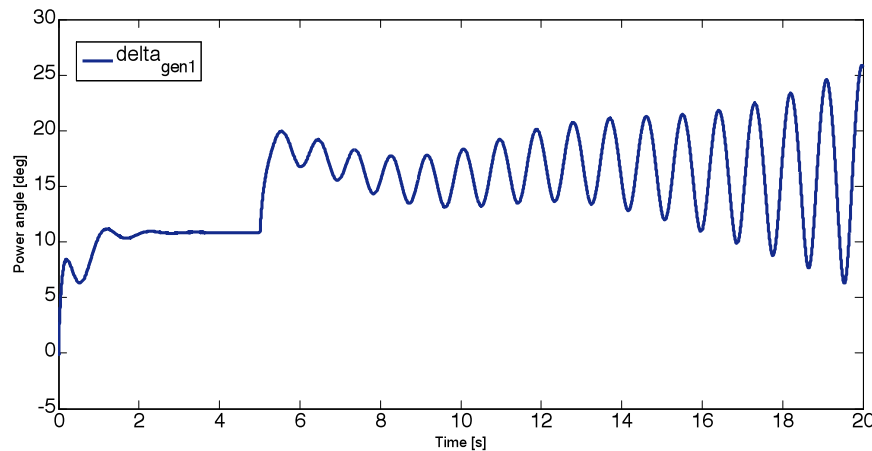


Figure 67: Generator 1 power angle before and after the transient (Generator 2 disconnected at 5s)



It is evident that the low-frequency instability (swinging) started happening after the transient at 5s. The generator was uncontrollably oscillating regardless of the fact that the total load demand was way below their power capabilities.

The turbine time constant ($\tau_{turbine}$ shown in Figure 12) played the major role in this instability scenario. The bigger it is, the more severe instability occurs. The similar behavior can be observed in the following figures showing dynamics of the generator 3 after this transient.

Figure 68: Generator 3 active and reactive power waveforms before and after the transient (Generator 2 disconnected at 5s)

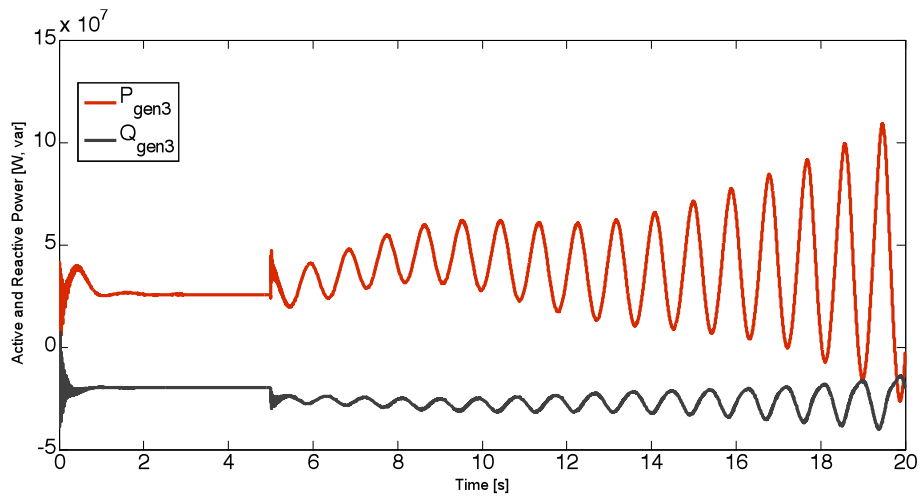
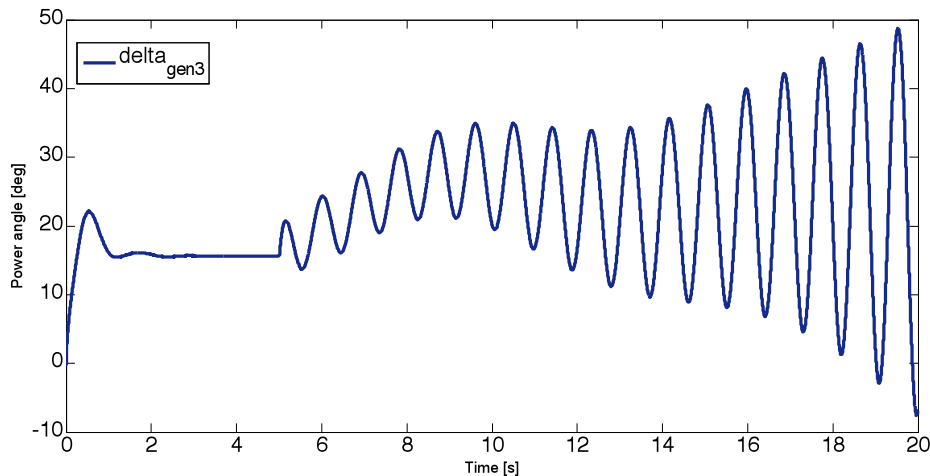


Figure 69: Generator 3 power angle before and after the transient (Generator 2 disconnected at 5s)



The next simulation performed (*Test case 2*) was the same loss of generation (generator 2 off) in the WECC system when generator 3 was connected to the system at its bus No.3, but instead of the generator 1, grid-interface converter was connected at the bus No.1.

It should be noted that in this scenario, model D (section 1.3.4) of the power converter was used.

The same transient as in the *Test case 1* (disconnecting generator 2 at 5s) was then repeated and the waveforms captured. Below shown are the active and reactive power, and power angle waveforms of the generator 3 before and after the transient.

Figure 70: Generator 3 active and reactive power waveforms before and after the transient (Generator 2 disconnected at 5s)

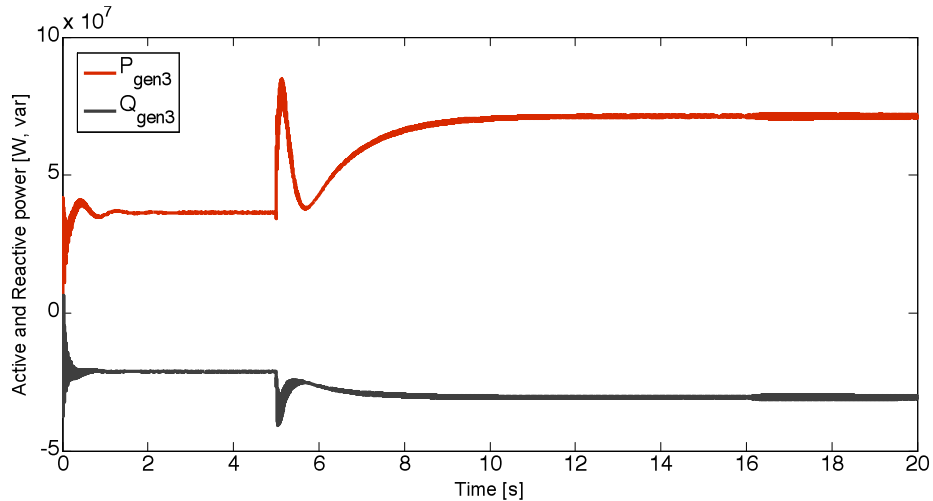
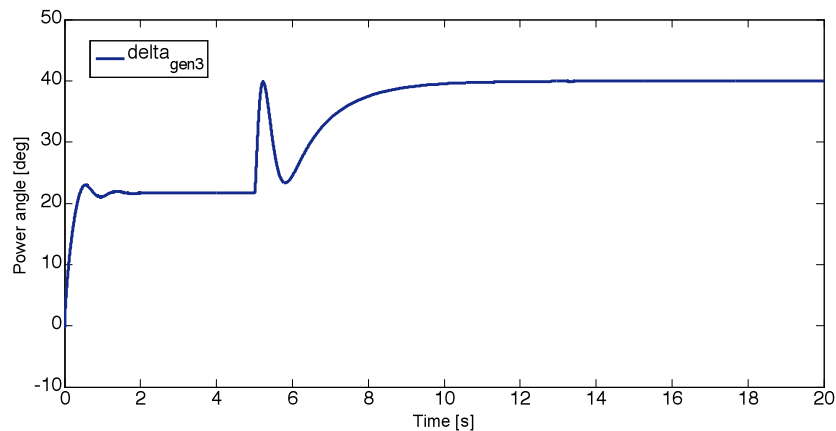


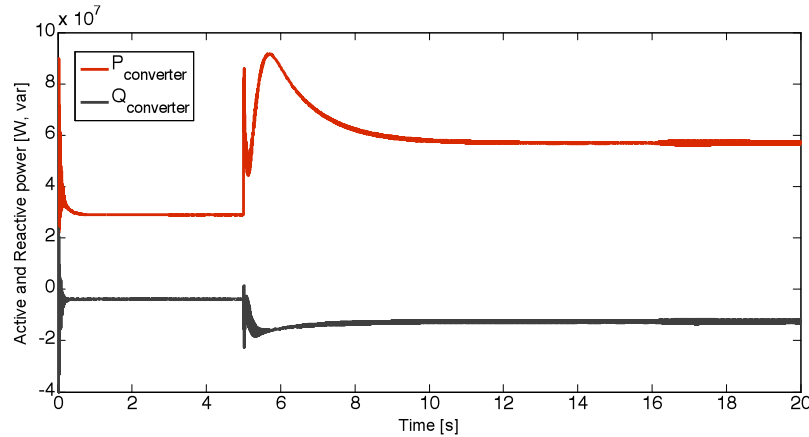
Figure 71: Generator 3 power angle before and after the transient (Generator 2 disconnected at 5s)



It is evident that the loss of generation transient did not cause instability in the system this time when grid-interface converter was connected to the system; although more than two times smaller source in terms of its power capability, it had a significant stabilizing effect due to its fast response.

Figure 72 below shows a grid-interface converter’s active and reactive power waveforms during this transient.

Figure 72: Grid-interface converter active and reactive power waveforms before and after the transient (Generator 2 disconnected at 5s)



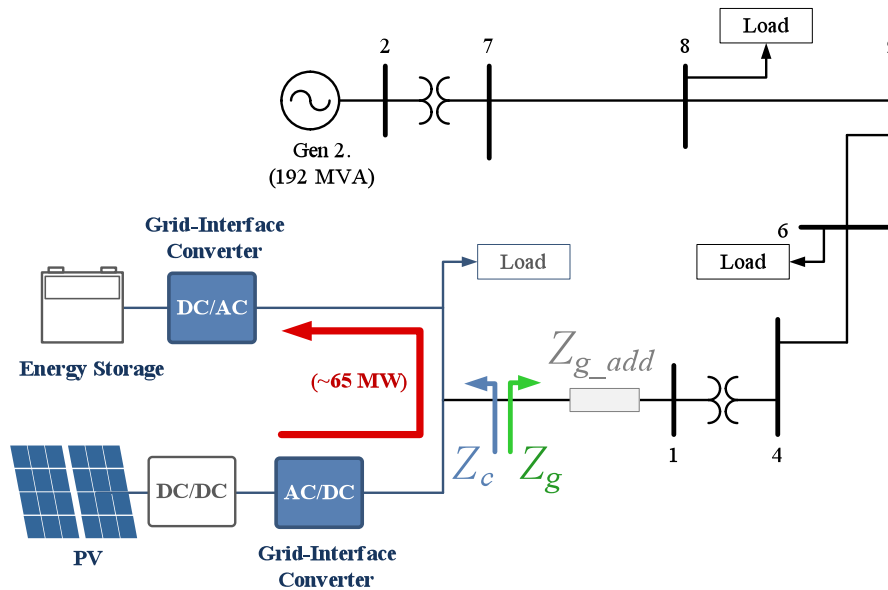
Deliverables:

MATLAB (Simulink /SimPowerSystems) model for the scenario I (Figure 65). The model called “**loss_of_generation.mdl**” has been uploaded to the NETL members SharePoint website. Please note that the model initialization *m*-file “**init_file.m**” has to be run before starting the model.

4.2.2 Scenario II

This scenario explores dynamics of two grid-interface converters connected to the reduced WECC system at the bus No.1 as show in Figure 73.

Figure 73: Reduced WECC 9-bus system with two grid-interface converters



The reason for reducing the WECC 9-bus system is to show how grid–interface converters (operating as current sources) behave under weak grid condition. Grid-interface converter model C (section 1.3.3) was used for this purpose.

Scenario is the following: PV system is delivering about 65MW of power to the energy storage system (e.g., charging the batteries). All the power produced by PV is delivered to the energy storage, and none is going to the rest of the system (WECC). Voltage at the bus No.1 is regulated by generator No. 2 only. Two converters’ PLLs feature slightly different PLLs with the following PI parameters:

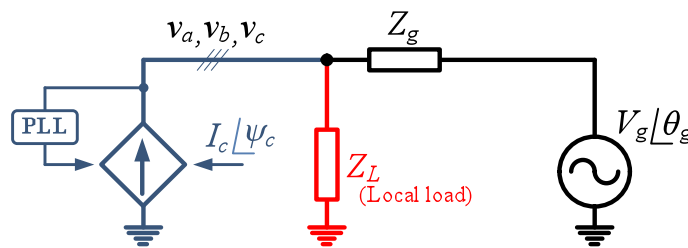
$$PI_{Conv1PLL} = \frac{0.5 + 0.5s}{s}$$

$$PI_{Conv2PLL} = \frac{3.2 + 0.1s}{s}$$
(12)

----- A digression -----

In order to understand dynamics of above described system, condition for PLL-caused instability will be considered here.¹⁸ As shown in this reference, (synchronous reference frame) PLL model including grid output impedance inherently comprises negative and positive feedback loop. PLL can thus become unstable if (13) is not satisfied. Figure 74 shows simplified circuit that corresponds to the given criteria.

Figure 74: One-line diagram of the grid-interface converter connection to the grid – given here for better understanding of condition (13)



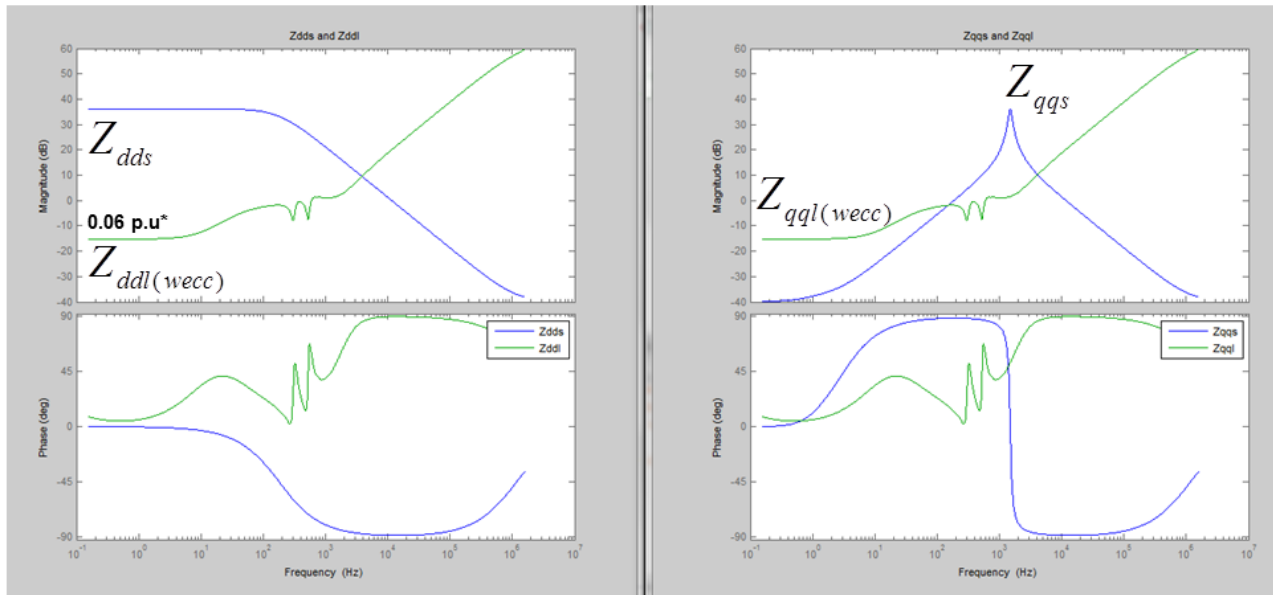
The system will be stable if:

$$(13)$$

¹⁸ D. Dong, L. Jin, D. Boroyevich, P. Mattavelli, I. Cvetkovic, and X. Yaosuo, "Frequency behavior and its stability of grid-interface converter in distributed generation systems," in *Applied Power Electronics Conference and Exposition (APEC), 2012 Twenty-Seventh Annual IEEE*, 2012, pp. 1887-1893.

To obtain the reduced WECC system output impedance (Z_g), system was linearized in MATLAB and the following bode plots of the grid output impedances in $d-q$ were obtained at the point between the bus No.1 and the power converters as depicted in the Figure 73. Due to the symmetry, only dd and dq impedances are shown below.

Figure 75: Reduced WECC system (—), and the equivalent source (—) output impedances in $d-q$



*0.06 p.u. \sim 0.2 Ω

It can be seen that the dc-gain of the grid output impedance is still very small to cause any instability according to (13).

Thus, additional series impedance Z_{g_add} had to be added in order to increase total output impedance of the reduced WECC system and start causing severe dynamics interactions (instability) in the system. The following figures show this PLL-caused instability when grid output impedance became very high at 1s (in this case Z_{g_add} was 400 Ω , or about 120 p.u.). This is not quite realistic to happen in practice during normal system operation, but can be regarded as a system islanding case confirming that the islanded systems cannot work stable with all converters behaving as current sources (what is today a practice when renewable energy and distributed generation are concerned). There must be either synchronous generator, or much more preferably, a grid-interface converter performing voltage regulation in the isolated subsystem.

Figure 76 shows active and reactive power of two grid-interface converters before and after the grid output impedance had increased. It can be seen that the converter 1 interfaced to PV was delivering 65 MW to the energy storage system before the transient. Reactive power was negligible slow due to the accurate information about the grid frequency / phase provided to current sources by their PLLs.

Figure 77 shows angular frequencies of both PLLs before and after the transient. The instability is evident.

Figure 76: Active and reactive power of the two grid-interface converters before and after the transient (increasing grid output impedance at 1s)

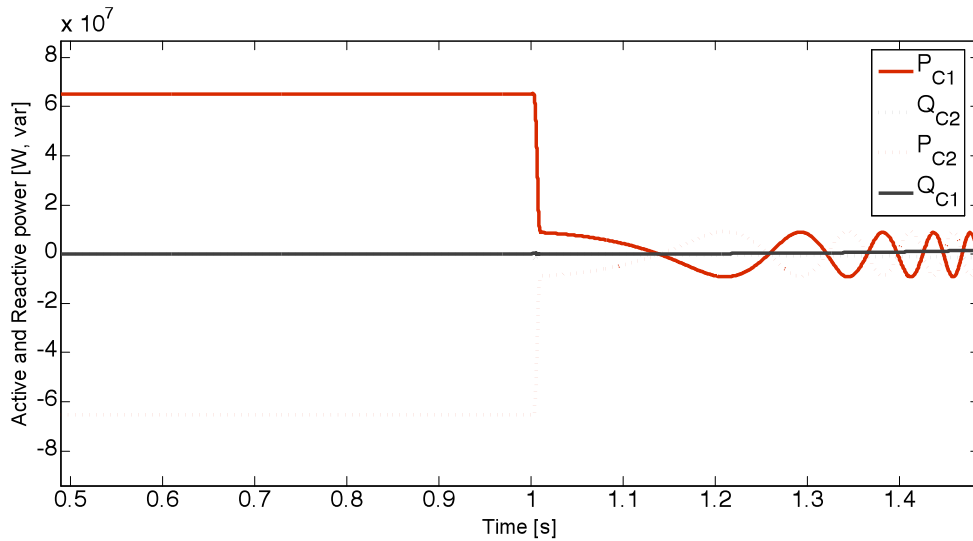
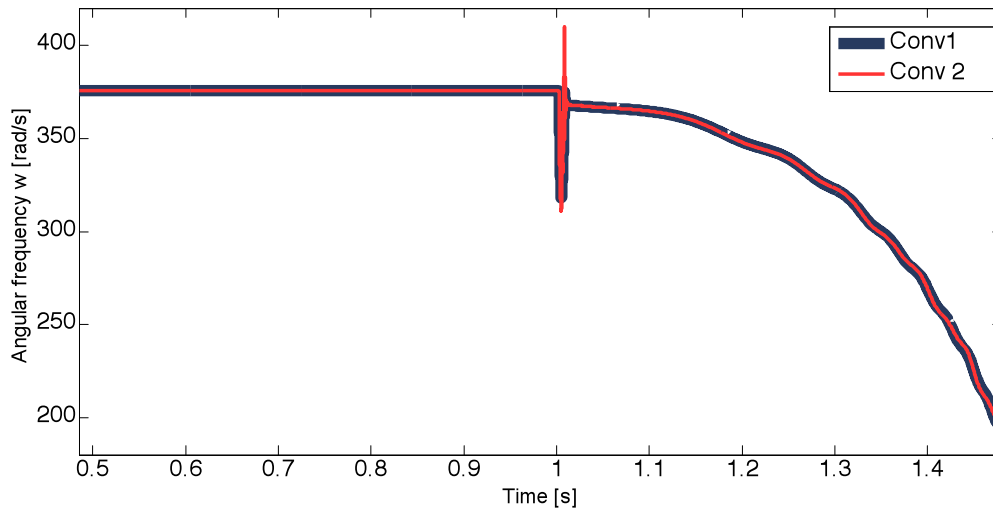


Figure 77: Angular frequencies of both converters' PLLs before and after the transient (increasing grid output impedance at 1s)



Deliverables:

MATLAB (Simulink /SimPowerSystems) model for the scenario II (Figure 73). The model called “**pll_instability.mdl**” has been uploaded to the NETL members SharePoint website. Please note that the model initialization *m*-file “**init_file.m**” has to be run before starting the model.

4.3 COMMUNICATIONS AND INTERFACE PROTOCOLS

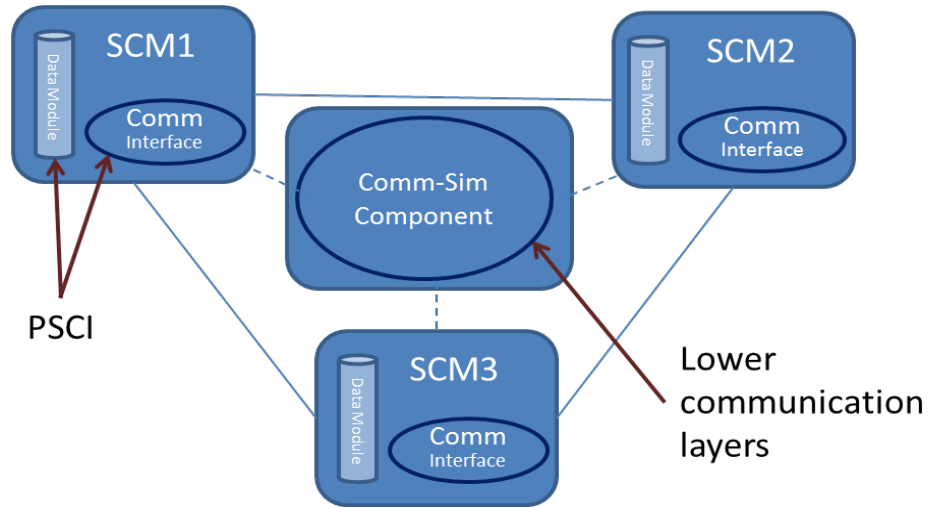
The work presented in this project complements the existing methods and takes a different approach by providing an embedded simulation environment inside the widespread commercially available tool PSCAD. PSCAD is a framework currently used in study of dynamic behavior of power system components and transient phenomena. It can be used widely in assessment of renewable energies integration as well as evaluation of control strategies in power system. In this study we are using the existing time steps in PSCAD transient power simulator and couple the discrete event-based simulation of communication network at these time steps. So the high level idea of this work is to couple the communication simulator with power system simulation by implementing the network simulator within PSCAD and trying to imitate discrete event-based behaviors by using available capabilities inside PSCAD rather than going outside.

The importance of studying communication in accordance with power systems simulations is the impact of communication on the whole system from control and stability standpoint. These effects are mostly caused by network effects such as delay and loss. It is important to note that all the complexity involved in complete network simulators will end up in a list of events obtained from the simulator with their timestamp. These events are at high level packets sent, the time taken for each packet to be received (delay) and whether it is received at receiver or not (loss). Therefore, one main focus of this study was on simulating these network effects (seen in the form of delay and loss pattern profiles) within the PSCAD. In addition to these two elements, delay and loss, which were defined at lower levels of communication, each communication network at application layer features a communication protocol (how to establish communication) and communication strategy (when and where to communicate) defined for the entities to be able to communicate. The communication is established through protocols, and nodes act according to the accepted strategy to communicate. All these elements have been considered in the architecture introduced for this study; allowing almost any protocol and strategy to be implemented on top of the framework provided here. The other important problem is designing a point of integration between power system simulation and communication simulation. This is considered as communication interface within PSCAD which will be introduced and explained in the next section.

Power System Communication Interface Design

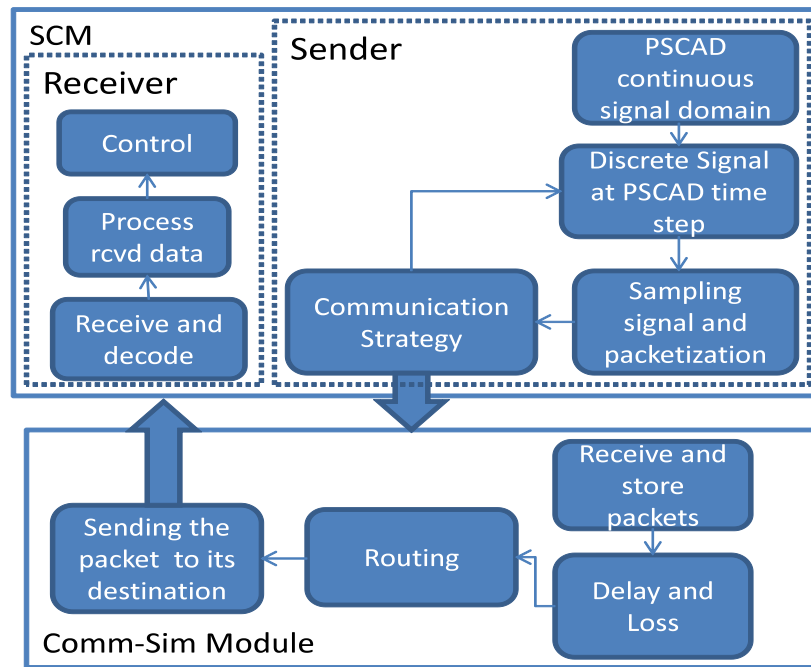
The communication interface in PSCAD can be separated into Application layer communication interface and lower level communication. The application layer interface is implemented in Sensor Control Modules (SCMs) while the lower level communication simulation has been implemented in Comm-Sim Component. These modules schematic can be viewed in Figure 78. SCMs are the points of communication which will need communication to mainly control the stability of the system. SCMs are basically regular modules within PSCAD which have Comm-Modules inside them as communication points.

Figure 78: Communication interface design within PSCAD, The whole system schematic



The nature of communication is discrete and event based, but in PSCAD we are dealing with a continuous time simulation process and consequently continuous signals. Therefore, the SCMs need to bring that continuous domain into discrete domain by use of sampling and then asynchronous packetization. This sampling mechanism is one of the most important features of the Comm-Modules within SCMs.

Figure 79: Communication network architecture coupled with PSCAD continuous time domain

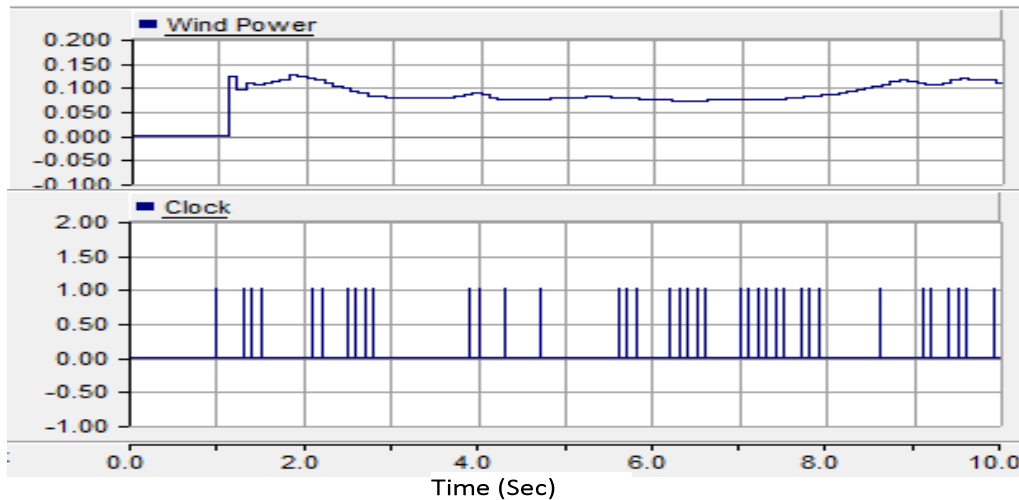


In real communication networks connected nodes send out their packets based on a communication strategy; they look at the values at a single point in time (sampled value) and perform some processing (for control purposes) and send out the packet if it is necessary. The same design has been considered in this work. The packet containing the sampled and processed data will be sent through Comm-Sim module to its destination. In Comm-Sim module, packets are stored and will be sent to the indicated receiver based on configurable delay and loss. The packet is received at its destination in a discrete fashion and will be decoded based on DNP-3 protocol data formats. The communication interface being applied so control will be performed, the control parameters will be taken out of the packet, processed according to the control being applied and then control actions will be performed in the destination SCM. The overall design of the communication interface can be seen in Figure 79.

Sensor Control Modules (SCM)

As described previously, these modules will be placed within the whole system and wherever communication is needed. The SCMs are the simulation of the application layer communication of the whole communication interface. Application layer interface consist of communication protocol and strategy. The communication protocol implemented in this study is DNP-3. The other element is communication strategy which can be applied by user and based on type of control. The SCMs are combination of a module within PSCAD, which has been chosen for communication, and a Comm-Module which is the point of communication for that SCM, this module can be interpreted as communication device installed on any element in the power system, such as storage or wind generator. SCMs are needed to be placed at both sender and receiver; the main functionality of these modules can be named as discretization, packetization, processing and making the decision to send out the packet or not based on communication strategy. At receiver side, they receive the packet decode it and wrap all the control variables based on DNP3 protocol and put them in a Fortran structure and do the control at receiver using these received data.

The sender can configure a sampling rate for the Comm- Module to sample the control variables, process and possibly reduce them to fewer numbers of control values and then put them into the packet for being sent over the communication network. These packets will then be sent based on communication strategy. In PSCAD we are working with continuous time signals as communication links. These signals are being sent using radio link components in PSCAD which have only the capability of sending continuous signals rather than discrete ones. Therefore, to determine the event of sending a packet we are using a clock which will be sent along with packets to the Comm-Sim module and the receiver consequently. This clock has an important role in packetizing process and will help simulate discrete events of communication coupled with this continuous time domain simulator. This can be observed for a sample case in Figure 80.

Figure 80: An example of sampled signal along with its clock signal

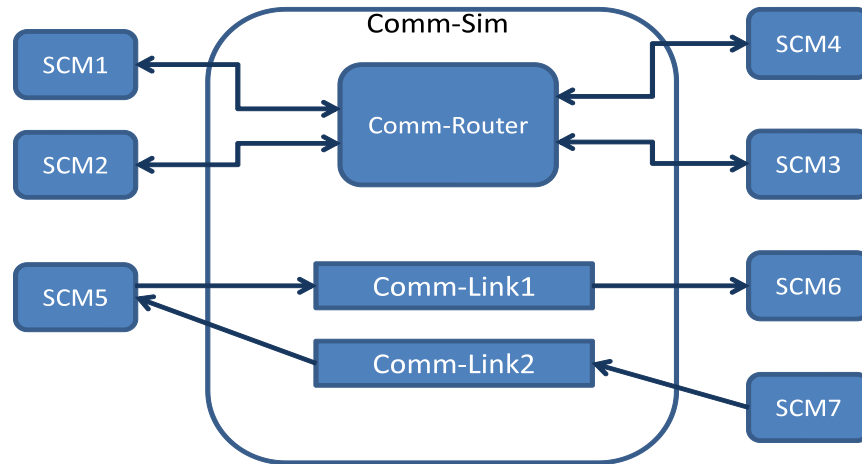
Communication Simulator Module

The Lower level of communication network has been designed as a separate module within PSCAD named Comm-Sim Module Figure 81. This module is designed to simulate lower layers of communication network while allowing the use of typical topologies in a communication network. There are two components within this module named Comm-Router and Comm-Link. Comm-Link component acts like a simple communication link and simulate a Point to Point (P2P) connection between 2 different SCMs.

This component simulates the network by applying delay and loss on the packets sent through this component. The delay value can be configured to be a fixed value, or it can be set to be a random value in a specified range, or it can be read from a delay profile; this profile can be simply a text file containing delay values obtained from a network simulator like NS3 or OPNET. The loss is applied by sending out a single packet to its destination or not. Loss is considered as one of the vulnerabilities of the communication network which should be considered in its simulation within PSCAD. The loss can be configured as random or it can be based on a profile, driven from a network simulator as well.

Comm-Router component is used for having more complex topologies than a simple P2P connection. Using this component user can set up links between different SCMs and allow sending from any of them to any other SCM while this component allows broadcasting too, so any of the SCMs can send a packet to all other SCMs connected to the Comm-Router.

Figure 81: Comm-Sim module components and how they can be used to have different network topologies



Case study: IEEE 13 Node Test Feeder

The IEEE 13 node feeder is used as a test platform to study the effects of communication in power systems.¹⁹ The test feeder is simulated in two versions of PSCAD 4.2 and X4. Both versions have been uploaded to the NETL members SharePoint website as IEEE_13Nodes_Test_Feeder_WVU* and IEEE13_node_Model_Roopa, respectively. The PSCAD X4 version was exclusively used in the communication studies. The test system also consists of a wind turbine connected to an induction generator at feeder 675. A storage component with a bidirectional converter is also connected to feeder 675.^{20,21} The storage component capacity is designed to absorb the power generated by the wind generator. The storage component stores the real power generated by the wind turbine and provides power when real power produced by the wind decreases. The converter is designed in such way as to control the direction of power flow either into the storage component or out of it. The converter control compares the wind power and the power from the storage and generates a reference current signal which determines the direction of power flow across the converter.

Initially the wind speed is kept constant at 6m/s and then stepped up to 20m/s. After 2 sec the wind speed is stepped down to 10 m/s. These values are chosen only to see the effect of communication in two different cases, when there is a step up in wind speed from low value to a high value and the step down in wind speed from high value to an average value. The turbine torque and the real power generated by the wind generator vary according to the wind speed. The wind power goes from -4 p.u. to 0.65 p.u. and then to -0.5 p.u. In the case of ideal

¹⁹ IEEE 13 Node Test Feeder. Available at: <http://ewh.ieee.org/soc/pes/dsacom/testfeeders>

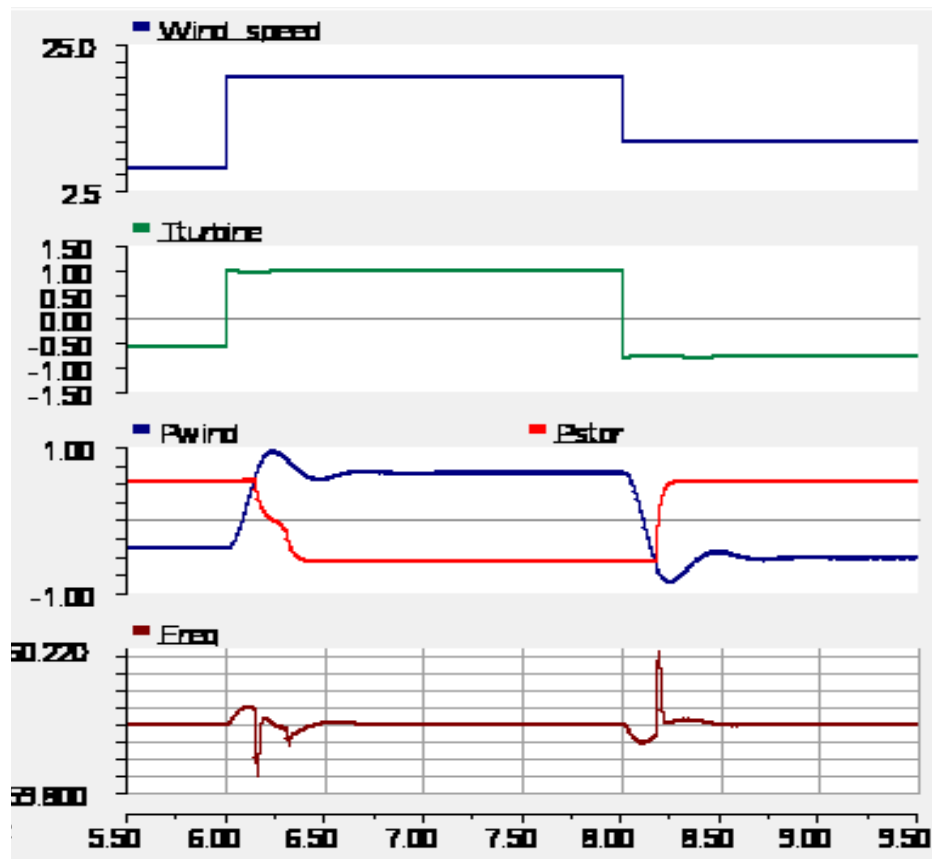
* contribution of WVU Research Assistant Professor Jignesh Solanki

²⁰ Mohamed, M. Elshaer, and O. Mohammad, "Bi-Directional AC-DC/DC-AC Converter for Power Sharing of Hybrid AC/DC Systems," in *2011 IEEE Power and Energy General Society Meeting*, pp. 1-8.

²¹ M. Hilal, M. Maaroufi, and M. Ouassaid, "Doubly Fed Induction Generator Wind Turbine Control for a Maximum Power Extraction," in *2011 International Conference on Multimedia Computing and Systems*, pp 1-7.

communication, a radio link is used to communicate the real power generated by the wind generator module to the storage converter module. Initially the wind component acts as a load due to the low wind speed. The storage component provides the necessary power to keep the system stable at a frequency of 60 Hz. When the wind steps up, the wind power increases to 0.65 p.u. and this power is stored in the storage component. During this time the frequency at the point of grid integration deviates from 60 Hz and comes back in about 0.5 seconds as shown in Figure 82. Similar results can be seen when the wind speed changes from 20m/s to 10m/s.

Figure 82: Wind Speed, Turbine Torque, Wind Power, Storage Power and Frequency for ideal communication



The ideal communication link is replaced with a Comm-Sim module which communicates the real power generated by the wind generator to the converter control circuit in the storage component at different delays and packet loss. Comm-Module samples the signal at a desirable rate and then the SCM decides whether to send the sample out or not. The sampling rate of the Comm-Module is given as 10 samples per second and the loss is considered as random loss. Here wind generator and storage modules are the two SCMs.

At delay equal to 0.1 and 0.5, the control signal at the storage SCM is delayed due to the delay in communication and hence the instant at which the power flow direction changes is delayed. The effect of this delay can be seen in the storage power signal represented as P_{stor} in

Figure 83, Figure 84 and Figure 85. The frequency also deviates from the steady state value for about 0.6 seconds for 0.1 delay and approximately 0.9 seconds for delay equal to 0.5 as shown in Figure 82 and

Figure 83. The real power values of the wind generator communicated to the storage converter control through the Comm-Sim communication link is shown in Figure 84.

Figure 83: Wind and Storage Power, Frequency for 0.1 delay

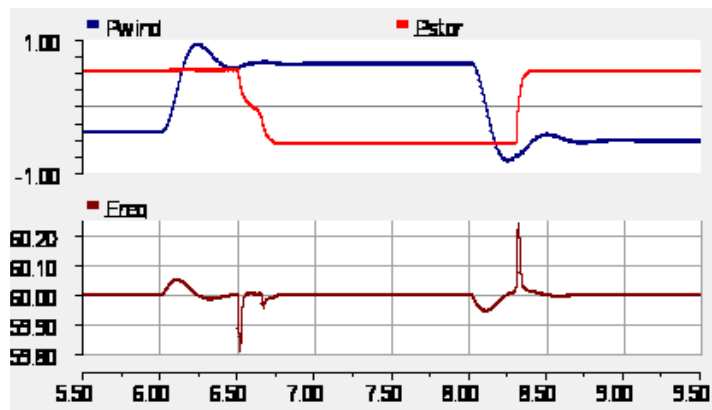


Figure 84: Wind and Storage Power, Frequency for 0.5 delay

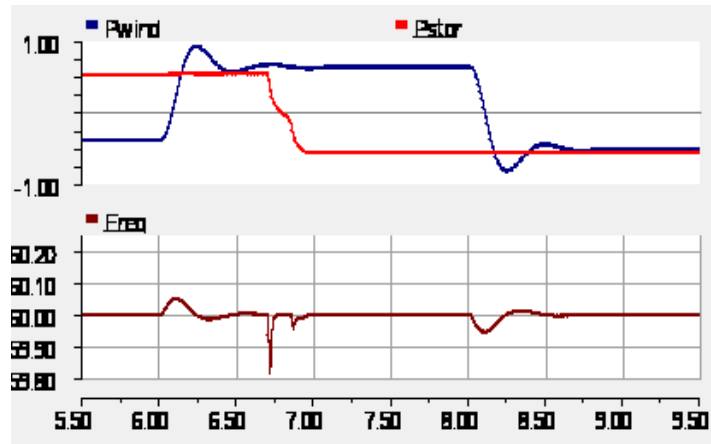
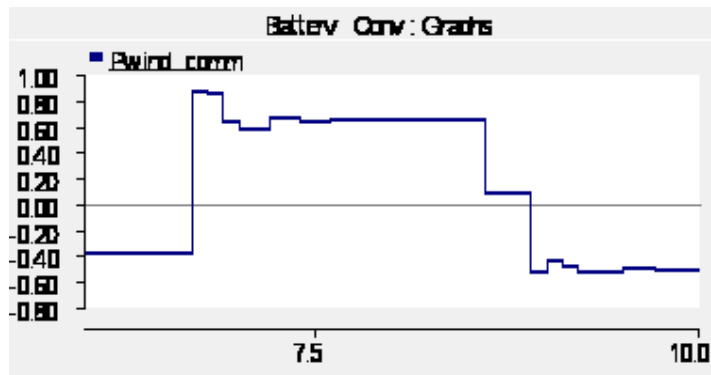


Figure 85: Wind Power Communicated to Storage component



In Figure 85 we are showing one instance of change and control action. For a dynamic situation where a controller should follow the change in wind generation, the larger delay will mean more prolonged frequency instability. Hence we can say that frequency instability increases for increased delay in communication. This effect will become more prominent in situations where the rate of change in wind speed is very high. Here we have demonstrated the implementation of the Communication Simulation module in a power sharing case, but since the module is very generic it can be extended to other applications of power system where communication is required.

4.4 SMART CONTROL METHODOLOGY

With the increased connection of variable and intermittent renewable energy sources (RESs) such as wind and solar, the energy management mechanism to avoid an unacceptable increase in frequency deviations becomes much more challenging and needs to be revisited due to the limited prediction accuracy for these resources. Most of the renewable energy sources cannot be dispatched like conventional generators because their power output is highly dependent on environmental factors such as wind speed and solar irradiation. On the other hand, the fast ramping required for conventional generators to follow the RES power variations is increased significantly due to their variable and intermittent nature, which greatly increases wear and tear losses of the generating units.

The emerging large scale energy storage technologies together with the energy converters are being recognized as a natural fit to overcome the challenges related to these variable and intermittent energy sources and have received increased attention. However, the question is how these new devices fit into the operational structure of power systems, which has evolved over decades without consideration of large scale storage. Not only the power limits but also the energy limits on energy storage devices have to be taken into account.

The main effort with regards to the development of smart control methods is focused on the energy management problem on multiple timescales to coordinate energy storage and intermittent resources and conventional generation. We re-categorize the multi-timescale energy management into two levels: real-time frequency control and advanced economic dispatch. The level of real-time frequency control incorporates the main functions of the traditional primary control and secondary control and additionally takes into account the storage model and limits, while advanced economic dispatch on the timescale of several minutes is designed to optimally schedule generation and storage to serve the forecasted system demand in the most economical manner subject to various physical constraints and uncertainties of renewable generation.

Another relevant question that must be addressed with regards to the inclusion of energy storage devices into a power system is that of their energy and power ratings. How much capacity is needed to integrate intermittent resources into the system and reduce the overall cost of generation while taking into account the operational losses and capital cost of storage? Where is the most optimal location for storage devices when taking into account line congestions and generator limits? Thus, the problem of optimal sizing and placement of storage devices is also investigated as a complementary research topic to the development of the energy storage enabled smart control methodology.

Real-time Frequency Control

Overview

This section describes a novel H_∞ -based and structure-preserving approach called advanced frequency control (AFC) to integrate energy storage into the framework of real-time frequency control. Unlike the traditional frequency control investigation method where a uniformed frequency is assumed within each control area, the structure-preserving approach utilizes the power flow model to connect different components in the control area retaining the frequency information at each individual generator bus. Under AFC, the power balancing responsibilities between two types of resources are divided according to their capabilities, i.e. the conventional generators are mainly responsible to balance the low frequency components of the RES and load variations whereas the energy storage devices are employed to alleviate high frequency components. Such a frequency differentiated power balancing scheme essentially enables effective state-of-charge (SOC) regulation as the storage largely compensates high frequency power variations. Another benefit is that the required ramp rates from conventional generators and therefore the associated wear and tear effects on generators are reduced.

Modeling

The state-space structure-preserving model needed for control design is derived in this section based on component-level models and the DC power flow model. Component-level models include models of conventional generator, energy storage device, and RES generator.

The model of the conventional generator is a fourth order governor-turbine-generator model including the dynamics of the speed governor and the turbine²² and is given by

$$\begin{bmatrix} \Delta \dot{\omega} \\ \Delta \dot{\theta} \\ \Delta \dot{P}_m \\ \Delta \dot{Y} \end{bmatrix} = \begin{bmatrix} \frac{-k_D}{2H} & 0 & \frac{S_N}{2HS} & 0 \\ \omega_0 & 0 & 0 & 0 \\ 0 & 0 & \frac{-1}{T_{CH}} & \frac{1}{T_{CH}} \\ 0 & 0 & 0 & \frac{-1}{T_G} \end{bmatrix} \begin{bmatrix} \Delta \omega \\ \Delta \theta \\ \Delta P_m \\ \Delta Y \end{bmatrix} + \begin{bmatrix} 0 \\ 0 \\ 0 \\ \frac{1}{T_G} \end{bmatrix} [\Delta P_G^{ref}] + \begin{bmatrix} \frac{-S_N}{2HS} \\ 0 \\ 0 \\ 0 \end{bmatrix} [\Delta P_e]$$

The parameters and variables in this model are:

²² P. Kundur, *Power system stability and control*, McGraw-Hill, USA, 1994.

S_N : power network VA base	S : generator VA base
H : inertia constant based on S	ω : rotor speed
Δ : deviations from operating point	θ : voltage angle in radians
P_m : mechanical power	P_e : electrical power
k_D : damping factor	T_{CH} : turbine time constant
Y : valve position	T_G : governor time constant
P_G^{ref} : control input	ω_0 : nominal speed in rad/sec

We denote the state space model of the i th conventional generator in a compact form as

$$\dot{x}_{G,i} = A_{G,i} \cdot x_{G,i} + B_{G,i} \cdot u_{G,i} + E_{G,i} \cdot P_{e,i}$$

The storage device consists of the actual storage and the power electronic inverter connecting the device to the grid. The model for the storage captures the relationship between charging/discharging power and the energy level. The dynamics of the inverter can be modeled using a first order model with time constant T_S capturing the response of the inverter to the control signal. Hence, the model for the storage device is given by²³

$$\begin{bmatrix} \Delta S \dot{O}C \\ \Delta \dot{P}_S \end{bmatrix} = \begin{bmatrix} 0 & \frac{-1}{E_{cap}} \\ 0 & \frac{-1}{T_S} \end{bmatrix} \begin{bmatrix} \Delta SOC \\ \Delta P_S \end{bmatrix} + \begin{bmatrix} 0 \\ \frac{1}{T_S} \end{bmatrix} [\Delta P_S^{ref}]$$

where the parameters and variables are:

E_{cap} : energy capacity in p.u.sec	T_S : inverter time constant
Δ : deviations from operating point	SOC : state of charge
P_S : storage power injection	P_S^{ref} : control input

We further denote this reduced order model of the i th storage device in a compact form as

$$\dot{x}_{S,i} = A_{S,i} \cdot x_{S,i} + B_{S,i} \cdot u_{S,i}$$

Regarding the renewable resources (RES), the main focus is on wind and solar generation. Most of the modern wind and solar generation types such as doubly fed induction generator and photovoltaic generator are connected to the grid via power electronics.²⁴ Typically, these power electronic devices are controlled by the maximum power point tracking algorithm to maximize

²³ T. Goya, E. Omine, Y. Kinjyo, T. Senjyu, A. Yona, N. Urasaki, and T. Funabashi, "Frequency control in isolated island by using parallel operated battery systems applying H infinity control theory based on droop characteristics", *IET Renewable Power Generation*, vol. 5, no. 2, pp. 160–166, 2011.

²⁴ J. M. Carrasco, L. G. Franquelo, J. T. Bialasiewicz, E. Galvan, R. C. P. Guisado, Ma A. M. Prats, J. I. Leon, and N. Moreno-Alfonso, "Power-electronic systems for the grid integration of renewable energy sources: A survey", *IEEE Trans. Industrial Electronics*, vol. 53, no. 4, pp. 1002–1016, 2006.

the RES power output. In addition, usually wind and solar generators do not participate in frequency control. Hence, the RES generators are modeled as negative loads.

By stacking all the states of the dynamic components, we obtain the following preliminary model for the entire system:

$$\dot{x} = A_0x + B_0u + E_0h,$$

Where,

$$\begin{aligned} x &= [x_{G,1}^T, \dots, x_{G,N_G}^T, x_{S,1}^T, \dots, x_{S,N_S}^T]^T, \\ u &= [u_{G,1}, \dots, u_{G,N_G}, u_{S,1}, \dots, u_{S,N_S}]^T, \\ h &= [P_{e,1}, \dots, P_{e,N_G}]^T, \\ A_0 &= \text{diag}(A_{G,1}, \dots, A_{G,N_G}, A_{S,1}, \dots, A_{S,N_S}), \\ B_0 &= \text{diag}(B_{G,1}, \dots, B_{G,N_G}, B_{S,1}, \dots, B_{S,N_S}), \\ E_0 &= [F_0^T \quad 0_{N_G \times N_S}]^T, F_0 = \text{diag}(E_{G,1}, \dots, E_{G,N_G}), \end{aligned}$$

N_G and N_S are the number of generators and the number of storage devices, respectively.

Based on the DC power flow model, the electric power h produced by generators can be given as a linear function of the states x , control inputs u and RES disturbances w , i.e.

$$h = G_0x + H_0u + J_0w.$$

where G_0 , H_0 , J_0 are coefficient matrices derived from the DC power flow model. Hence, the structure-preserving state-space model of the entire system is

$$\dot{x} = Ax + B_1w + B_2u,$$

where $A = A_0 + E_0G_0$, $B_1 = E_0J_0$, $B_2 = B_0 + E_0H_0$. The model here is consistent with the standard H_∞ problem formulation.

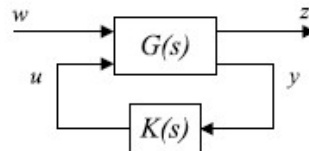
Control Design

H_∞ control is suitable for disturbance attenuation problems such as frequency control in power systems. Via the H_∞ control synthesis, the robustness and stability of a dynamic system subject to model uncertainties and/or bounded disturbances can be achieved simultaneously.²⁵

²⁵ K. Zhou, J.C. Doyle, and K. Glover, *Robust and Optimal Control*, Prentice Hall, 1995.

The standard configuration of the H_∞ control problem is depicted in Figure 86, where $G(s)$ is the transfer function of the plant, $K(s)$ is the transfer function of the controller, w is the exogenous input including disturbances, references and measurement noise, u is the control input, z is the performance vector that we want to minimize to satisfy the control objective and y is the measurement vector.²⁶

Figure 86: Standard H Infinity Problem Configuration



The objective of H_∞ control is to find the optimal stabilizing controller $K(s)$ that minimizes the H_∞ norm of the transfer function $T_{zw}(j\omega)$ from w to z , which is defined as the peak of the maximum singular value of the complex matrix $T_{zw}(j\omega)$ over all frequencies ω . Based on the specific design requirements and the focus of the exogenous input signals, weighting functions are typically assigned to the performance vector and the exogenous input to define the importance of the individual control objectives.

The objectives of the H_∞ -based AFC design are to minimize the influence of RES variations on frequency deviations and the state of charge deviations of the storage devices, and to achieve the frequency differentiated power balancing goal. The weighting functions for the frequency deviations and the state of charge deviations are chosen to be constant values, i.e. not frequency dependent. The values of these constants reflect the trade-off between tightly regulating the frequencies to their nominal values and to keep the SOCs of the energy storage devices close to a predefined value. The frequency differentiated power balancing goal is achieved by choosing frequency dependent weighting functions for the power output of the two types of resources. For the power output from the conventional generators, higher penalties are put onto the high frequency region so that by minimizing the weighted power output the generators are less responsive to the high frequency components of the RES disturbances. For the power injection of the storage devices, higher weights are put on the low frequency region, which forces the storage to be less sensitive to the low frequency components in RES fluctuations. The matrix-valued weighting functions are then realized and integrated into the system model. In order to reduce the complexity in controller implementation, the decentralized static output feedback is adopted to obtain suboptimal but decentralized and low order controllers. Once the controllers are designed, only local information is used as control input. For the conventional generator, this is the local frequency and the rotor angle which could also be derived as the integral of the local frequency. For the storage device, the measured values are the local frequency and the SOC. The control law for the i th generator and i th storage device under AFC is mathematically defined by

²⁶ K. Zhou and J.C. Doyle, *Essentials of robust control*, Prentice Hall, 1998.

$$\Delta P_{Gi}^{ref} = k_{1i} \Delta \omega_{Gi} + k_{2i} \Delta \theta_{Gi}$$

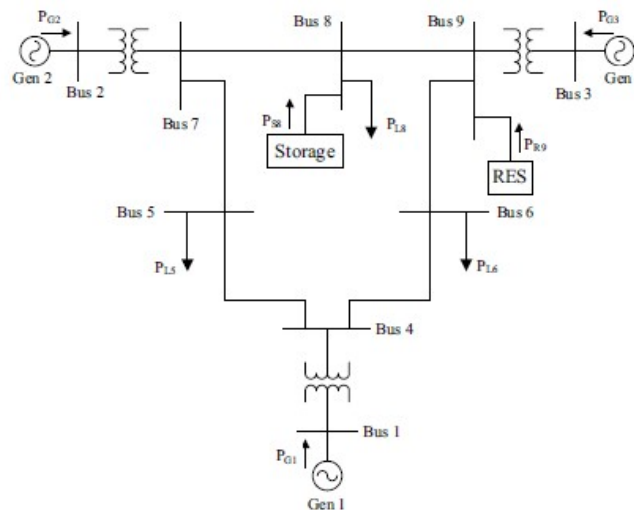
$$\Delta P_{Si}^{ref} = k_{3i} \Delta \omega_{Si} + k_{4i} \Delta SOC_{Si}$$

where the subscripts G_i and S_i denote the local information of the i th generator and the i th storage device, respectively. The weighted H_∞ problem with decentralized static output feedback is then solved by applying a linear matrix inequality algorithm.

Simulation

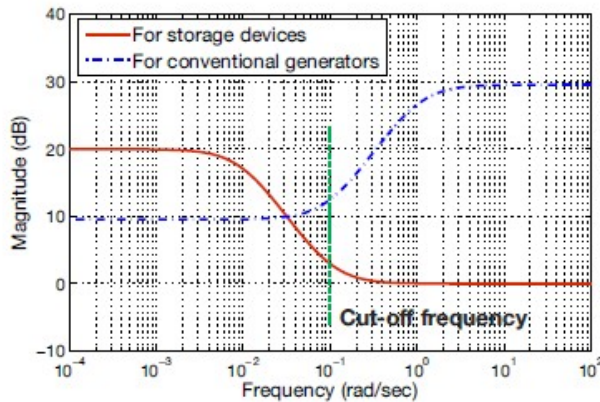
The proposed controllers are applied to the WECC 9-bus test system shown in Figure 87 to illustrate the performance of the AFC approach. The RES generator is installed at Bus 9 and the energy storage device is placed at Bus 8, which is a load bus. The RES variations are within about $\pm 5\%$ around the average value of 600 MW. The load is assumed to be constant with a total of 1,000 MW for the considered time frame. The base case corresponds to the situation where the traditional primary and secondary control is applied. The secondary control signal is set to be equally assigned to each conventional generator and the storage device. The base case is termed as CFC, i.e. conventional frequency control.

Figure 87: WECC 9-bus Test System



The frequency dependent weighting functions for generator and storage power output are shown in Figure 88. The separation frequency (cut-off frequency) of the frequency differentiated power balancing scheme is defined at 0.1 rad/sec.

Figure 88: Weighting Functions for Generator and Storage Power Output



The Bode magnitude diagram of the transfer functions from the RES disturbance w to the real power output of the three generators and the storage device is depicted in Figure 89. It is clear that the frequency differentiated power balancing objective is successfully achieved with the separation frequency at around 0.1 rad/sec. Moreover, the storage device in the base case acts like a conventional generator as it is simply requested to follow the secondary control signal.

Figure 89: Real Power Output in Frequency Domain

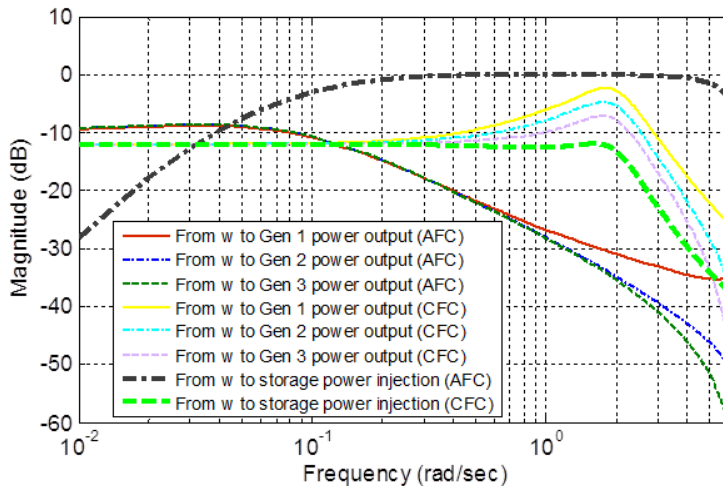
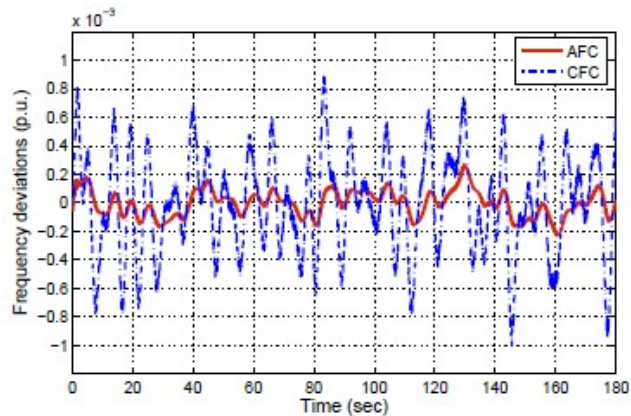
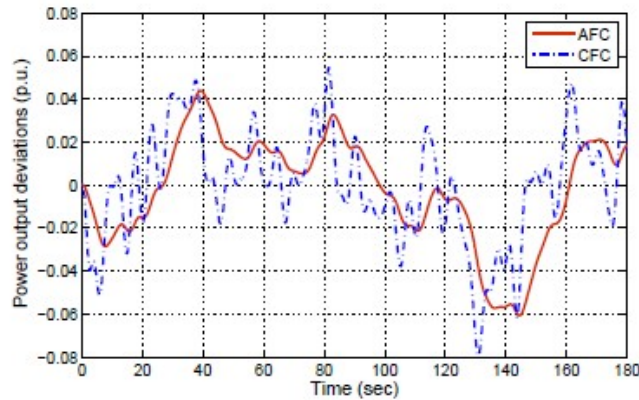
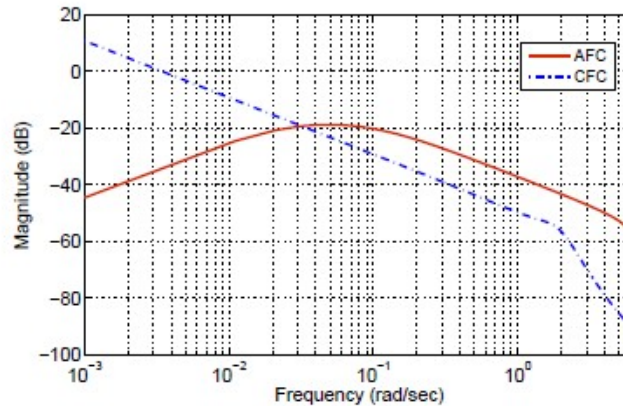


Figure 90 shows the comparison of frequency deviations at Bus 3 between AFC and CFC. The frequency deviations under AFC are further reduced and narrowed within a tighter band than the base case. The power output deviations of Generator 3 from its operating point are plotted in Figure 91. Similar power output deviation curves are observed for the other two generators. Compared to the base case, the power output of the three generators under AFC is smoothed out and high frequency fluctuations in the power output are greatly attenuated.

Figure 90: Frequency Deviations at Bus 3**Figure 91: Power Output Deviations of Gen 3 from the Operating Point**

The comparison of SOC between AFC and CFC in the frequency domain is plotted in Figure 92, showing the magnitudes of the transfer functions from the RES disturbance w to SOC under AFC and CFC over the entire frequency spectrum. It can be seen that the peak magnitude of the closed loop transfer function from disturbance w to SOC under AFC is bounded at around -20 dB. In contrast, there is no upper bound on the peak magnitude of the same transfer function under CFC. The SOC under CFC is prone to exceed its limit with the increase of the low frequency components in RES variations.

Figure 92: Bode Diagram of the Transfer Function from w to SOC

Advanced Economic Dispatch

Overview

This section addresses the energy management problem in the slower time scale. The advanced economic dispatch provides a promising solution to the emerging generation/storage dispatch problem in power systems under uncertainties introduced by renewable resources. The new economic dispatch problem with uncertainty is modeled as a two-stage stochastic model predictive control (SMPC) problem typically resulting in a large-scale optimization problem. The optimality condition decomposition technique is then employed to speed up the calculation of the large optimization problem by solving small subproblems in parallel.

Problem Formulation

The new generation/storage dispatch problem is casted as a two-stage scenario-based stochastic model predictive control optimization problem where a detailed energy storage model considering self-discharge and different conversion efficiencies for charge and discharge is employed to predict the SOC of the storage devices under different scenarios for variable generation. The decision variables are the storage charge/discharge rates and the power output of conventional generators for each scenario. The objective function in each scenario includes the generation costs and the ramping costs of conventional generators, and the costs for conversion losses of energy storage devices. The overall objective function is the sum of the scenario objective functions weighted by the probabilities of the corresponding scenarios. The storage model, the ramp limits of the conventional generators, the power balance equation, and the so-called nonanticipativity conditions compose the constraint set of the SMPC optimization problem. The nonanticipativity conditions are used to make sure that the decision variables in different scenarios at the first stage are identical.

The general form of the considered economic dispatch problem is mathematically formulated as:

$$\begin{aligned}
 & \min \sum_{s \in \Omega} \pi^s \cdot \sum_{k \in \Gamma} l^s[p^s(k), u^s(k)] \\
 & \quad x^s(k+1) = A_0 x^s(k) + B_0 u^s(k) \quad \dots (1) \\
 & \quad x^{\min} \leq x^s(k+1) \leq x^{\max} \quad \dots (2) \\
 & \quad 0 \leq u^s(k) \leq u^{\max} \quad \dots (3) \\
 & \quad p^{\min} \leq p^s(k) \leq p^{\max} \quad \dots (4) \\
 \text{s.t.} \quad & -RD \cdot T \leq p^s(k) - p^s(k-1) \leq RU \cdot T \quad \dots (5) \\
 & 1^T \cdot u^s(k) + 1^T \cdot p^s(k) + 1^T \cdot r^s(k) = 1^T \cdot d^s(k) \quad \dots (6) \\
 & f^{\min} \leq f^s(k) \leq f^{\max} \quad \dots (7) \\
 & u^i(0) = u^j(0), \forall i, j \in \Omega \quad \dots (8) \\
 & p^i(0) = p^j(0), \forall i, j \in \Omega \quad \dots (9)
 \end{aligned}$$

Where,

Ω : the set of scenarios,

Γ : the set of look-ahead time steps,

π^s : the probability of Scenario s ,

l^s : the objective function for Scenario s ,

p^s : the power output of generators in Scenario s ,

u^s : the power injection of storage devices in Scenario s ,

x^s : the SOC of storage devices in Scenario s ,

RD, RU : maximum rates of ramp down and ramp up for generators,

T : time step size,

r^s : the renewable generation in Scenario s ,

d^s : the load consumption in Scenario s ,

f^s : the line flows exclude the tie line flows in Scenario s .

The energy storage model is represented by (1)-(3), where (1) is the general formulation of the dynamics of the energy storage device. The generator model is given in (4)-(5). Constraint (6) is the power balance equation for the grid. The line flows are limited by (7). The nonanticipativity constraints are stated in (8)-(9).

The foregoing SMPC optimization problem possesses an underlying decomposable structure with complicating constraints stated in (8)-(9) such that the original problem can be decomposed into simple subproblems based on scenarios if the complicating constraints are relaxed. Thus, the primal dual decomposition techniques can be used to tackle the complicating constraints in the original problem by incorporating the complicating constraints into the objective function.

Optimality Condition Decomposition

Due to the large size of the yielding SMPC optimization problem, decomposition and parallel computing techniques have to be applied for the purpose of practical implementation. The decomposition method adopted in this report is the optimality condition decomposition.

The optimality condition decomposition (OCD) is an extension to the Lagrangian relaxation decomposition and used to decompose a large-scale optimization problem into smaller subproblems.²⁷ Consider the overall problem defined as:

$$\begin{aligned} & \min_{x_1, \dots, x_n} f(x_1, \dots, x_n) \\ \text{s.t. } & c_i(x_i) \leq 0, \quad i = 1, \dots, n \\ & g_i(x_1, \dots, x_n) \leq 0, \quad i = 1, \dots, n \end{aligned}$$

where x_i is the vector of decision variables assigned to the i th subproblem. Each subproblem has its own constraint set given in the first inequality. The second inequality which is called the complicating constraint depends on decision variables from multiple subproblems. The i th subproblem using OCD is formulated as:

$$\begin{aligned} & \min_{x_i} f(\bar{x}_1, \dots, \bar{x}_{i-1}, x_i, \bar{x}_{i+1}, \dots, \bar{x}_n) \\ & + \sum_{j=1, j \neq i}^n \bar{\lambda}_j^T g_j(\bar{x}_1, \dots, \bar{x}_{i-1}, x_i, \bar{x}_{i+1}, \dots, \bar{x}_n) \\ \text{s.t. } & c_i(x_i) \leq 0 \\ & g_i(\bar{x}_1, \dots, \bar{x}_{i-1}, x_i, \bar{x}_{i+1}, \dots, \bar{x}_n) \leq 0 \end{aligned}$$

where \bar{x}_j , $\bar{\lambda}_j$ are determined by the j th subproblem and fixed in the i th subproblem. By including the complicating constraint in the i th subproblem as a hard constraint, the corresponding Lagrangian multiplier vector λ_i is obtained after solving the subproblem, which then provides an automatic update for multipliers in the next iteration. The general OCD algorithm is given below.

- 1) Initialize all variables \bar{x}_i and Lagrangian multipliers $\bar{\lambda}_i$.
- 2) Solve subproblems mentioned above.
- 3) Update \bar{x}_i , $\bar{\lambda}_i$ for all i by the values obtained in Step 2.
- 4) If stopping criteria are fulfilled, stop. Else, go to Step 2.

²⁷ A. J. Conejo, E. Castillo, R. Minguez, and R. Garcia-Bertrand, *Decomposition Techniques in Mathematical Programming*, Springer, 2006.

Generally speaking, the advantages provided by OCD over the other primal-dual decomposition techniques are that: 1) the update for the Lagrangian multipliers is implicitly given by each subproblem; 2) there is no need for parameter tuning; 3) the subproblems can be solved either until optimality or just for one Newton-Raphson iteration.²⁸

Two types of OCD are implemented for the considered SMPC economic dispatch problem. The main difference between the two types lies in Step 2 of the algorithm. One type is to solve each subproblem until optimality and the other version is to only implement one Newton-Raphson iteration step. Comparisons between the two different implementations regarding OCD are made in the simulation section.

Unlimited Point Method

This section describes one specific method named unlimited point method to transform the inequalities in the KKT optimality condition into equalities to facilitate the implementation of the Newton-Raphson based optimality condition decomposition (the second version of OCD).

Since any Newton Raphson based method is to deal with equation systems, we first need to find the equation system corresponding to the optimization problem. The well-known KKT optimality condition yields a mixed system with equalities and inequalities. We apply the so-called unlimited point method to transform the KKT condition into an equation system. In the following, we will demonstrate the unlimited point method on the subproblem of the two-stage stochastic model predictive control problem.

For each subproblem, we have the following optimization in general.

$$\begin{aligned} \min \quad & \frac{1}{2} x^T F x + c^T x \\ \text{s.t.} \quad & Ax \leq b \quad (10) \\ & Dx = d \quad (11) \end{aligned}$$

where F is semi-positive definite; the limits on decision variables and the line flow constraints are included in (10); the power balance equations and the internal system model including the models of generators and storage devices are included in (11).

The modified Lagrangian function is

$$L(x, \lambda, \mu^2) = \frac{1}{2} x^T F x + c^T x + \lambda^T (Dx - d) + (\mu^2)^T (Ax - b).$$

Note that here we are assigning a squared term to the Lagrangian multiples associated with the inequality constraints so that the non-negativity of the multipliers is guaranteed.

²⁸ A. J. Conejo, E. Castillo, R. Minguez, and R. Garcia-Bertrand, *Decomposition Techniques in Mathematical Programming*, Springer, 2006.

Additional squared terms are also added to the inequality constraints to transform them into equality constraints. It is obvious that the non-negativity of the additional squared terms ensures that the original inequalities are always true. The resulting KKT condition is

$$\begin{aligned}\nabla_x L &= Fx + c + D^T \lambda + A^T \mu^2 = 0 \\ Dx - d &= 0 \\ Ax - b + \varepsilon^2 &= 0 \\ \text{diag}(\mu) \cdot \varepsilon &= 0\end{aligned}$$

Due to the fact that there are no non-negativity constraints on μ and ε , this method is therefore called the unlimited point method. The corresponding Jacobian matrix at each iteration is

$$\begin{bmatrix} F & D^T & 2A^T \text{diag}(\mu) & 0 \\ D & 0 & 0 & 0 \\ A & 0 & 0 & 2\text{diag}(\varepsilon) \\ 0 & 0 & \text{diag}(\varepsilon) & \text{diag}(\mu) \end{bmatrix}.$$

When the second version OCD is implemented, the Jacobian matrix above is used to calculate the updates of the coupling variables and Lagrangian multipliers.

Discussion on Singularity of Jacobian Matrix

One key issue of the Newton-Raphson based method is the singularity of the Jacobian matrix at the optimal solution. In order to avoid a singular Jacobian matrix, we first need to remove all the redundant constraints in each subproblem of the SMPC economic dispatch. For instance, the control input at $k=0$ in each subproblem is fixed due to the constraint $\bar{u}^s(0)$, all the other constraints restricting $u^s(0)$ need to be removed. The bar here indicates that the variable is fixed. However, such a precautionary measure cannot guarantee that the Jacobian matrix at the optimal point is non-singular. Further investigation has to be carried out. In the following, we will analyze the reason behind why the Jacobian matrix still could possibly become singular even after the removing of all redundant constraints and then provide a possible solution to this singularity issue.

In general, each subproblem has the following formulation:

$$\begin{aligned}\min & f(x) \\ \text{s.t.} & g(x) = 0 \quad (12) \\ & h(x) \leq 0 \quad (13)\end{aligned}$$

The corresponding modified KKT condition based on the unlimited point method is:

$$\begin{aligned}\nabla_x L &= \nabla_x f(x) + \nabla^T g(x) \lambda + \nabla^T h(x) \mu^2 = 0 \\ g(x) &= 0 \\ h(x) + \varepsilon^2 &= 0 \\ \text{diag}(\mu) \cdot \varepsilon &= 0\end{aligned}$$

The corresponding Jacobian matrix is:

The Jacobian matrix will become singular when the gradient of the binding constraints (including all the equality constraints) does not have full row rank. In other words, we need to make sure that the following matrix has full row rank.

The singularity issue is caused by the constraints related to the storage devices. For illustration purpose, we assume that the number of storage devices is just one.

The relevant variables corresponding to the storage constraints are:

$$x = [E(k) \quad u^c(k) \quad u^d(k) \quad E(k+1)]^T.$$

The storage constraints are:

$$\left\{ \begin{array}{ll} E^{\min} \leq E(k) \leq E^{\max} & (14) \\ E^{\min} \leq E(k+1) \leq E^{\max} & (15) \\ 0 \leq u^c(k) \leq u^{c,\max} & (16) \\ 0 \leq u^d(k) \leq u^{d,\max} & (17) \\ E(k+1) = \alpha E(k) + T \cdot \eta^c u^c(k) - T \cdot (\eta^d)^{-1} u^d(k) & (18) \end{array} \right.$$

where $E(k)$ and $E(k+1)$ are the energy levels of the storage device at time steps k and $k+1$, respectively; $u^c(k), u^d(k)$ are the charge and discharge power, respectively; α is the coefficient associated with standby losses; η^c, η^d are the conversion efficient coefficients. Here, the limits for the storage energy levels are assumed to be identical for all time steps.

Consider the situation where the optimal solution is $E(k) = E^{\min}$ and the lower limit of the energy level E^{\min} is zero. It is obvious that the gradients of the binding storage constraints are linearly dependent as there are five binding constraints in total with only four variables.

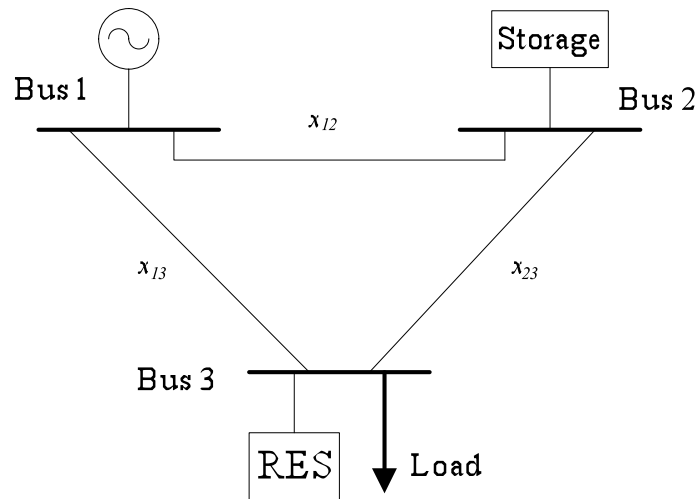
This singularity problem can be solved as long as at most three of the constraints (14)-(17) are binding at the same time. In practice, we simply need to make sure that the condition $E(k) > E^{\min}$ is satisfied. Intuitively, we make sure that there are always standby losses associated with the storage device by imposing the foregoing condition. For example, if (14) and (15) are binding in terms of the lower limit, constraint (17) becomes binding and constraint (16) is non-binding as the storage operates in the charging mode to cover standby losses to maintain the energy level. In such a scenario, it is rare in reality that the charging power reaches its

maximum limit. We choose the lower limit of the energy level to be 0.0001p.u.h and the coefficient for standby losses to be 0.95 in the simulation.

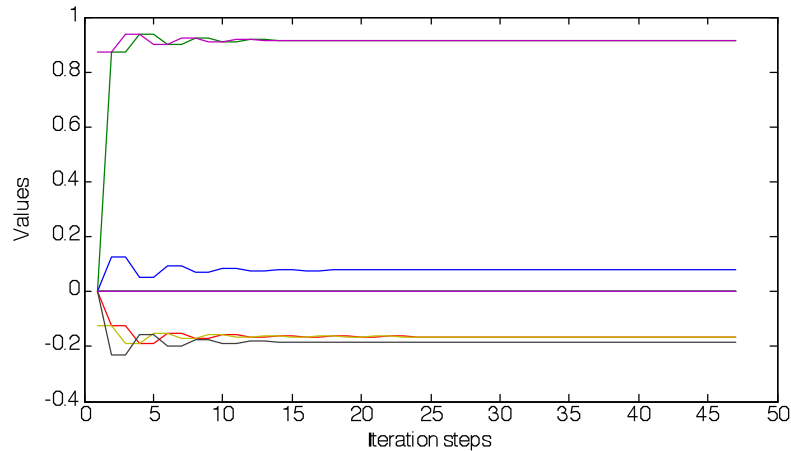
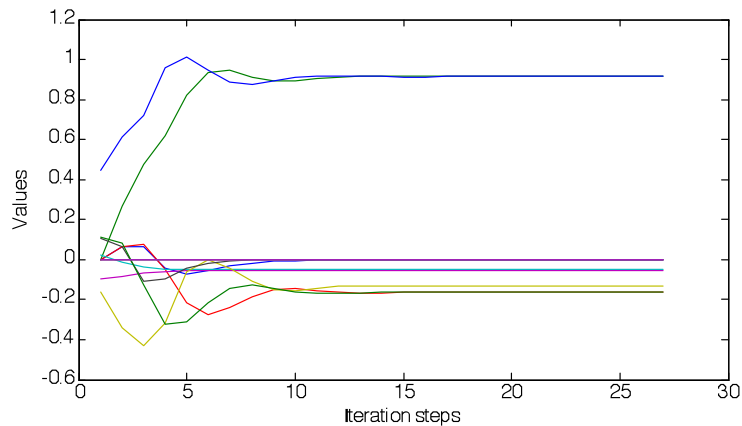
Simulation

The two versions of optimality condition decomposition are implemented in the simulation. Comparisons between the two versions are firstly made in a small 3-bus test system (see Figure 93). The commercial software TOMLAB is employed to solve optimization problems in the first version of OCD (denoted by OCD_v1) where each subproblem is solved until optimality. The second version of OCD (denoted by OCD_v2) adopts the Newton-Raphson based method and solves subproblems by performing only one Newton-Raphson iteration step.

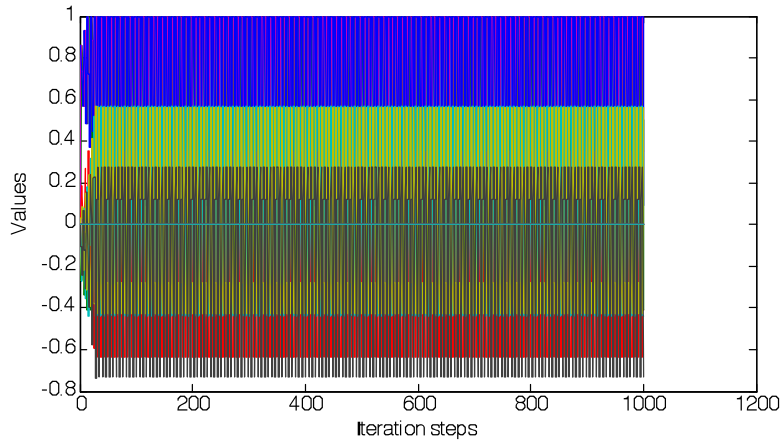
Figure 93: 3-bus Test System



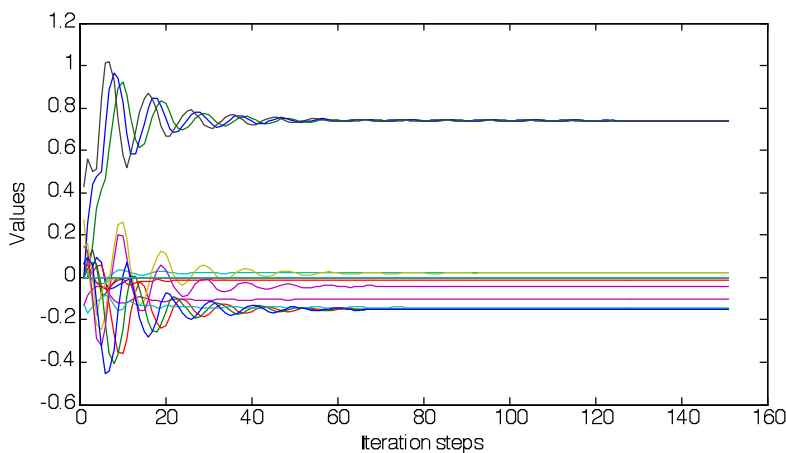
The number of scenarios is chosen to be 2 and the length of the look-ahead horizon is chosen to be 6 and the length of each time step is 5 minutes. The scenarios of load and RES generation are randomly generated at this moment. Actual data will be used in the later stage of this project. The decomposition is based on different scenarios. Even for this small 3-bus test system, there are 60 variables and 213 constraints for the corresponding overall SMPC problem. The evolution of the coupling variables and Lagrangian multipliers for OCD_v1 and OCD_v2 is shown in Figure 94 and Figure 95, respectively. The coupling variables in the considered problem are the states and control variables in the first time step of all scenarios. Each iteration step indicates one round of information exchange among subproblems. The optimal solutions are verified by checking the centralized solution of the overall problem without decomposition. As can be seen from the simulation result, the number of iterations needed for achieving global convergence in the second version of OCD is slightly less than the number in the first version of OCD where subproblems are solved until optimality using TOMLAB.

Figure 94: Evolution of Coupling Variables and Multipliers using OCD_v1**Figure 95: Evolution of Coupling Variables and Multipliers using OCD_v2**

It is actually not necessary to solve each subproblem until optimality. There are cases where the first version of OCD diverges while the second version is still able to calculate the optimal solution. Take the 3-bus test system as an example again. The only parameter change is that the number of scenarios is changed to three. All the scenarios are randomly generated again. In this case, the first version of OCD does not work anymore and divergent behavior is observed from the evolution of coupling variables and multipliers shown in Figure 96.

Figure 96: Divergent Evolution of Coupling Variables and Multipliers using OCD_v1

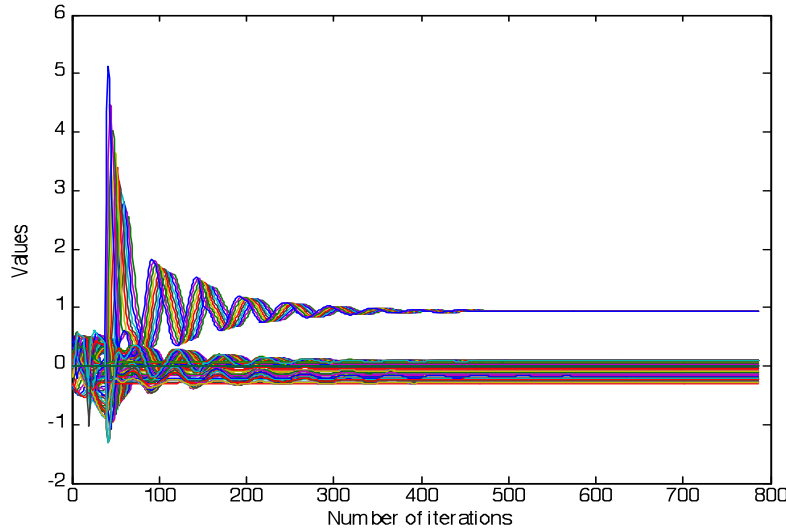
In contrast, the algorithm converges when the second version of OCD is applied for the same case. Solutions are checked by comparing with the result obtained from the overall problem. Figure 97 depicts the convergent behavior of the evolution of coupling variables and multipliers using OCD_v2. Simulation results favor the second version of OCD where only one Newton-Raphson step is needed to improve solutions of subproblems, which is believed to be the biggest advantage of the optimality condition decomposition compared to other decomposition techniques. For example, the well-known Benders' decomposition which is also widely used to decompose a two-stage stochastic optimization problem requests that we solve subproblems until achieving optimality.

Figure 97: Convergent Behavior for Evolution of Coupling Variables and Multipliers using OCD_v2

To extend the proposed advanced economic dispatch based on the algorithm of OCD_v2 to a larger system, the modified WECC 9-bus test system (see Figure 87) with 1 hour look-ahead

horizon (12 time steps) and 10 scenarios is used to further verify the convergence performance of the algorithm, which is demonstrated in Figure 98. It can be seen that the algorithm converges approximately within 600 iterations.

Figure 98: Evolution of Coupling Variables and Multipliers using OCD_v2 for the WECC 9-bus Test System

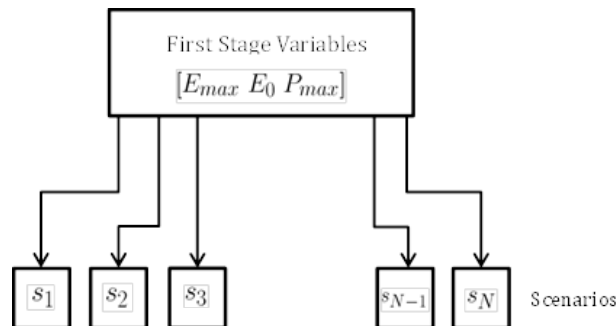


Optimal Sizing of Storage Devices

The problem of optimal sizing and placement of storage devices is investigated in this section as a complementary research topic to the development of the energy storage enabled smart control methodology.

To quantify the optimal storage capacity, a two-stage stochastic optimization approach is used. This approach seeks to minimize the total cost over a certain number of scenarios. In two-stage stochastic optimization, there are first stage variables, common to all scenarios, and second stage variables, which are scenario-specific. Each scenario is weighted by its probability of occurrence. A depiction of this relationship is seen below:

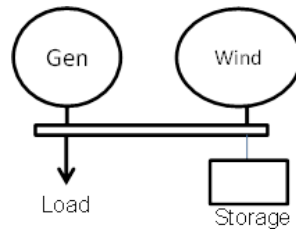
Figure 99: Two-Stage Stochastic Optimization



The first-stage variables in this case are the optimal storage size E_{max} , the initial state of charge E_0 , and the power converter rating P_{max} . The storage is also characterized by its roundtrip efficiency, which depends on the storage technology assumed.

Focus with regards to quantifying the optimal storage capacity is firstly being considered without system constraints as in Figure 100 and with only the optimal storage size E_{max} as a first stage variable. The optimal capacity of a storage device with parameters corresponding to a fast charging/discharging ultracapacitor (also called a supercapacitor) is considered to balance intraday (5-minute interval) fluctuations caused by variations in wind and load.

Figure 100: Economic Dispatch Model



Two-stage stochastic optimization using scenarios of 24-hour data for wind and load outputs from Bonneville Power Administration (BPA)²⁹ are considered. The objective to be minimized is the cost of generation (modeled as quadratic) over each scenario and the capital cost of the storage assuming a 10-year lifespan and a roundtrip efficiency of 95%. The total cost function is as follows:

$$f(x) = \sum_{i=1}^{numB} (C_1 E_{max,i}) + \frac{L}{N} \sum_{s=1}^N \sum_{i=1}^{numG} \sum_{t=1}^T a_i P_{G_i}^2(s, t) + b_i P_{G_i}(s, t)$$

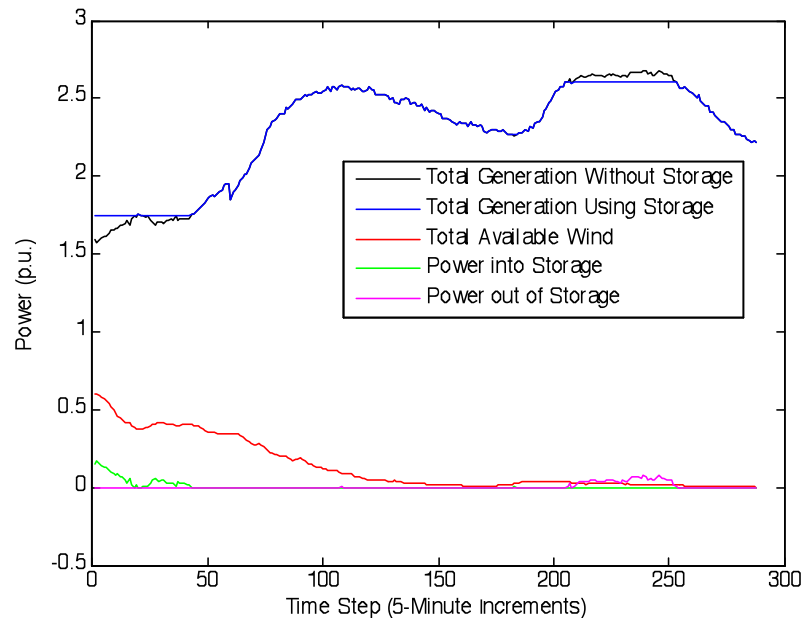
Where,

- numB: Number of buses in the system
- C_1 : Penalizing factor for storage capacity
- L: Lifetime of fully functional storage
- N: Number of scenarios
- numG: Number of generators in the system
- T: Total number of time points in a scenario
- P_{G_i} : Active power generation at generator i

²⁹ Bonneville Power Administration, *Wind Generation Forecast*.
 [Online] Available: <http://transmission.bpa.gov/business/operations/wind/forecast/forecast.asp>

For example, the optimal output for one 24-hour scenario (5-minute increments; $T = 288$) is shown below. The optimal storage size for this single scenario alone is $E = 0.1806$ p.u.

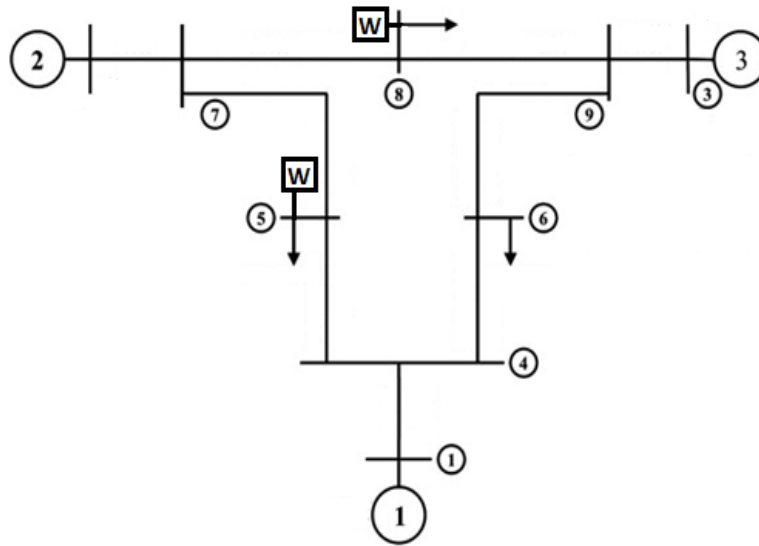
Figure 101: Optimal Generation and Storage values for 24 hours



The generators are ordered from cheapest to most expensive in order of their generator number 1, 2, and 3. Generators 1 and 2 have limits and these limits are always met. The wind generators are modeled as “must-take”; i.e., all of their output (which is always lower than the load) is used to supply the demand.

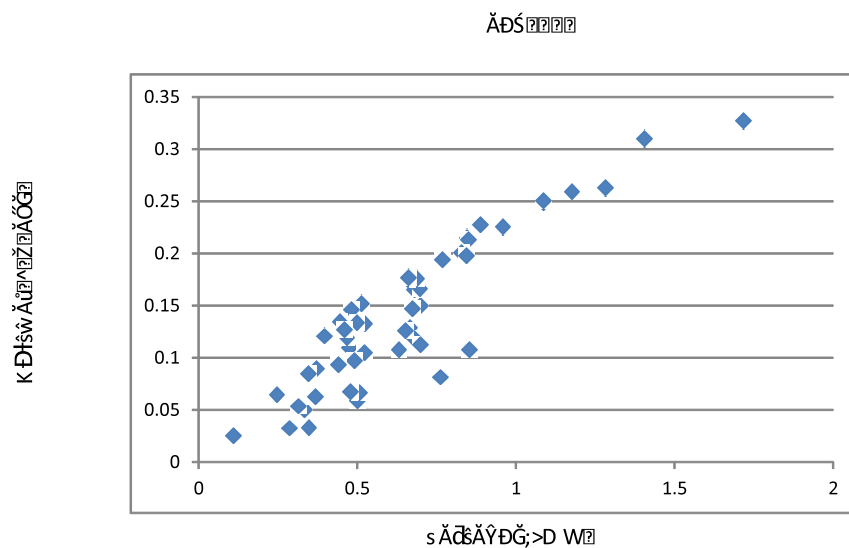
After this economic dispatch model is used to quantify the capacity of the storage, the system is extended to include multiple buses and generation and line constraints. Potential storage devices are placed at each bus – that is, the optimization is run not with storage at one particular bus, but at every bus. The problem to be solved is then the sizing of this storage; if the optimal capacity of the storage at a particular bus is zero, it is assumed that it is not optimal to have storage at that bus. The relationship found between optimal storage size at a bus and variance in locational marginal price (LMP) at that bus is being explored further to incorporate an analysis on optimal storage location. The following 9-bus system is used in the simulations, with added wind generators at buses 5 and 8.

Figure 102: Modified WECC 9-bus Test System with Two Wind Generators



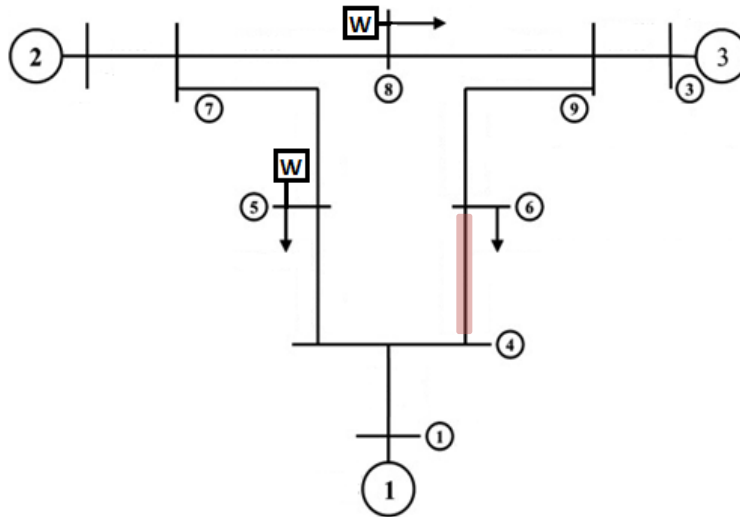
Two-stage stochastic optimization, with each scenario being a 24-hour time period of available wind and requested load, is run for up to 50 scenarios. The objective function of the optimization seeks to minimize the energy capacity and power rating of the storage device, as well as power generation from the generators. Cost parameters for these variables are taken from actual storage device datasheets for various forms of energy storage. Storage is initially placed at every bus and DC optimal power flow is performed to determine the optimal storage size at that bus. Without congestion, this storage size is evenly distributed among the buses and follows the relationship mentioned earlier of being related to variance in LMP as seen in Figure 103.

Figure 103: Optimal Storage Capacity and Variance in LMP Relationship



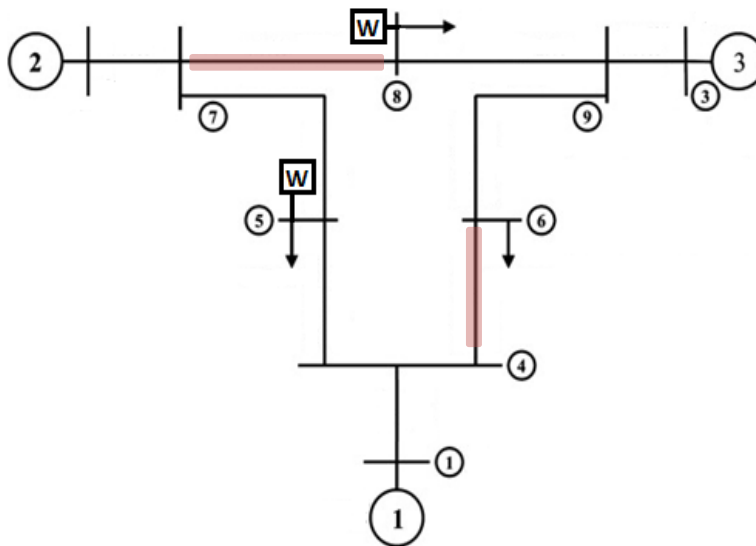
This size is the same at all buses because without congestion in DC power flow the LMP is the same at all buses. Moving to include line limits, we now have cases where the optimal storage capacity at each bus is not directly related to the variance in LMP at that bus. For example, when line limits are added between buses 4 to 6:

Figure 104: 9-Bus System with Line Limits Between Buses 4 and 6



The optimal capacity vs. variance in LMP is plotted for each bus. For all 50 scenarios, the optimal capacity at each bus is near zero and the optimal capacity at bus 6 is nonzero and follows the same trend seen in Figure 103. When two lines are congested:

Figure 105: 9-Bus System with Line Limits Between Buses 4 and 6; 7 and 8

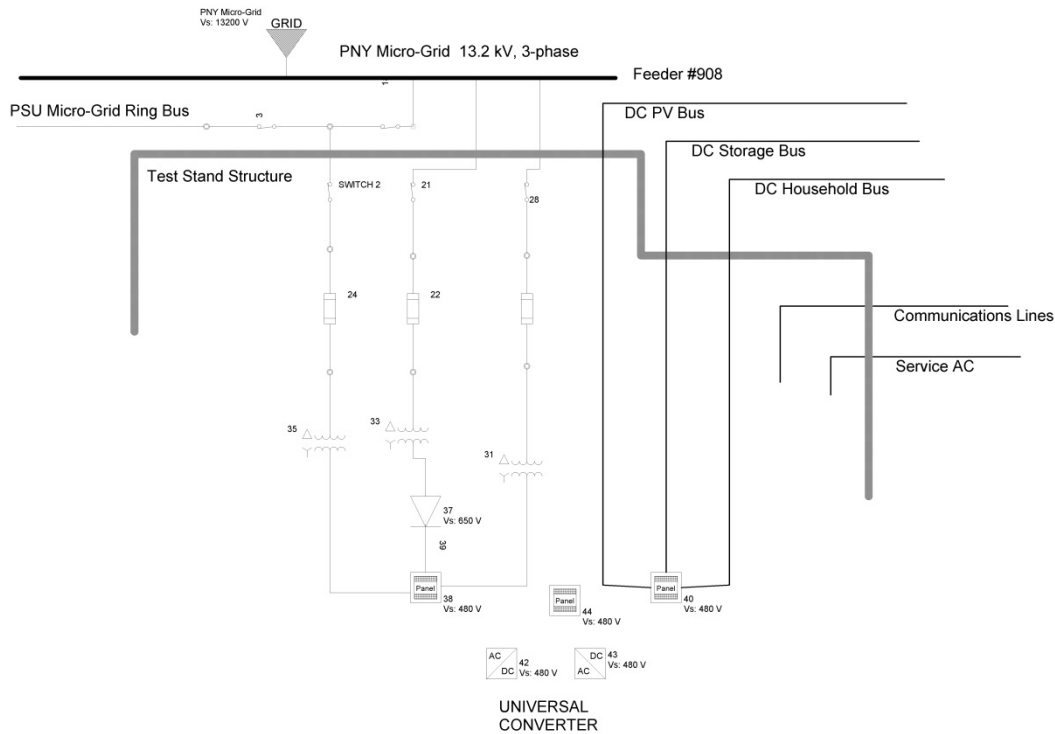


Across the 50 scenarios it is optimal to have found non-zero optimal storage capacities at buses 3, 6, 8, and 9. Because the system is modeled without line losses, the optimal storage size at buses 3 and 9 is evenly distributed; i.e., the solution is to have two storage devices at buses 3 and 9 with equal size. It would be an equivalent solution to have one storage device at either bus 3 or 9 with double that amount of storage.

In conclusion, the main finding is that without congestion, the optimal capacity of a storage device at a particular bus is correlated with the variance in the locational marginal price at that bus. With congestion, the conclusion gets a little more complicated. In general, the areas affected by congestion (such as in the second case, buses 3, 6, 8, and 9) benefit the most from storage devices. Depending on the application, this analysis could be useful for multiple reasons. If the storage device is going to be most beneficial in contingency situations or in normal day operations, different scenarios could be used in the stochastic optimization to decide on the optimal storage size.

4.5 THE POWER CONVERSION TEST STAND

The power mainframe of the prototype converter will support bi-directional transmission of energy between a DC power system and an AC power system. Functionality of the mainframe (whether controlling power factor or regulating voltage, for example) is determined by dedicated digital signal processing software (or firmware) mounted on the chassis of the converter. For developmental expediency, the controlling software is developed and evaluated in modules. The functionality of the power controlling mainframe can thus be changed by installation of an appropriate software module. An installation for in-line testing of the converter would consist of an enclosed exterior space for placing the converter power mainframe and its supporting control systems, along with wiring to and from each of the energy-carrying systems with which the converter is to be connected. The space should be designed so the mainframe may be readily installed and removed, and provide enough space around the hardware for technical support staff to adjust and modify the unit. For AC-to-AC and DC-to-DC applications, two of the prototype converter modules would ideally be wired back-to-back. For safety reasons, the enclosure would be placed away from other structures, but in a position so as to minimize energy loss in the power cabling running to and from the installation. Fire suppression equipment, cameras, and hazard detection sensors would also be present in the installation. An electrical schematic diagram of a workable Power Conversion Test Stand is shown in Figure 106.

Figure 106: Power-Conversion Test Stand

4.5.1 Initial Converter Test Configurations

As the first converter will likely be limited to AC voltages of 480 volts, any energy exchange with the 13.2-kV #908 PNY feeder will initially require connection through a step-up transformer. All taps but one on the GridSTAR system are conventional 120/240 VAC, 60-Hz, with a 100-kW maximum power. Under certain test conditions, it might be appropriate for the converter to exchange power directly with an individual distribution line, tapped off the microgrid on the load side of the line breaker and step-down transformer. This will require supplemental breakers and cabling. Only one line, the 480-VAC line intended for peak-shaving activities, has a power handling capacity that exceeds that of the converter. Direct connection to this line would require taking appropriate precautions to prevent overloads.

Below are listed likely testing scenarios for the converter on the ring bus. They appear in ascending order of anticipated complexity, with the simplest implementations listed first. (Future changes in hardware might affect this ordering.)

1. Interface between battery storage and the 13.2-kV ring bus. Here the converter would be transmitting power bi-directionally between the battery storage resource and the ring bus via a 480-V-to-13.2-kV step-up transformer. During periods when demand is low, the converter would rectify grid-sourced energy, transmitting it to a DC input in the energy storage system. During periods of high energy demand or for testing, and under the control of software, DC energy would be converted to AC by the inverter to augment the energy flowing on the PNY #908 radial feeder. (See Figure 107.) Alternately, this same functionality might be applicable to smaller storage systems operating at 240 VAC.

2. Power-factor control of the PNY #908 feeder. Here the converter would be supplied power-factor signals from an Eaton Power Xpert® 8000 Power Quality Monitor sampling the #908 feeder line. Working at 480 VAC, on the secondary of a step-down transformer bridging the #908 feeder, the UC would appropriately adjust the relationship between P and Q power so as to obtain a unity power factor on the feeder. The cycle-to-cycle energy storage required to control the P-Q relationship is provided by placing a capacitor bank on the open end of the converter. (See Figure 108.)
3. Rectification of grid AC to supply a residential nanogrid. There is growing interest in employing DC power in residences to improve overall energy efficiency. Here, the converter would rectify three-phase 480 VAC from a step-down transformer operating on the ring bus, providing DC for driving DC appliances and constant-power devices designed for use with DC systems. It would act as an energy control center. Energy surpluses generated by the household would be passed on to the grid. (See Figure 109.)
4. Interface between a PV array and the system. Here, the converter would interface between the DC output of a string of photovoltaic panels and the 480-VAC three-phase transformer supplying the collected and inverted solar-sourced electrical energy to the ring bus. Due to the natural fluctuations of solar insolation, in addition to converting the collected DC energy to AC, the converter must perform the function of what is called a *maximum-power-point tracking* (MPPT). An MPPT algorithm dynamically adjusts the electrical load impedance seen by the array at the input to the converter. The adjustment serves to electrically match the PV source and converter load impedances so as to maximize the energy transferred to the converter. (The connections would be similar to that of Figure 107, but with the battery storage system replaced by the PV array. Energy flow would be uni-directional.
5. Testing of the converter under dynamic loads. The stability of the converter operating with AC loads typical of conventional residences and small offices may be more severely tested with the ring bus disconnected from the feeder. Initially, for this test, the converter may invert a DC source to provide the AC output for the household or office load. The DC might be supplied by the rectified output of a diesel generator or the rectified output of 480-VAC transformer supplied by the feeder. Once a DC demonstration capability is introduced into the residence, the presence of constant-power loads will present another stability challenge to the converter. In later implementations, the converter could be tested under the condition of dynamic loads and a simultaneously varying AC-grid source. (See
6. Figure 110.)

Figure 107: The Converter Interfacing between Storage and the Ring Bus

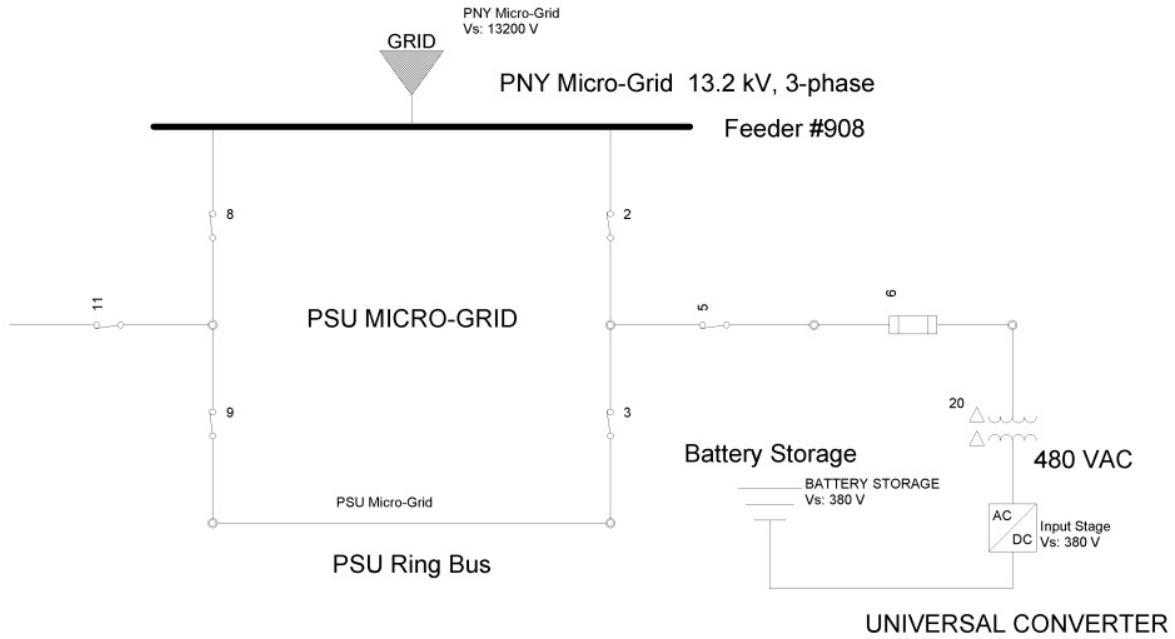


Figure 108: The Converter Controlling Power Factor on the Ring Bus

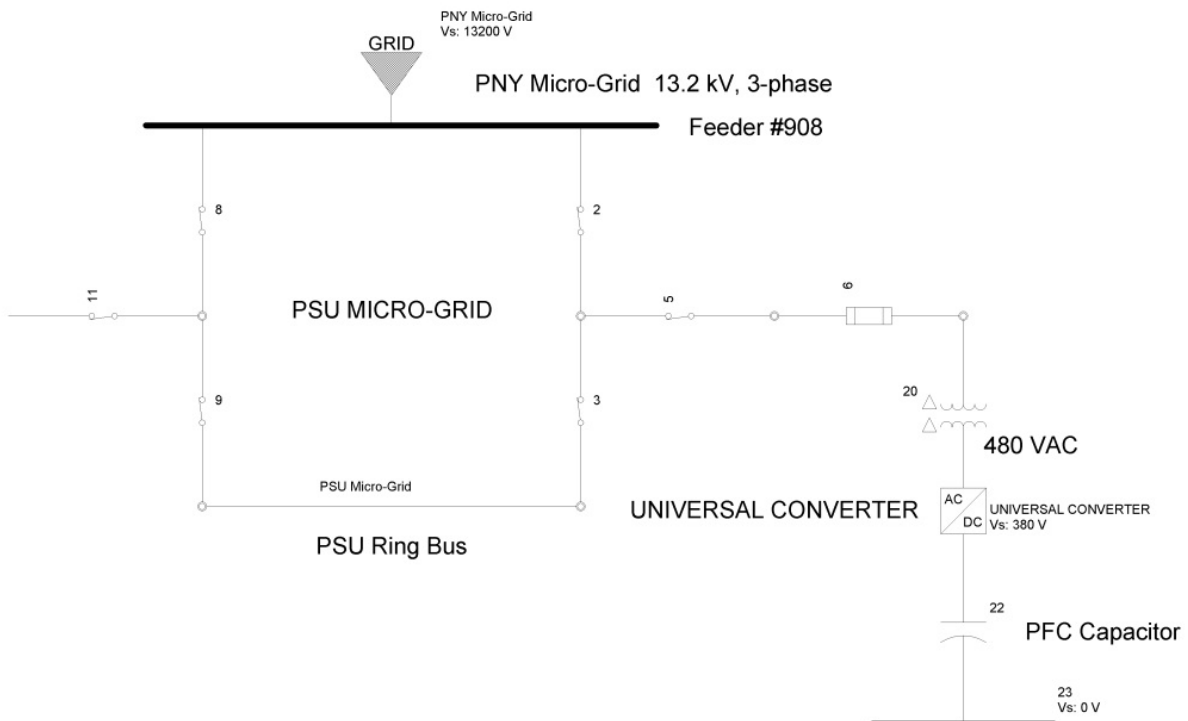


Figure 109: The Converter Operating as an ECC for a DC Household.

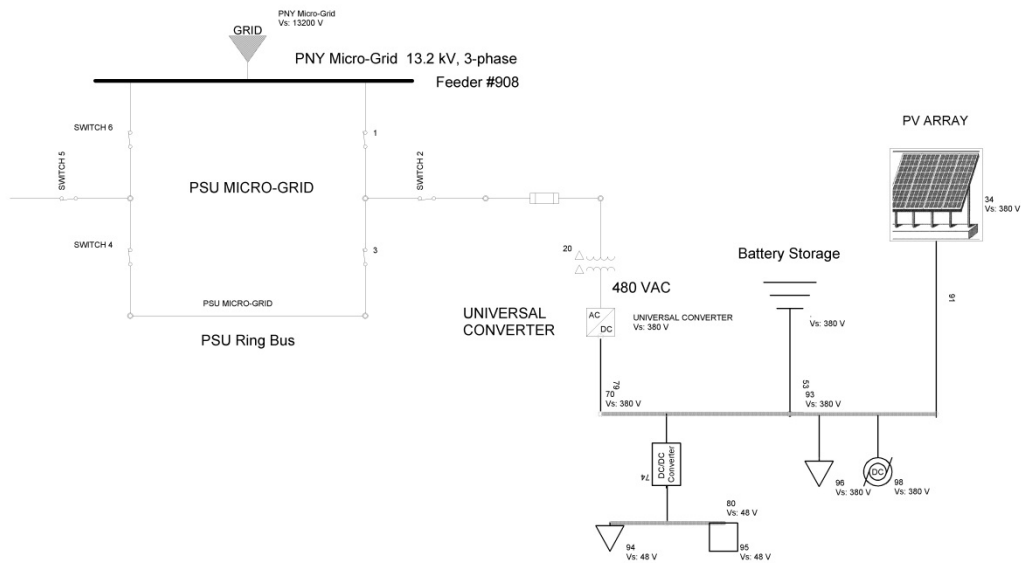
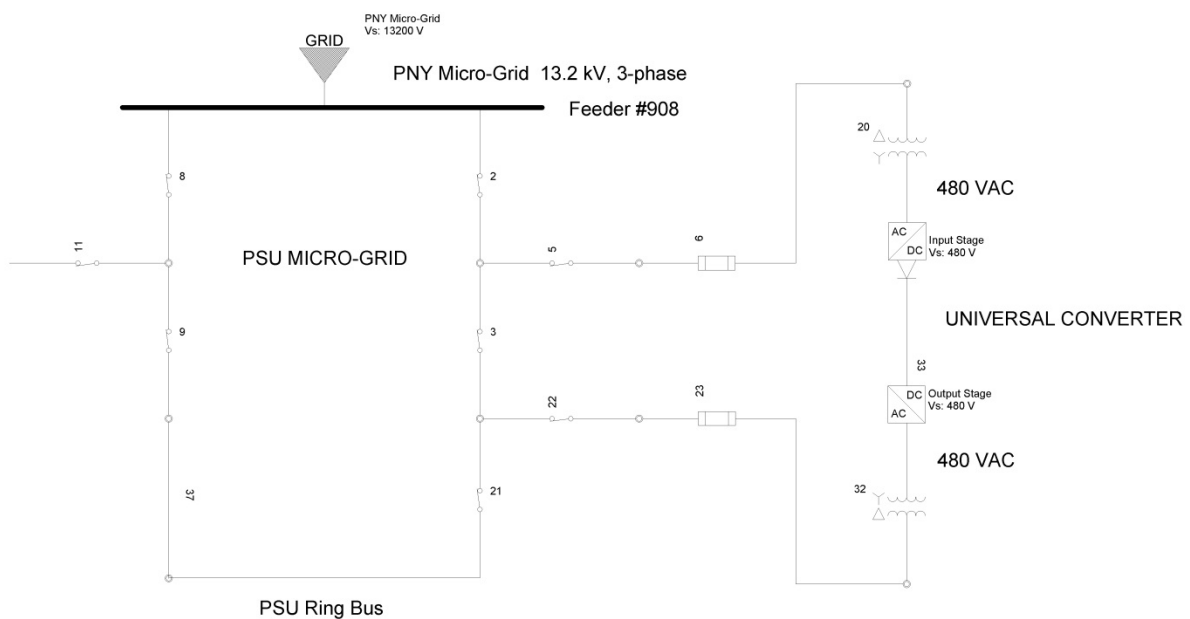


Figure 110: The Converter Operating Under a Dynamic AC Load



As seen from Figure 107 through Figure 110, these evaluation scenarios for the converter require only simple re-arrangements of the resources, yet provide the kind of real-world test challenges necessary to demonstrate the reliable operation of sophisticated hardware intended for widespread use.

4.5.2 Test Configurations Details

Conventional solid-state power converters have become commonplace in industrial equipment, computers, and home appliances and electronics. Their advantages in weight, efficiency, flexibility, and cost are significant. Power flows one way in these converters. The number of subsystems in these converters is usually limited to two or three. Once bidirectional power flow is required, along with the ability to handle AC or DC power of differing voltages, the system becomes more complex. High operating voltages and large operating voltage ranges also complicate the circuitry. Because of the sophisticated nature of the converter concept, the pace of development of a hardware prototype in an academic environment is limited. Fortunately, the generality of the converter system allows some of its capabilities to be developed independently of others. The two core elements of the converter are most readily applied to bidirectional AC-to-DC power conversions suitable for use in an energy control center (ECC), a transition device operating between an AC-grid and a DC-household. (This system envisions a main power bus operating at 380-V DC on the household side, with a possibly smart controller providing an additional 48-V DC bus for supplying secondary loads.) The two-way operation of this simplest of converters, provides the option of employing local renewable generation and storage on the household side. This is Test Scenario #3, outlined earlier.

Another application for the first UC converter chassis is power factor control of the PNY #908 feeder. This is Test Scenario #2. This is the simplest application envisioned for the first, simplified converter prototype. It requires no load on the DC side, only an appropriately sized bank of capacitors. It will require control software different from that used for Test Scenario #3. If the power factor on the 908 feeder is poor, there would be motivation for the PIDC to maintain operation of the converter as long as possible. Except in the case of a catastrophic failure, this system could be activated without interrupting power on the feeder.

While hardware development of the UC proceeds, installation of the storage and small PV array is expected to proceed. As these systems incorporate their own DC-to-AC converters, they may be directly connected to the grid-sourced power available, via appropriate transformers only if necessary. Operation of these more conventional energy resources would be fully monitored by the power quality monitors on site. Staff might employ the systems for training and to study long-term performance.

Field testing of hardware produced by independent entities might also be considered.

4.5.3 Evolution of UC test configuration

As the development of the converter progresses, alternate testing regimens come into play. Depending on the path of the converter development, alternative testing scenarios would evolve. If the DC-AC converter topology of the converter is retained in favor of increasing its maximum operating voltages, the five scenarios outlined above as initial test configurations would be simply extended to higher voltages—principally on the AC side. For each of the five aforementioned scenarios, the interface at the AC end of the upgraded converter would be connected to the ring bus via transformers dropping from the 13.2 kV of the feeder to an intermediate voltage, such as 2400 or 4160 VAC. As the DSP-based converter control algorithms would have been proven for the different operating scenarios during initial testing, testing at the intermediate AC voltages would be simply confirmation that the converter voltage-handling capabilities meet requirements.

Once it became possible to operate any converter prototypes on the 13.2 kV AC feeder, evaluation of the converter's efficiency would be more convenient, as losses in the step-down interface transformer would be absent.

4.5.4 AC-to-AC Converter Testing

If hardware development of the converter proceeds to provide AC-to-AC capabilities, alternative test scenarios would be appropriate.

- Interface with PNY feeder. Whether through a step-down transformer to conform to voltage limitations or not, this connection would allow testing of the capability of the converter to transfer AC power in either direction between the grid and the ring bus, while maintaining desired voltages and optimum power factor. With the ring bus powered by PV or via storage, the "islanding" capability of the converter could be evaluated. If the array were supplying more energy than demanded on the ring bus, the converter would pass the excess onto the feeder and the AC grid.
- Feeder control. Once the design of the converter allowed operation at the 13.2 kV AC feeder voltage, it would be feasible to operate the converter in series with the #908 feeder line. This would allow dynamic adjustment of power factor and near instantaneous control of line droops. Essentially the converter would be operating as a *line conditioner*.

4.5.5 DC-to-DC UC Testing

If hardware development of the converter proceeds to provide DC-to-DC capabilities, other test scenarios would be appropriate.

- Interface between storage and a DC residence. Here the converter would dynamically adjust the transmission between an energy storage system and a DC-fed home. The converter would need to respond to transients in the household load, while adjusting for the steady decline in the storage battery voltage. Any excess in energy available in the household grid would be returned to storage.
- Interface between a PV array and a DC residence or storage. This duplicates the energy flow from the array to the household bus, but with the maximum-power-point tracking. Power flow in the reverse direction would be blocked.

Ultimately, DC-to-DC conversion at grid voltages is considered a long-range goal for the converter application. At present, there appear to be no avenues for testing the converter at the PNY in this mode.

4.5.6 Ancillary Testing Opportunities

The GTC took on the development of technologies appropriate for distributed energy resources of the power grids of the future. The converter is at core of this effort. But, distributed generation significantly complicates the long-standing issues of economic dispatch and the maintenance of grid stability. Fittingly, supporting technologies that deal with these issues are part of the overall development efforts.

4.5.7 Power System Simulation

The difficulty of experimenting with complex, high-power grid transmission and distribution (T&D) systems motivated the development of powerful software tools for grid simulation. Today's computation capabilities and simulation tool options provide various levels of modeling and analysis to be performed. With distributed generation (DG) and the stochastic character of renewable sources being incorporated into the development plan (and eventually a test bed environment), the incorporation of new hardware and control strategies must be verified. Part of the GTC project previously discussed establishes T&D models implementing the industry-standard simulation tool, PSCAD, including development of enhanced user models to more accurately represent the dynamics of a DER grid.³⁰

The test bed infrastructure, with its local generation and storage capability, will provide the hardware elements and a basic operational environment required to verify the accuracy of the modeling enhancements and the simulations under certain scenarios. To that extent four Eaton Model 8000 Power Xpert® power-quality monitors (PQM) operating on the microgrid can provide the real-time operational data necessary to corroborate the software modeling and results. Using a PC-based data-collection system and data-analysis software, enough real-time information can be readily processed to provide initial verification of the upgraded grid modeling as it progresses.

4.5.8 Communications and Smart Grid Simulation

System communications will be critical to the dynamic behavior and stability of the anticipated smart grid structures being developed. Simulation tools not incorporating the temporal behavior of the communication channels and protocols used to carry the many grid status and control signals expected in the new grids will not accurately model real behavior. Anticipating this issue, another part of the program effort has been the development of routines to simulate common protocols and transmission characteristics for incorporation in PSCAD.³¹ Initially, control of the test bed infrastructure will not be centralized. This will limit the verification of simulations on the system to the collection of status signals. The on-site Wi-Fi capability at PNY, along with the four Eaton PQM units, will readily enable time-of-arrival comparisons between the simulations and the hardware-generated signals. However, the nature of this testing is such that it may be handled nearly as well in more controlled environments, such as in laboratories, or on well-instrumented extant grids. As development of the test bed infrastructure progresses, more closed-loop systems and their enhanced testing opportunities will present themselves. Early exploitation of these opportunities will speed the development and deployment of more efficient and cost-effective grid infrastructure.

Distributed renewable generation presents new challenges to grid operation as a result of both its physical distribution and its stochastic variation. At high penetrations of renewable generation, the irregular placement of generators and the statistical variation in their power output present major hindrances to reliable and economical grid operation. Cognizant of the potential

³⁰ GTC Monthly Technical Report, November 2012, University of Pittsburgh.

³¹ GTC Monthly Technical Report, November 2012, West Virginia University.

roadblocks posed by these factors, and the need for energy storage in DER grids, another part of the first year activities of the program initiated development of optimization algorithms for power balancing—important for the economic operation of the converter. When incorporated optimally, storage offers the potential to shift loads, to reduce energy congestion in transmission, and to increase the allowable penetration of distributed generation in large smart grids. The inclusion of forecast data and stochastic prediction techniques promise improved performance.³²

Two aspects of energy balancing optimization, short-term frequency control (both primary and secondary) and the more general economic dispatch problem, are relevant to even small grids. Ultimately this optimization is to be implemented in real time and will allow smart grids to most economically balance the dynamic constraints of generation, transmission, and distribution. Once the algorithms have been proven in simulations, their implementation in PC-based supervisory equipment within a microgrid environment will be one avenue to prove their efficacy in energy balancing in small systems with storage.

4.6 MODELING PRODUCTION COST DECLINES FOR UNIVERSAL POWER CONVERSION TECHNOLOGIES

This section provides a summary of work done to support the effort to develop prototypes, models and controls for advanced bi-directional power converters in the area of production cost modeling and system-level economic benefits estimation. The task for the second half of 2012 was to design a study methodology that could be used to estimate declines in production costs for advanced bi-directional converter technologies as they move from bench to commercial production scale. Towards this goal, discussions were held with the GTC institutions to identify data sources and collaborative modeling opportunities, including the following topics: prototype costs for bench-scale converters (essentially custom-built for specific research purposes); availability of production cost data for commercially available power converter systems and the primary production cost drivers; modeling control strategies at the grid scale and how those models could be adapted to estimate system-level benefits associated with wide deployment of advanced converters. This last topic is important but additional work would be necessary to build a simulation environment where system-level benefits could be defined and estimated, conditional on a specific control strategy.

4.6.1 Summary of Findings

As advanced universal converters move from bench scale to commercial scale, production cost declines can be expected due to a variety of factors, including economies of scale and learning in manufacturing. Economists can estimate learning rates based on declines in reported production costs over time, but a challenge in implementing such an approach with converters is the lack of substantial publicly-available data on component costs even for mature technologies. A review of publicly-available resources found virtually nothing in the public domain relevant to estimating production cost *levels* for commercially-available systems, let alone sufficient data to directly estimate production cost decline curves for next-generation technologies. Project pricing and component breakdown are difficult to obtain; anecdotal evidence from discussions with

³² GTC Technical Monthly Report, November 2012, Carnegie Mellon University.

other GTC researchers would suggest that commercially available VSCs might run from \$75 - \$100 per kW of installed capacity while Static VAR Compensators (SVCs) might run at about \$60 per kVA. Both of these cost estimates would be for “large” utility-scale installations, on the order of 100 to 200 MW (or MVA). Profit margins on converter systems are usually low (less than 10%); the highly competitive market ensures that commercial prices stay close to production costs.

The advances in semiconductors, especially the development of insulated-gate bipolar transistors (IGBTs) and integrated gate-commutated thyristors (IGCTs) have allowed solid state power converters to become economically feasible. While transforming power from alternating current to alternating current (AC to AC) has been cheap and efficient for 100 years, transforming direct current (DC) current and voltage, and converting AC to DC and vice versa has been more expensive and much less efficient. While there has been a small amount of market penetration for large bi-directional power converters (>1 MW), the rapid increase of variable renewable energy connected to the electric grid and the hope for the widespread deployment of massive batteries means a market is developing for utility scale converters (>10 MW).

The converter systems envisioned by the GTC are perhaps one order of magnitude smaller – around 20 MW (or MVA). Again, anecdotal evidence from conversations with other GTC researchers suggests that these smaller scale converters would have perhaps twice the production cost. The inflection point in any learning curve, however, is highly uncertain. The difference in production cost for bench-scale versus commercial-scale systems is perhaps one order of magnitude, but there is also substantial uncertainty in this figure.

5. CONCLUSIONS

The work of the GTC from August through December, 2012 is presented in this final report on "The Next Generation Power Converter: Applications for Enhanced T&D Grid Performance and Resource Integration." Significant progress was made by the GTC team in advancing the development of power electronics conversion technology through this first year effort.

Each university represented on the GTC had assumed a defined lead role responsibility in the project, along with strong ties to input and support from the other organizations, while also providing similar input and support to others' lead scopes. This synergistic approach proved to work extremely well, and also provided strong team interactions and interdisciplinary collaboration among the university partners and NETL.

The initial year's project efforts focused primarily on modeling and simulation to develop validated steady state and dynamic models of system interactions at the converter-grid interface, including consideration of a next generation power converter. It was concluded in this effort that the converter development going forward will be established as a scalable bi-directional three-phase AC-DC interface for utility scale high power applications at the transmission and distribution (T&D) levels.

As such, initial system applications for this advanced power electronics based converter topology were selected in the 2012 work, to address T&D grid performance including advanced control methodology development, interface and communications protocols, and integration of various renewable energy resources, energy storage, and evolving load entities, as well as emerging hybrid AC/DC systems.

Modeling platforms for the initial year efforts were chosen to include industry-standard tools and programs that are also common to each university's capabilities and expertise, and are centered on models utilizing the PSCAD/EMTDC and MATLAB/Simulink program environments. The system models for initial project development consisted of an accepted and widely used IEEE standard WECC transmission level test case system, as well as an IEEE standard distribution feeder test case system.

These models were established as a baseline to allow the ability to analyze interactions between T&D networks for both the converter and the control and interface methodologies to be developed. With this foundation established, various additional resources and loads can now be integrated into these models, as well as the advanced converter model that is being developed separately.

Basic conclusions from the different components of the 2012 work are provided in the following sections (5.1 through 5.5), along with a brief discussion on future work and considerations (5.6).

5.1 SYSTEM MODELING CONCLUSIONS

With the conclusion of the IEEE 13 Node Test Feeder validation, the team now has a model that generates the same power flow functionality that the IEEE 13 Node Test Feeder report dictated. The results provide validation and verification of the model development for the intended purposes of the converter development. Specifically, the validation results given in this report show that the PSCAD model created is an accurate model of the IEEE 13 Node Test Feeder system. The documented explanation provided in this report will make the modeling thought process more clearly understood going forward, and allow an expansion of the model for the various application scenarios that are envisioned.

5.2 CONVERTER PERFORMANCE, FUNCTIONALITY & DESIGN CONCLUSIONS

Although power electronics can undoubtedly improve system controllability, reliability, size, and efficiency, its penetration in power systems is still quite low. The often-cited barriers of higher cost and lower reliability of the power converters are quite high if power electronics is used as a direct, one-to-one, replacement for the existing electromechanical equipment. However, if the whole power distribution system were designed as a system of controllable converters, the overall system cost and reliability could actually improve, as is currently the case at low power levels within computer and telecommunications equipment. Further penetration will strongly depend on the progress in our ability to model, understand, design and dynamically control desired and undesired subsystem interactions in the new, electronic power distribution systems. The work completed in 2012 on this part of the project establishes a strong foundation for the performance, functionality, and design of the next generation power converter.

5.3 COMMUNICATIONS AND INTERFACE PROTOCOLS CONCLUSIONS

The emergence of distributed communication based control schemes in power systems emphasizes the need for a realistic power systems simulation tool that allows inclusion of communication components. Communication performance parameters, such as delay and loss in transfer of measurements and commands, can affect the result of control and should be taken into account while studying a control mechanism over power system dynamics. In the project efforts thus far, methods and tools have been developed to allow simulation of communication networks inside off-the-shelf product for power system transient simulation in PSCAD. In particular, the structural designs and interfaces of modules that are needed for implementing an embedded communication network simulator in PSCAD have been developed, and provide a brief guide on how power system engineers can use these modules in their designs. The presented simulation environment allows for simulation of emerging distributed control and monitoring schemes in advanced smart power systems. The main contribution of this work is in coupling the dynamics of power systems and communication networks, given that they are considerably different (continuous vs. discrete event-based dynamics). The coupling was made possible using a synchronization mechanism embedded in PSCAD (as opposed to other methods that use synchronization with outside tools). A communication interface has been implemented to enable power system designers to integrate their system with communication links and routers, to provide a more thorough perspective over the entire system as one coupled entity. The IEEE 13-node test feeder was used for the case study, with wind generator and storage modules connected to the system to add more dynamic behavior. A control for the system was designed which

works with communication interface and modules implemented in PSCAD. The test system was used to validate and verify the embedded communication simulator and its implementation.

5.4 SMART CONTROL METHODOLOGY CONCLUSIONS

From the perspective of smart control development, an energy storage enabled smart control methodology was developed for the future power system with uncertainties introduced by renewable generation, which provided a promising solution to the problem of seamlessly integrating variable energy sources and energy storage devices into the electric power systems in terms of multi-timescale energy management. Simulation results on the modified WECC 9-bus test system validated the feasibility of the proposed optimal control and scheduling methodologies that were developed in the 2012 project efforts. In addition, the optimal sizing and placement problem of storage devices was investigated from the viewpoint of stochastic optimization. The close correlation between the optimal size of a storage device and the variance in the locational marginal price at the bus where the storage is installed was found. This work extends from and can be integrated in the future on the communications and interface protocols that were also developed, providing a holistic approach to the converter smart control development overall.

5.5 DEMONSTRATION SITE PLAN CONCLUSIONS

The principal conclusion of the demonstration site plan investigation is that the Philadelphia Navy Yard facilities and associated GridSTAR capabilities could provide an environment for the convenient and economical in-line testing of novel power-conversion equipment and systems. Installation of advanced equipment for the generation and storage of electrical energy, along with the electronic energy conversion equipment that can support experimentation with developmental concepts, such as DC household power for example, is currently in development. The technologies represented are those expected to form the core of the distributed energy resources of the future electrical grid, providing opportunities for operation and experimentation under realistic operating conditions. Based on the un-regulated electrical microgrid set up of the Philadelphia Navy Yard, novel energy-saving strategies and grid-based applications may be established and evaluated without the regulatory constraints facing most grid-tied entities. In addition, incorporation of energy storage and renewable generation equipment within the test bed facility provides an opportunity for evaluation and demonstration of devices such as newly developed converter technologies. Additionally, opportunities for DC distribution experiments are present. Power-electronic hardware exists to handle the narrowly defined tasks required of interfaces between DER and the grid, or energy storage systems and the grid, for example. To support evaluation and demonstration activities for the converter development, the concept for a power conversion test stand was developed. As converter development advances, other opportunities for its deployment for demonstrations exist, which can be leveraged, including testing and verification at system voltage levels up to 13.2 kV.

5.6 FUTURE WORK AND CONSIDERATIONS

This final report of the Phase 1 project documents the group's initial accomplishments, representing a period of performance of August thru December, 2012. The modeling platforms for the initial year efforts were chosen to include industry-standard tools and simulation/analysis programs that are also common to each university's capabilities and expertise, and centered on

models utilizing PSCAD/EMTDC and MATLAB/Simulink program environments, offering opportunities for more seamless interaction with future industry partners - this approach will continue in 2013.

Considerations to multi-platform modeling and simulation capability development with NETL for the converter, system, and applications were also integrated into the first year efforts, and will be expanded upon in the future work. In 2013, these models will be adapted to specific utility system topologies for future analysis and simulation of specific networks, designs, and operation. This will also allow the ability to develop interactions between T&D networks for the converter development, as well as the smart control and communications interface methodologies under development. Various additional resources and loads will be integrated into these models, as well as the advanced converter model that is being developed separately.

Future Phase 2 R&D Project Description: The Next Generation Power Converter

The Next Generation Power Converter will serve as a key interface to power grid modernization and advancement, providing an efficient, bidirectional connection and control point, and enabling the operation of emerging hybrid AC/DC systems. Initial applications of the converter will be at the utility-scale distribution level with extension of control concepts and interfaces to the transmission system, including aspects of renewable energy integration, energy storage, and evolving load entities. The key deliverables for the 2013 research project will include the following:

- Development of a simulation-quality distribution model of the Philadelphia Navy Yard micro-grid, in MATLAB/Simulink and PSCAD
- Collect Simulink and/or PSCAD inverter models, perform laboratory tests on inverters and verify model performance
- Transition 2012 MATLAB/Simulink models to PSCAD
- Continue and expand simulation and analysis of system interaction at interfaces and connection points for various types of technology integration
- Design a hybrid AC/DC test bed for future experimental validation of research results
- Multi-time scale control of storage devices
- Optimal sizing of Inverter and storage and determination of optimal location
- Advanced converter materials and devices development
- Develop and test network estimation strategies and protocols, identifying rate control mechanisms
- Identify and test DNP3 and IEC61850 features needed in evaluation of grid cyber-infrastructure, implementing an abstract version of the features for small-scale study
- Study interaction of communication protocols and network estimation strategies, and their effects on system performance
- Study vulnerabilities of communication protocols and estimation strategies, and identify methods to improve robustness
- Collect sufficient information to support development of a simulation-quality distribution model of the Philadelphia Navy Yard micro-grid
- Multi-scale modeling and optimization
- Production cost modeling

These main deliverables, as well as joint conferences and journal publications resulting from the work, will be the emphasis of the future contributions.